



Learning from offshore field performance

P. Jeanjean*

bp, Houston TX, USA

K. Hampson

bp, Sunbury-on-Thames, UK

L. Majzlik, J. Bronikowski, A. Zakeri, A.W. Hill

bp, Houston TX, USA

**philippe.jeanjean@bp.com (corresponding author)*

ABSTRACT: This paper, the written version of the 7th ISSMGE McClelland Honor Lecture, documents and shares the learnings from the field performance of full-size offshore foundations under installation and operation loads. It details the events that led to the buckling of driven piles at the Valhall field during installation and compares the measured performance of MODUs anchors and mooring systems, jackets, and free-standing caissons to North Sea and Gulf of Mexico extreme environmental loads. It shows that the predicted performance of these structures is consistent with the field observations, if modern approaches to foundation modelling are used.

In addition, rather than focusing on natural geohazards as is often the case in the literature, the paper addresses anthropogenic geohazards by publishing two case histories where deepwater seafloor instabilities were triggered by human activities. Hard grounds and seafloor alterations resulting from drilling activities and the hazard they pose are also discussed.

Keywords: anthropogenic geohazards; pile buckling; field performance; p-y curves

1 INTRODUCTION

I would like to thank the International Society for Soil Mechanics and Geotechnical Engineering (ISSMGE) and its Technical Committee 209 on Offshore Geotechnics for inviting me to present the 7th McClelland Lecture. This is truly a great honour and a landmark event in my career.

Although having never worked with Mr. McClelland, I have had the privilege to work closely with all previous six ISSMGE McClelland lecturers as mentors, educators, and colleagues on projects or as part of industry committees on codes and standards. The first course dedicated to offshore geotechnics that I took in 1990 during my graduate studies at Texas A&M University was taught by J. D. Murff, the inaugural Lecturer. It was A. Young, the 4th Lecturer, and me who met with Mr. McClelland's widow in 2010 to ask her permission to use the "McClelland" name for this Honor Lecture series. Every interaction with every Lecturer has been a learning experience which I fondly cherish.

The six previous lectures focused on numerical modelling and analytical solutions for offshore foundations, soil laboratory testing and development of design parameters, integrated geoscience studies, physical modelling, and the bearing capacity of foundations from small to medium scale 1-g testing.

Offshore operating companies have access to field performance data that is not always available to consultants, service companies, or members of academia. Therefore, the topic of offshore field performance of full-size foundations, and what can be learned from it emerged as a theme that had not been explored in the Lecture series and for which an original contribution could be made.

This paper documents performance that can only be experienced in the field when full-size design loads are applied to full size foundations, either during installation or operation. These performances represent the ultimate test of industry design practices and often come at a considerable cost to the industry. It is therefore imperative to document them, learn from them, and publish the learnings so that they can be included into our practices to verify and improve our design methodologies. This is the primary purpose that this paper aims to accomplish by sharing these case histories.

The paper also addresses the topic of man-made or anthropogenic geohazards and gives examples of how the offshore seafloor can be affected by human activities.

"Offshore field performance" therefore refers to the performance of the seafloor and seabed under anthropogenic effects and the performance of foundations during installation and operations.

2 ANTHROPOGENIC GEOHAZARDS

2.1 Introduction

One of the first activities undertaken during the early stages of a hydrocarbon or renewable energy offshore project is the identification of geohazards, which are typically divided in two broad categories: natural geohazards occurring through geological, hydrological, and other environmental processes and anthropogenic geohazards which result from human activities.

Natural geohazards are the primary concern and represent almost the totality of the published literature. They include earthquakes, liquefaction, slope stability, debris flow propagation, hurricane-induced seafloor instability, fault movement, mud volcanoes, rapid sedimentation, gas and fluid expulsion features including pockmarks, authigenic hard ground, and gas hydrate dissolution.

Anthropogenic geohazards are also addressed in the literature with assessments of whether drilling, installation or operational activities can negatively impact, and potentially destabilize, the seabed. However, very few examples of anthropogenically-triggered events have been published where such events have occurred in the (deepwater) offshore environment.

Two marine seafloor instabilities caused in part by human activities famously include the 1979 Nice, France, harbour disaster where the triggers included loads induced by the harbour expansion and the construction of an embankment (Dan et al., 2007) and the 1994 Skagway, Alaska, harbour underwater slide which formed during the collapse of a cruise ship wharf undergoing construction at the head of Taiya Inlet (Kulikov et al., 1996). However, for both events, although the seafloor instability propagated offshore, the anthropogenic trigger occurred at the shoreline above the water level.

The paper first gives examples of seafloor alterations caused by drilling activities and deposition of drill cuttings and cement and then describes two case histories of deepwater seafloor instabilities with anthropogenic triggers.

2.2 Anthropogenic seafloor sediment changes

2.2.1 Top-hole drilling

When a deepwater well is spudded, the seafloor conductor is typically jetted. Then the first casing section is drilled and cemented without a BOP and a marine riser in place. The drilling mud and drill cuttings up to this point are returned to the seafloor, spilled over from the wellhead, and deposited around

the wellhead. This operation is known as “open-hole” or “top-hole” drilling with, in some cases, mud “pump and dump” techniques used to control slight formation overpressures. A typical open-hole deepwater subsea wellhead system is shown on Figure 1.

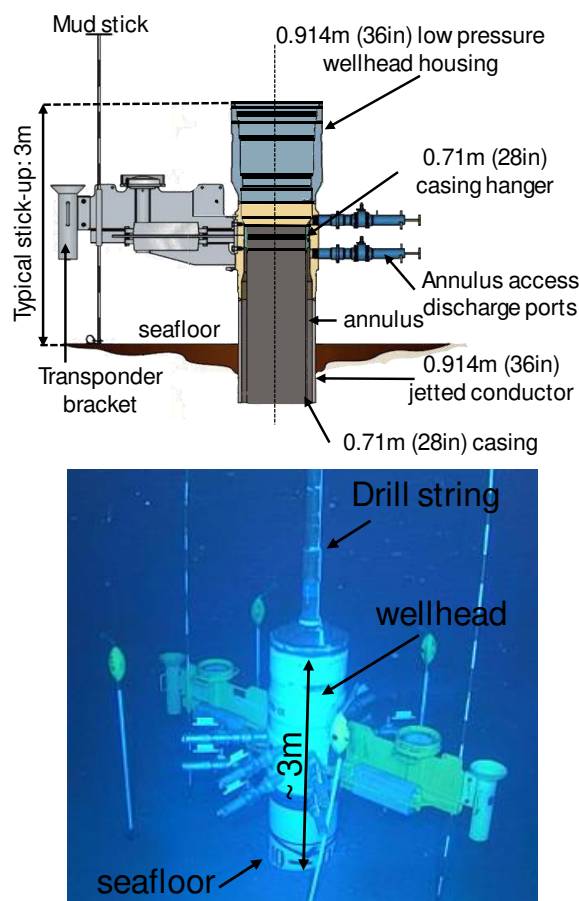


Figure 1 top) sketch and bottom) ROV view of typical deepwater open-hole wellhead system.

An ROV view of pump and dump drilling operations with cuttings flowing over the wellhead onto the seafloor is given in Figure 2.

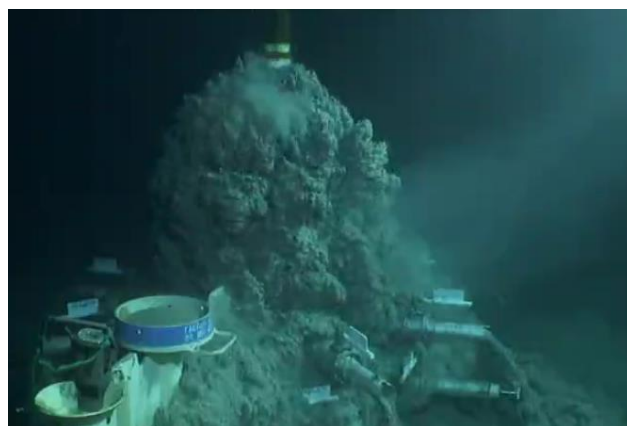


Figure 2 Typical “pump and dump” open-hole drilling operations with drill cuttings return to seafloor.

When the first casing string is cemented, the annulus between the casing and the soil or conductor is overfilled to ensure annular cement full coverage. Returns to the seafloor are monitored by ROV seeing cement flowing from the ports and spilling across the seafloor, forming a crust (Figure 3).

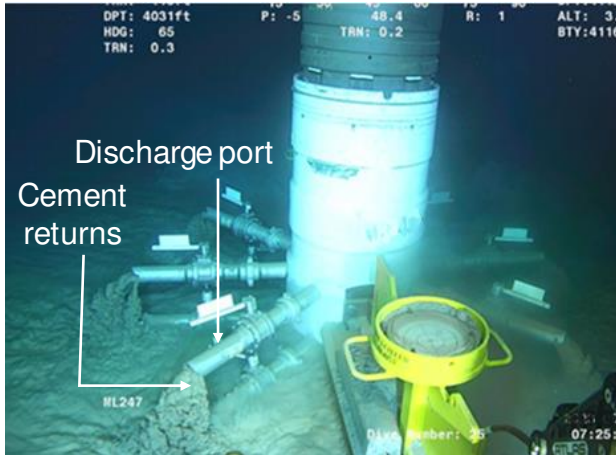


Figure 3 Typical cement return monitoring with ROV.

Top-hole drilling challenges include encountering reactive formations where the natural clay reacts with the drilling mud and swells, causing the formation of “gumbo”, a soft, sticky, mass resulting from cuttings agglomeration. This is known as a “gumbo attack”. This gumbo can clog the discharge ports, stick to the drill pipe and exit the well through the top of the wellhead in a blocky mass on the seafloor in greater volume and height than normal (Figure 4).

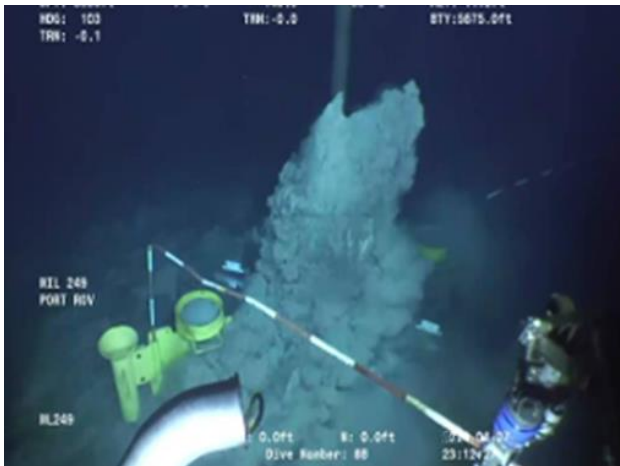


Figure 4 Example of “gumbo attack” being extruded through the top of the wellhead and piling up on top and around it.

2.2.2 Geophysical characterisation of cuttings

Because cuttings and cement present a hazard to the installation of subsea structures, their areal extent and thickness need to be understood. They are typically

mapped using an AUV equipped with a multibeam echosounder (MBES), side-scan sonar (SSS), and sub-bottom profiler (SBP). The areal extent can be determined from MBE backscatter data, SSS reflectivity, and by changes in bathymetry between the pre and post drilling seafloor. SBP records can also be used to provide cutting thickness.

In the example in Figure 5, the drill cuttings were deposited as far as 200m from the nearest wellhead, and their maximum thickness exceeded 3m close to some of the wellheads.

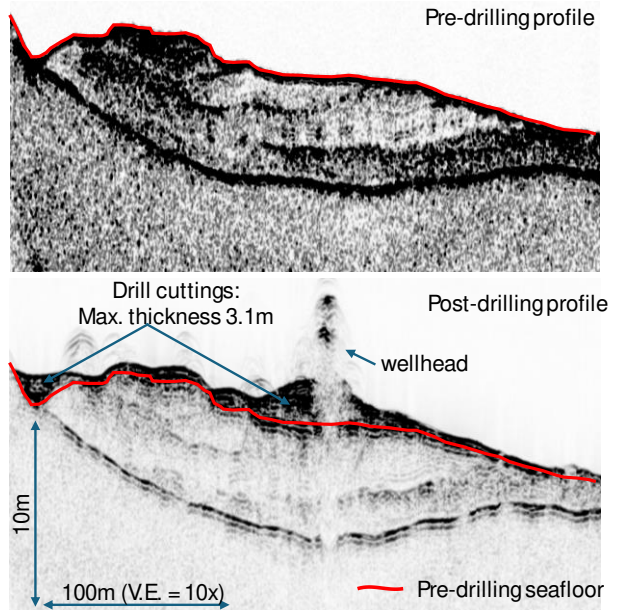
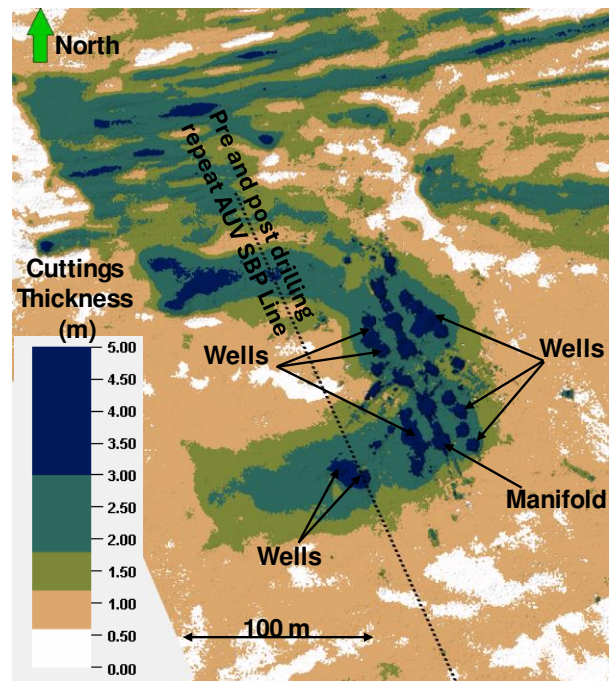


Figure 5 top) Example of drill cutting contours obtained from repeat pre- and post-drilling bathymetry surveys and bottom) Example of repeat AUV SBP records showing drill cutting thickness at multi-well drill center.

2.2.3 Geotechnical characterisation of cuttings

Once the extent and thickness of the drill cuttings have been established, a geotechnical site investigation can be performed, if further quantification of the risk to subsea foundation is warranted.

Depending on the cement content, cuttings can be tested in-situ with mini CPT, or mini T-bar tools, and sampled with piston cores for laboratory testing. Cement-rich cuttings can be sampled via rotary coring, hydraulic breaker (e.g. jack hammers) circular saws or diamond saws.

Three types of cuttings are typically encountered: drill-mud-rich uncemented cuttings, very weakly cemented cuttings, and cement-rich hard cuttings. Their typical geotechnical properties are now described.

2.2.3.1 Uncemented cuttings

Uncemented cuttings are usually made of natural clay materials mixed with drilling mud (e.g. bentonite, barite) and do not contain cement. Their texture can easily be identified in cores and their strength can be lower than that of the natural seabed (Figure 6).

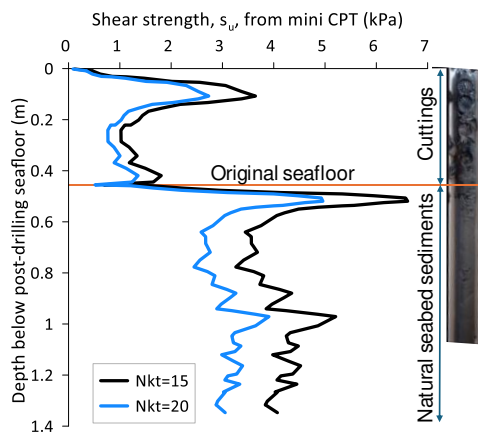


Figure 6 Example of shear strength measurement in uncemented drilling mud-rich drill cuttings.

Such cuttings do not represent a hazard for the installation of skirted foundations but can have an impact on the sliding capacity of the foundation. For example, if the length of the foundation skirt was 0.4m and the foundation was installed at the site where the strength profile of Figure 6 was measured, the shear strength at the skirt tip would be about 1kPa instead of about 3kPa if the cuttings were not present. The presence of cuttings would therefore reduce the sliding resistance by a factor of about three.

2.2.3.2 Very weakly cemented cuttings

The second type of material encountered consists of very-weakly to weakly cemented cuttings with

typical cone resistances less than 4MPa. This type of material can be broken apart by hand with little effort and tends to occur as plates of typical thicknesses of 0.1m on top of, or embedded into, uncemented cuttings. Figure 7 presents shear strength profiles derived from mini-CPT testing in locations where the cuttings were present and absent. It shows that these very weakly cemented materials can be up to 1.5m thick with shear strength in excess of 100kPa. They can pose a hazard to the installation of skirted foundations by preventing the skirts from penetrating to their design depths and by causing non-uniform embedment across the footprint of the foundation, resulting in foundation inclinations above allowable limits.

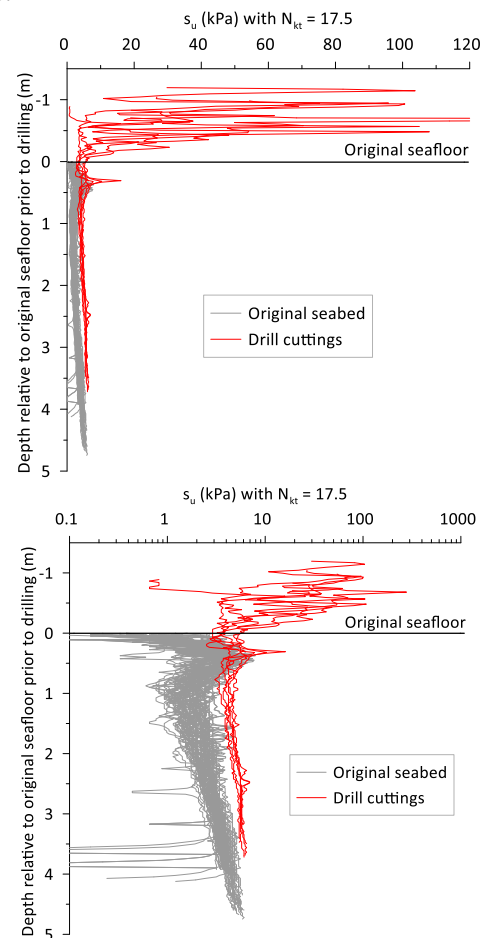


Figure 7 Example of shear strength measurements in very weakly cemented drill cuttings top) linear scale and bottom) logarithmic scale.

2.2.3.3 Cemented cuttings

A third type of sediment encountered consists of cemented cuttings with typical cone resistances greater than 4MPa. This type of material requires significant energy to be broken apart. The amount of cement in these materials can vary highly and reach up to 100%. Figure 8 shows an example of mini-CPT

refusal in such a material which was also rotary-cored to determine that its total thickness was about 0.11m.

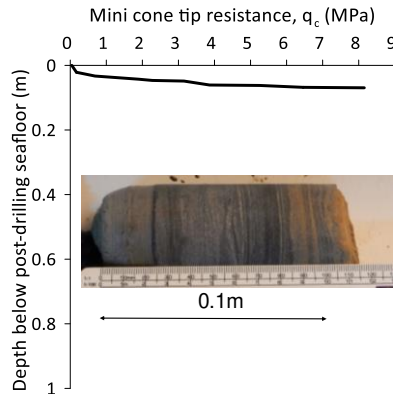


Figure 8 Example of mini-CPT record refusing in cemented cuttings about 0.11m thick.

These cemented blocks can also be recovered from the seafloor using an ROV and tested in the laboratory to measure the maximum pressure that is required to break them. Figure 9 shows a test where a loading bar intended to model the tip of a shallow foundation skirt is progressively loaded up to the point where the cemented block breaks.

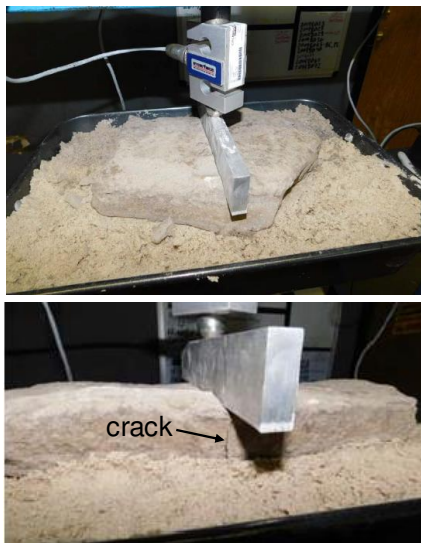


Figure 9 Testing of 50mm-thick cemented cutting block with loading bar: top) test set-up; bottom) crack in block at 2mm vertical displacement.

The recorded pressure, calculated as the applied force divided by the contact area between the bar and the sample, as a function of vertical displacement, shows that the cemented block behaved in a brittle way and broke at a mobilized vertical displacement of only 1.4mm and for an applied pressure of 505kPa (Figure 10). The pressure immediately decreased to 200kPa with further displacement of up to 6mm.

By comparing the required pressure to break the cement block with the actual pressure on the

foundation skirt during installation, the likelihood of skirt refusal in the cement can be estimated.

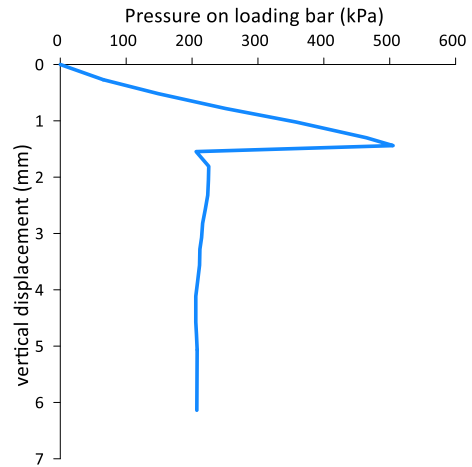


Figure 10 pressure-displacement curve on block of cemented cutting.

2.3 Anthropogenic seafloor instabilities

2.3.1 Drilling-triggered instability

A case history is first presented for which, during deepwater well top-hole drilling operations, the cuttings and cement accumulated to such a height and extent that they became unstable and triggered a seafloor instability. The areal extent of the resulting debris flow was mapped using MBES backscatter data (Figure 11).

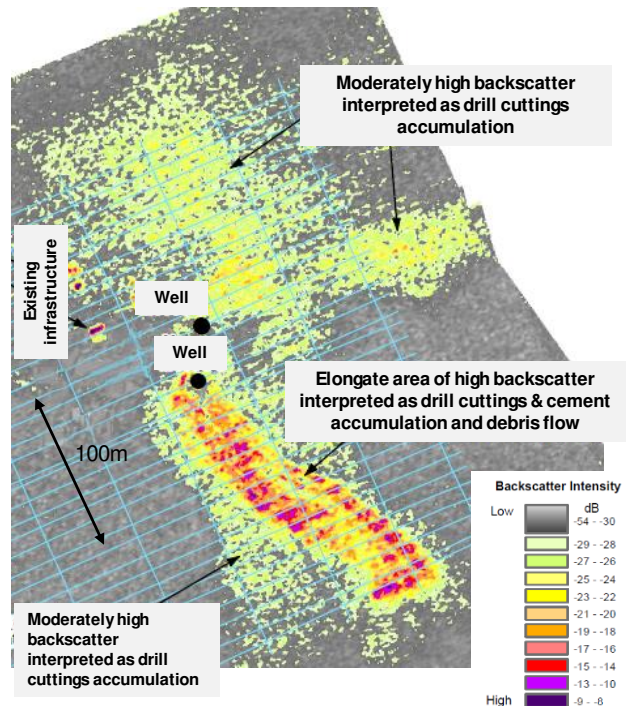


Figure 11 Identification of drill cutting and debris flow using multibeam backscatter

For this well, the 0.914m (36-inch) conductor was jettied and a 0.71m (28-inch) casing was drilled and cemented. Both activities were completed without issues. A 0.66m (26-inch) hole was then advanced during which minor gumbo was seen extruding from the wellhead. Drilling continued and the 0.66m (26-inch) hole reached target depth 12 days after the well had been spudded.

About 13mins after completing the drilling, an ROV observed seafloor instability in progress in the drill cuttings to the south-southwest of the well. The

instability lasted a couple of minutes and generated a debris flow at the seafloor.

Cutting thickness contours around the wells and within the debris flow are shown on Figure 12. After the event, the cuttings were 1.7m thick near the wellhead. They ran out about 260m on slopes with angles up to 8deg locally. The cuttings were imaged with AUV backscatter, SSS, and also with sub-bottom profiler data but only when they were thicker than 0.1m.

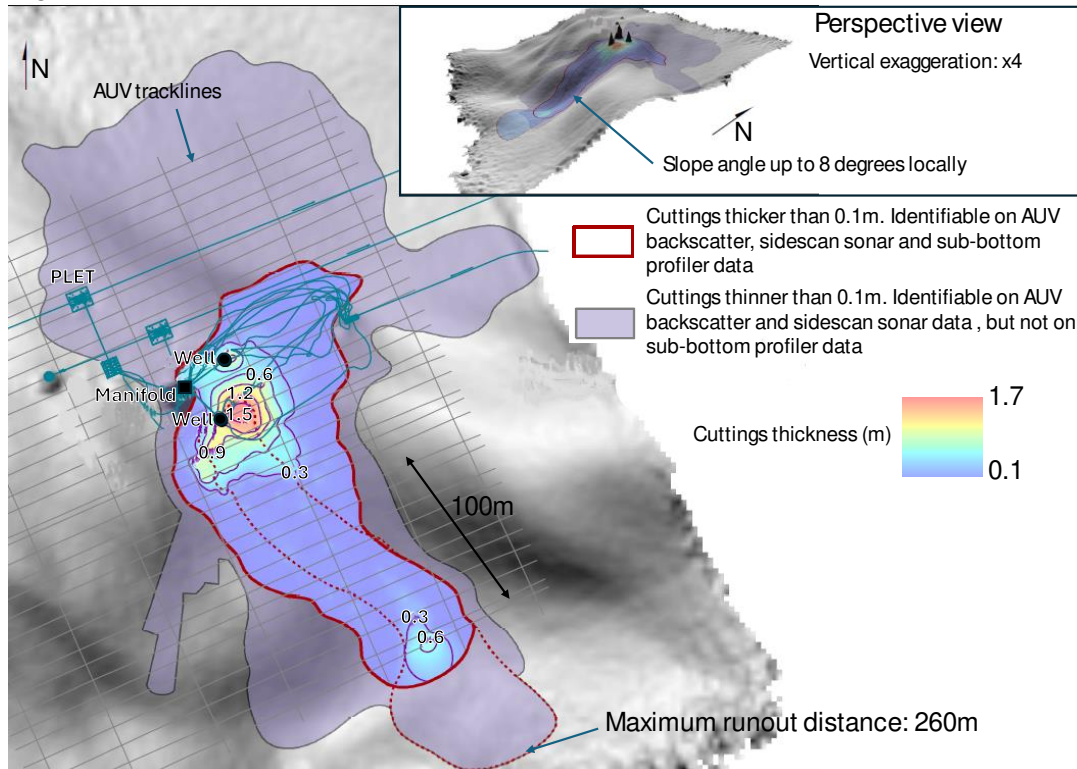


Figure 12 Areal extent and thickness of drill cuttings debris flow after occurrence of seafloor instability

This seafloor instability was caused by the accumulation of drill cuttings which overloaded the seafloor upslope very near an 8-degree slope. ROV-captured videos suggest the cuttings were up to 2.5m thick near the wellhead prior to the event.

Images of the seabed prior to jetting the conductor suggests the seabed already contained some amount of both cuttings and cement from neighbouring offset well(s) and this layer may have acted as a decollement layer which led to seabed instability after sediment loading.

2.3.2 Dragging-triggered seafloor instabilities

For this second case history, a deepwater seafloor area was recently imaged with AUV multibeam bathymetry data. The area includes an escarpment with numerous gullies, channels, and debris flows incising the seabed, as is commonly encountered at GoM deepwater sites.

An unusually linear, almost perfectly straight, scar feature was also identified running NNW-SSE. It was mapped for 4.3km across the site but clearly extends beyond the survey boundaries and its total length is unknown (Figure 13).

The headscarp of two recent-looking primary and secondary debris flows appear to coincide precisely with the scar feature suggesting that the debris flows may have been triggered as a result of the scar formation.

It is challenging to identify a natural geological process that could form such a long straight scar feature, thereby suggesting that the trigger is potentially anthropogenic in nature.

The debris flows depositional lobes are well imaged with AUV SSS mosaic and MBES backscatter data (Figure 14). These data show a clear contrast between a) the surrounding seafloor and the other gullies to the North and b) the inside of the

debris flows. In addition, no seafloor drape could be imaged in the SBP sections through the debris flow. These facts support the hypothesis that these flows are younger than the surrounding seafloor features.

At the headscarp, the local seafloor slope on the promontory is up to 25deg (Figure 15). A series of bathymetric cross sections across the linear scar are shown on Figure 16 and indicates a depth ranging from 0.5m to 3.1m and a width between 3.0m and 13.1m within the surveyed portion of the feature.

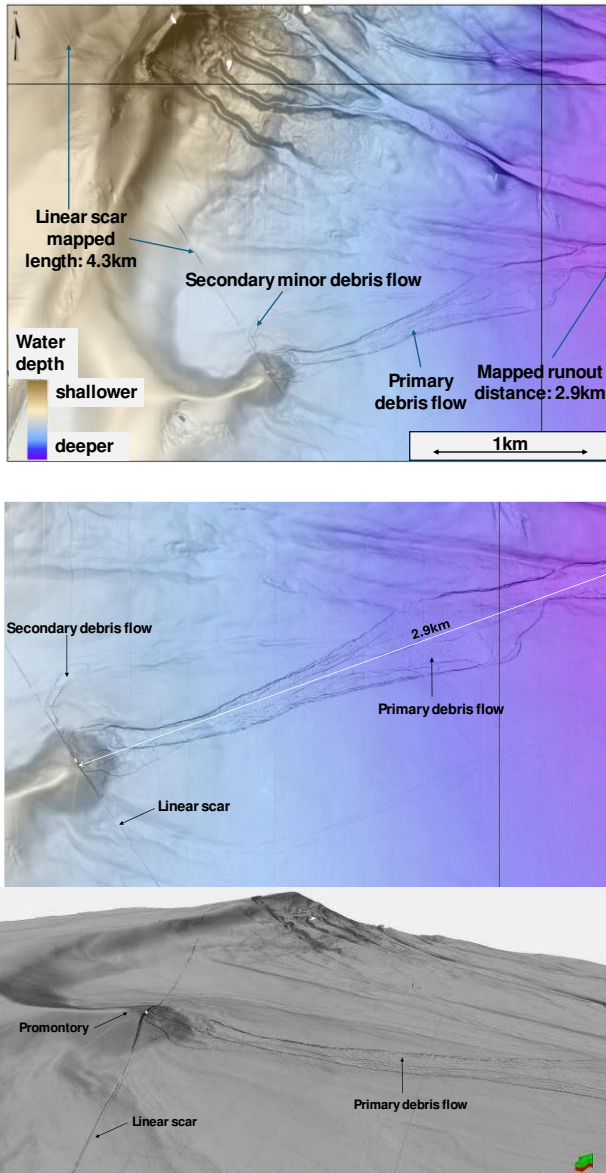


Figure 13 Seafloor rendering of deepwater area with suspected anthropogenically triggered seafloor instabilities. top) general view, middle) zoom on promontory and debris flows, bottom) perspective view.

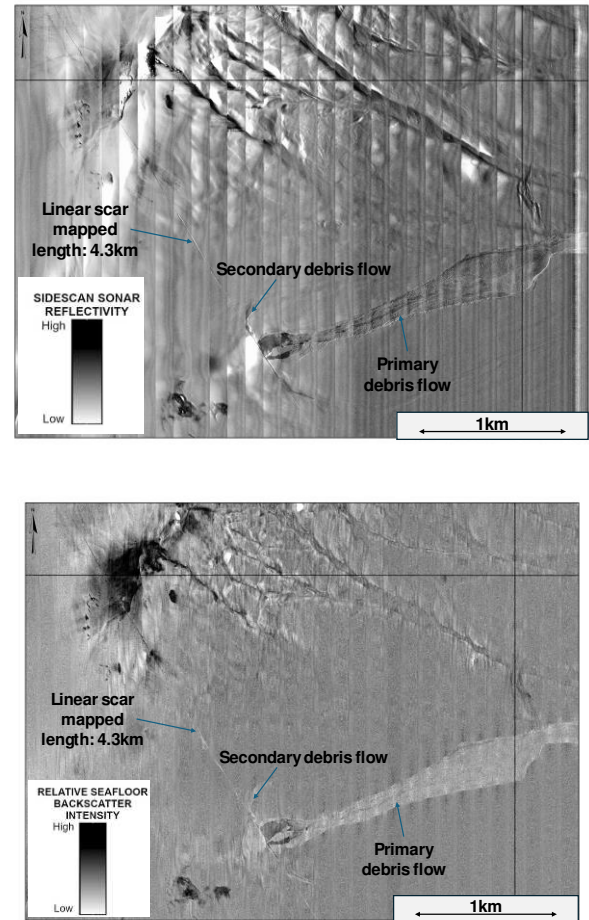


Figure 14 Imaging of anthropogenically triggered seafloor instabilities with top) SSS mosaic and bottom) MBES backscatter data.

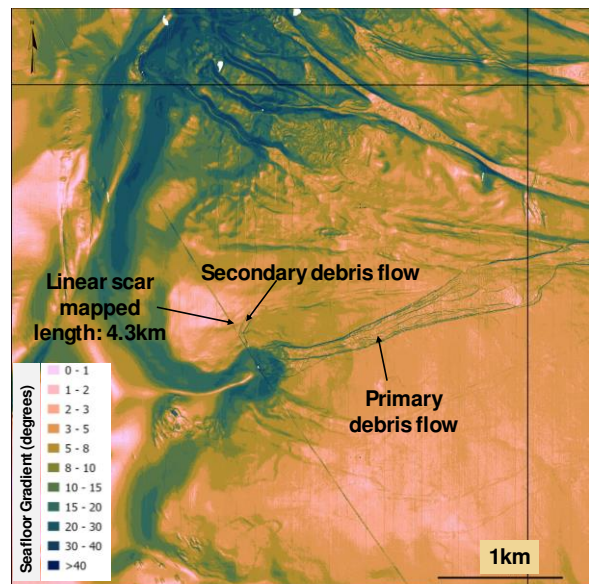


Figure 15 Seafloor gradient of area from AUV MBES bathymetry data.

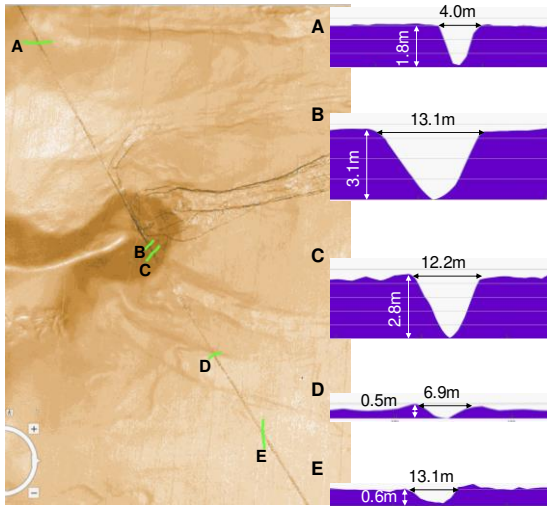


Figure 16 Bathymetric cross-sections of the linear scar feature.

Low-resolution bathymetry data obtained from a 3D seismic survey in 2001 are also available. Although these data provide fewer details of the seafloor features than the AUV MBES data, they strongly suggest, albeit not conclusively, that the two debris flows were not present in 2001, making them less than 24 years old.

The list of potential activities that could generate such a linear feature includes:

- The laying of a cable or fiber optic line,
- The dragging of a survey sled during a deep-tow geophysical survey,
- The dragging of a pipeline bundle sled during a bottom-towed installation,
- The dragging of a drilling rig anchor after the rig broke its mooring, lost position, and drifted during a hurricane.

These activities were assessed as follows:

- No records of a cable or fiber optic line being laid in the area could be located and the scar is too wide and too deep to be a cable.
- No records of a deep-tow survey, which had become rare in the GoM after 2001, in the area could be located and the scar is again too wide and too deep to be made by a towed sled.
- In the GoM, between 1985 and 2005, 14 pipelines were installed by towing from a beach in the Matagorda peninsula to offshore platforms along a well-established and documented route (Brown, 2006). This route is located well outside the area of interest and no available record of a towed pipeline installation that could have caused the linear scar could be found.
- An anchor drag mark left by a rig which was drifting during a hurricane is a possible trigger. It is challenging to positively confirm or rule out this trigger as the performances of MODUs

during hurricanes are not always sufficiently documented (see Section 5.1. of this paper).

Therefore, although the precise trigger for the two recent debris flows cannot be conclusively established, it is believed that it was anthropogenic and associated with the dragging of an object on the seafloor which caused a scar feature and destabilised soft clay sediments on the seafloor at a location where the natural slope was at a relatively high angle.

2.4 Learnings

The above case histories document the performance of the seafloor under anthropogenic activities and demonstrate that seafloor instabilities in deepwater can and have been triggered by dragging objects on the seafloor. They also show that drilling activities can affect the seafloor and the top few meters of the seabed in profound ways by depositing mixtures of natural clays, drilling mud (e.g. barite, bentonite) and cement in highly varying proportions, thereby creating heterogeneous deposits where they would be otherwise unexpected.

At the sites described, the thickness of cuttings was up to 3m with shear strengths ranging from 1kPa to over 500kPa. These test results give quantitative data which can be used to assess the likelihood of complete or partial shallow foundation skirts refusal in drilling cuttings and cement (Figure 17).



Figure 17 Example of uneven shallow foundation skirt partial penetration due to the presence of drill cuttings.

These drilling deposits can become unstable and generate debris flows with runout distance of several hundreds of meters. This hazard should be recognized when finalising the location of subsea equipment on the seafloor if slope angles exceed a nominal value of 5deg.

This industry experience emphasizes the need to understand the areal extent and geotechnical properties of the seabed which may have been affected by riserless top hole drilling activities after the geotechnical site investigation used to derive foundation design parameters was performed. This

understanding should be developed well in advance of installation activities to avoid surprises and potentially costly remediation in the field, post foundation installation.

These learnings from the Oil & Gas industry are also applicable to carbon capture projects if, for example, they include offshore wells used to re-inject and store CO₂ into aquifers or depleted reservoirs. They also have applications to offshore wind field activities such as the installation of anchors and the laying of cables since those can also potentially destabilize the seafloor.

3 THE VALHALL PILE REFUSAL EVENT

During the life of a project, the next field activity relevant to geotechnics is the installation of the foundation system. The paper now documents a case history where piles were driven into very dense sands and buckled prior to reaching their design depths.

The companies involved in the event, either during the initial design, the refusal investigation, or the pile remediation, include in alphabetical order: Aker Maritime, Aker Kvaerner, Aker Stord, Advanced Geomechanics, Arup Energy, BP Amoco, Det norsk Veritas (DnV), Fugro Ltd, GCG, Geo Survey AS, Heerema Marine Contractors, Imperial College, Norwegian Geotechnical Institute (NGI), Norwegian University of Science and Technology (NTNU), Rowan Drilling Inc., Seacore Ltd., Sintef, Saipem, the University of Western Australia (UWA) and individual consultants. Their contributions are acknowledged globally but it was not possible to credit the contribution of each party separately.

3.1 History of Valhall field development

The Valhall field is found in a water depth of about 75m in Block 2/8 in the southern part of the Norwegian Sector of the North Sea (Figure 18). The first three platforms of the Valhall complex, the Quarters Platform (QP), the Drilling Platform (DP), and the Production Compression Platform (PCP) were installed in 1982. Subsequent additions include the Wellhead Platform (WP) installed in 1996, the Injection Platform (IP) installed in 2002, and the Production and Hotel Platform (PH) installed in 2009 (Figure 19).

The paper discusses the pile refusal events that occurred during the installation of the IP jacket in 2002.

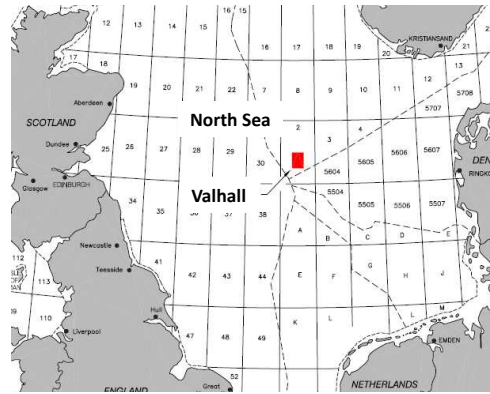


Figure 18 Location of the Valhall field



Figure 19 The Valhall complex, circa late 2000's

3.2 Site geology

The description of the geology at the site focuses on the foundation zone, taken as the top 100 m below seafloor (BSF). The sediments were deposited during the Quaternary period and affected by multiple glaciations. The ice sheet during both the last glaciation (Weichselian; 10,000–115,000 years B.P.) and the penultimate one (Saalian; 130,000–200,000 years B.P.) covered the Valhall area (Figure 20). During the Weichselian maximum, the thickness of the ice was around 150m to 200m while the Saalian ice sheet thickness in the area was at least 1,000m.

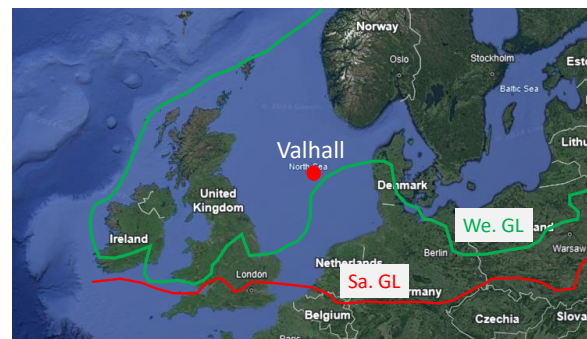


Figure 20 The last two glaciations at the Valhall field: We.Gl. = Weichselian Glacial Maximum (28-22kyears) extent of the Fennoscandian, UK and western Barents Sea ice sheets, (Sejrup et al., 2000). Sa.Gl. = Southern extension of the Saalian Glacial Maximum (130 – 200kyears) (Andersen and Borns, 1994).

The geology can be described with reference to four commonly encountered formations of the North Sea UK sector: the Forth, Fisher, Ling Bank, and Aberdeen Ground formations, although the latter typically occurs below 108m at Valhall (Table 1).

Table 1 Representative geological formations at the Valhall field within the foundation zone

Depth (m)	Formation	Sediment Description
0-19	Forth	Dense to very dense fine to medium sand with shells. Buried boulders and gravel lenses can occur.
19-26	Fisher	Hard, occasionally very hard, very silty clay with pockets and partings of silt
26-32	Fisher	Very dense, slightly silty, fine to medium sand
32-41	Fisher	Hard to very hard silty clay with occasional silt partings and thin layers of very dense sand
41-48	Intra Fisher	Very dense, slightly silty, fine sand with occasional shell fragments and occasional thin layers of clay at top
48-56	Intra Fisher	Interbedded layers of hard, slightly sandy, very silty clay and very dense, slightly silty, fine to medium sand
56-83	Ling Bank	Predominantly very hard very silty clay with lenses of silt and occasional very dense sand layers towards the base
83-108	Ling Bank	Predominantly very dense fine to medium sand with occasional thick layers of very hard, very silty clay
>108	Aberdeen Ground	Very dense fine to medium sand and very hard, silty clay

3.2.1 The Forth Formation

This formation of late Weichselian to Holocene age comprises dense to very dense fine sands (Whitethorn Member) to about 19m BSF. Buried boulders and gravel lenses can occur within this formation. In the Valhall area, the Forth Formation can be divided into two units; an upper cross stratified

unit (0-9m) and a less well-structured lower unit (9m to 19m BSF).

In the Valhall area, the presence of Forth Formation sediments resting directly on the much older Fisher deposits records a significant gap in the stratigraphic record of around 100,000 years, with sediments of Eemian to Weichselian age missing. The absence of Coal Pit deposits in the Valhall area is the result of non-deposition, or removal by later erosion, or a combination of the two.

3.2.2 The Fisher Formation

The Fisher Formation consists of a mixed sequence of sands and clays that are thought to have been deposited in a glaciomarine environment during the Saalian glaciation. The sands were probably deposited in a high energy shallow marine setting while the clays represent deposition from suspension during quieter conditions. Coarse cobble sized material found within both the sands and clays probably represent glacial sediments brought into the area by ice and deposited as either dropstones from melting ice or from the base of the ice as moraine.

The Fisher Formation lies below the upper sands of the Forth formation and comprises reasonably uniform sediments of hard to very hard very silty clays and very dense, slightly silty, fine to medium sands. It is present between the depths of 19m and 56m on average at the site.

3.2.3 The Ling Bank Formation

The upper Ling Bank Formation consists of reasonably uniform sediments of predominantly very hard, very silty, clay with lenses of silt and occasional very dense sand layers to 83m BSF. Below this, lie channel infill sediments predominantly comprising very dense fine to medium sand with occasional thick layers of very hard, very silty clay. At Valhall, the base of this unit at 108m BSF is marked by a major erosion surface.

3.3 Soil properties for the original design of the IP piles

The original 1978 site investigation for the design of the piles of the QP, DP, and PCP platforms consisted of three 78m deep geotechnical boreholes comprising sampling and CPT. The force available to push sample tubes or CPT rods into the ground was far less than it is today in modern site investigations. The lower force resulted in shorter recovered samples and shorter CPT pushes, the latter being at a maximum cone tip resistance typically between 35MPa and 45MPa.

Another main difference is that the drill string would not have been held stationary, which can affect sample quality, although not to a great extent in very hard soils. This can also affect estimated CPT penetrations since the drill string could move upwards during CPT pushes. If this happened the cone penetration, assumed to equal the cone rod extension out of the bottom of the drill string could be over-estimated. The CPT tip resistances measured in Boreholes B1, B2/2B, and B3 are shown in (Figure 21). Most CPT pushes refused in the sand layers and the maximum recorded values are not representative of the true in-situ values.

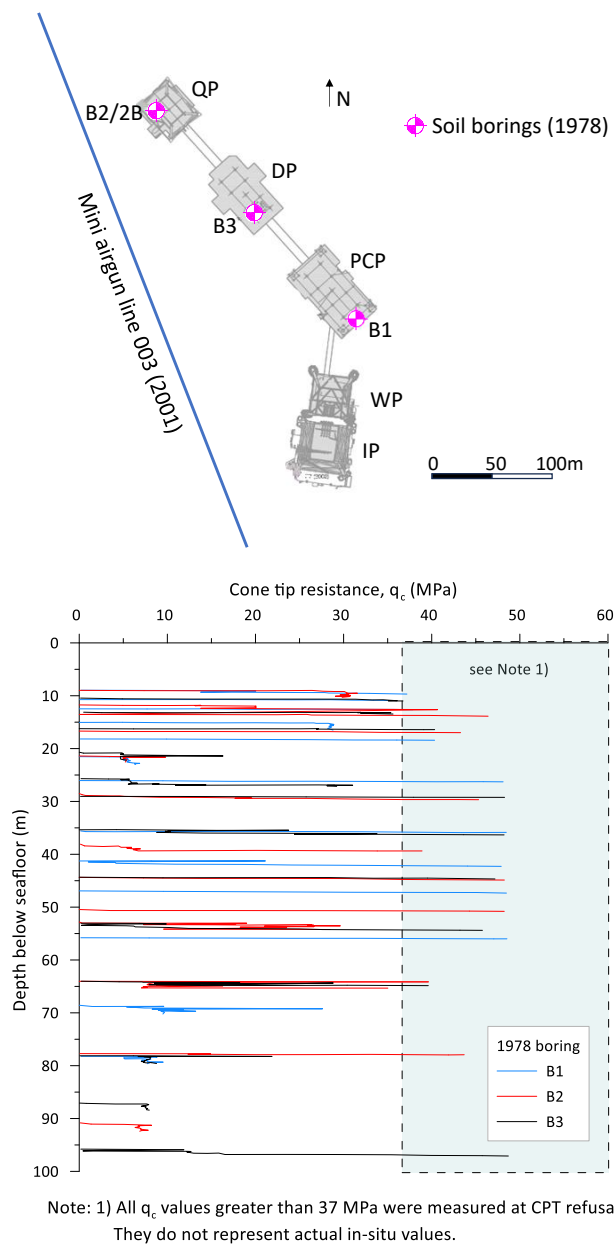


Figure 21 Base map and CPT records of the 1978 site investigation. Data also used for the original design of the WP and IP piles

The samples in clays were short (less than 0.5m) and their shear strength was measured using UU triaxial tests. PSD curves in the sand samples indicated no clay and little silts. Only two tests noted silt content greater than 2% and only one registered any clay at all, although fines may have been washed out by the sampling process.

The data of Figure 21 were successfully used in the design and installation of the WP platform piles in 1996, which went according to predictions.

In 2001, a geophysical site survey consisting of eight lines was conducted as close as possible to the QP, DP, and PCP platforms to tie the 1978 borings to the proposed IP platform location, which was not accessible due to the presence of a jack-up rig drilling over the WP platform. The location of the most relevant mini airgun line, Line 003, is shown on Figure 21. This survey was performed to verify that the IP geotechnical conditions were consistent with those of the 1978 boreholes.

Seismic Line 003 is shown on Figure 22 along with the stratigraphy and geological units encountered in the 1978 Boreholes B2 and B3. The results showed continuous beddings across the area of interest and channels were noticeably absent in the Forth formation at the IP location. Therefore the 1978 data were also used in the original design of the IP piles.

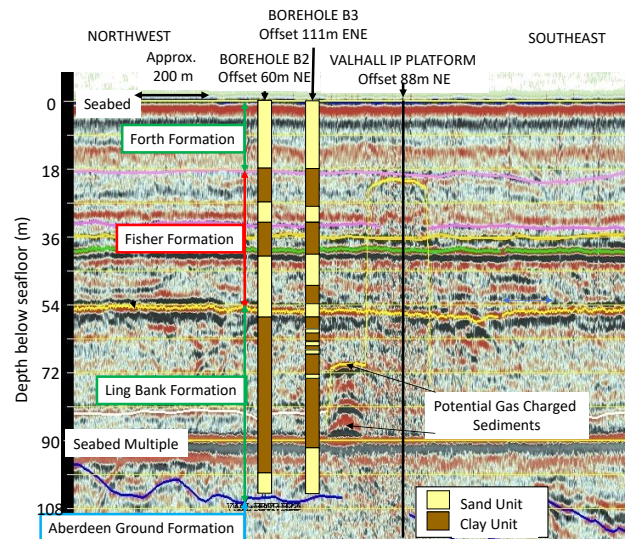


Figure 22 Mini airgun Seismic Line 003 with overlay of stratigraphy at Boreholes B2 and B3

The soil parameters used on the original IP pile design were mainly influenced by the results of Borehole B3 and are shown on Figure 23. The piles were designed using the API RP2A (1993) methods for both clay and sand units, i.e. the CPT data were used to estimate the sand relative density but were not used explicitly when calculating pile axial capacity.

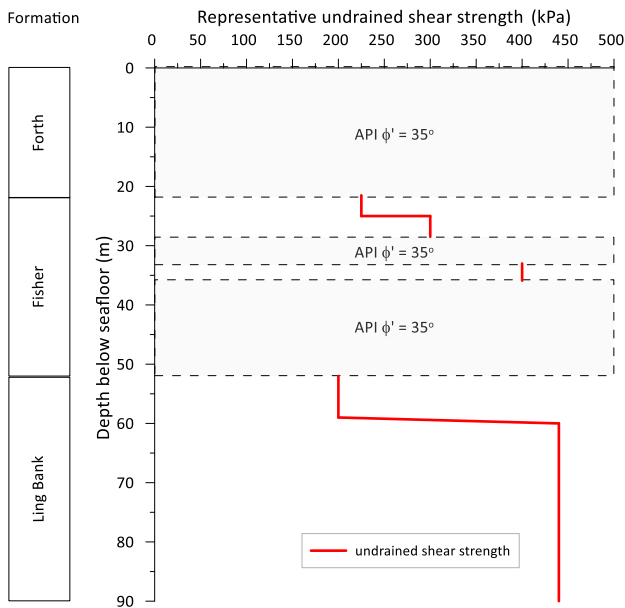


Figure 23 1978 soil properties used in the initial design of the IP platform piles

3.4 Original IP pile driving prediction

The original pile driving predictions were performed using the Alm and Hamre (1998, 2001) method. In principle, the soil layering of Figure 23 was used but the soil strength parameters were adjusted to match the recorded driving data at the neighbouring WP platform, as per Figure 24. The CPT resistance had to be increased to 95MPa from recorded values less than 40MPa in the Forth formation to calibrate the Alm and Hamre method and match the WP records. The measured Soil Resistance to Driving (SRD) for the WP piles and the original predictions for the IP piles are shown on Figure 25.

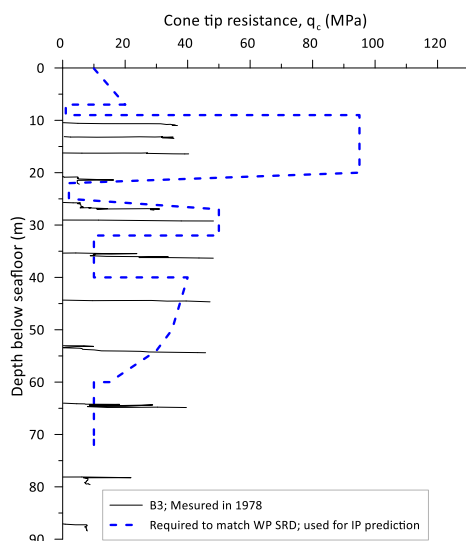


Figure 24 Calibration of the CPT input for the Alm and Hamre SRD calculation method against the WP piles

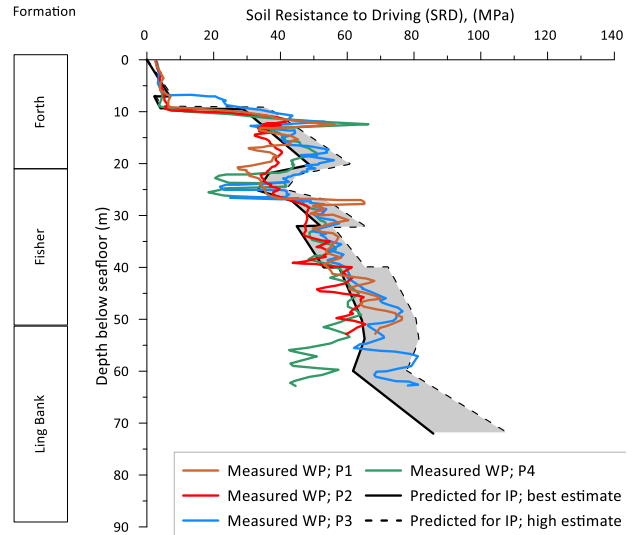


Figure 25 Original SRD prediction for the IP piles, calibrated against WP installation data.

3.5 The IP pile refusal event

The IP piles were driven in August 2002. Five out of the 8 piles refused at depths between 45.25m and 54.25m, which was 13m to 23m short of their target penetration depths (Figure 26). Operations were suspended and the jacket was left without its topsides installed (Figure 27).

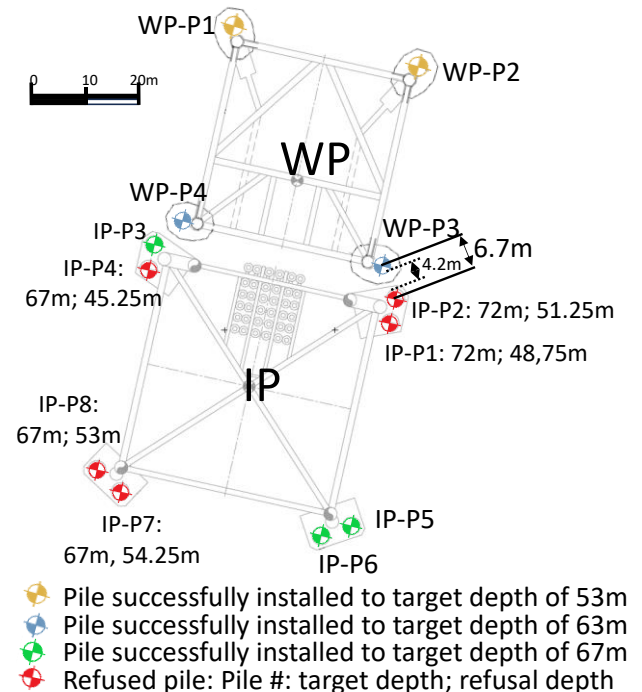


Figure 26 Depth of refusal of IP piles

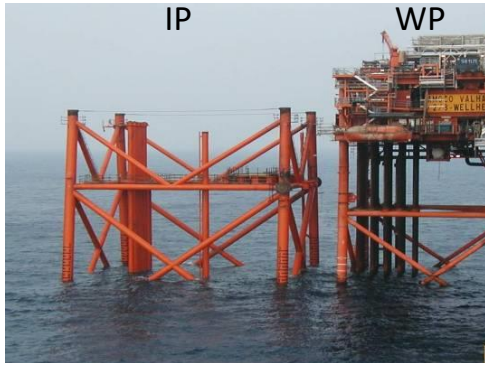


Figure 27 View of IP jacket after suspension of 2002 pile driving activities

3.6 Investigation of the pile refusal event

Two independent panels of world experts in offshore site investigation, pile design, structural design and installation were assembled to investigate the primary causes of the refusal.

The Delphic panel approach was followed with results being shared between panels as the work progressed rather than at the end of the work. Each panel had to consider the conclusions of the other panel, with the intent of reaching consensus. Both panels eventually reached similar conclusions, and their combined and harmonized findings are presented.

3.7 Predicted vs hindcast SRD for IP piles

Each panel independently performed a hindcast of the SRD for the IP jacket piles, based on the recorded pile installation data (e.g. hammer characteristics and recorded blow count). Although the details of the friction and end bearing distribution and the soil dynamic parameters were different between the two groups, these analyses showed similar results.

The actual SRD experienced by the piles was well in excess of the predictions and exceeded 130MN at the depths of refusal (Figure 28). Below the depth of 40m, the SRD of the IP piles was 30MN to 40MN higher than that of the WP piles of same diameter.

Noticeably, IP Piles P1 and P2 experienced a much higher SRD and refused at depths of 48.75m and 51.25m respectively in the lower Fisher formation whereas the WP Pile P3 of same diameter, located less than 10m away, was successfully installed to its target depth of 63m (Figure 29).

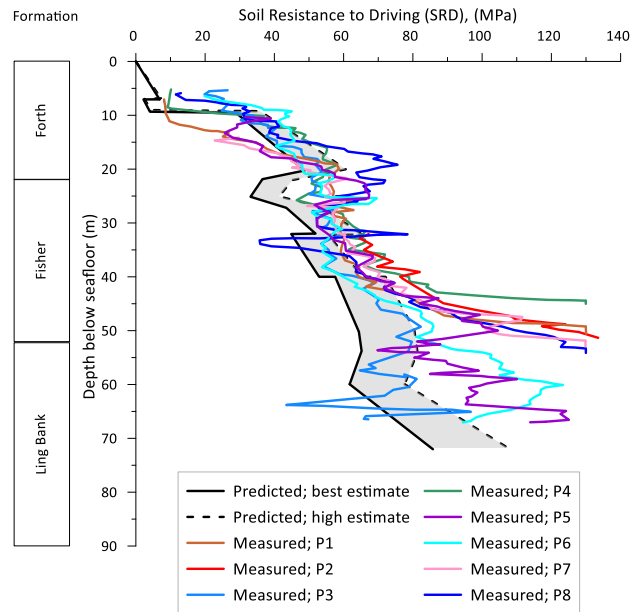


Figure 28 Measured IP pile SRD compared with pre-driving predictions

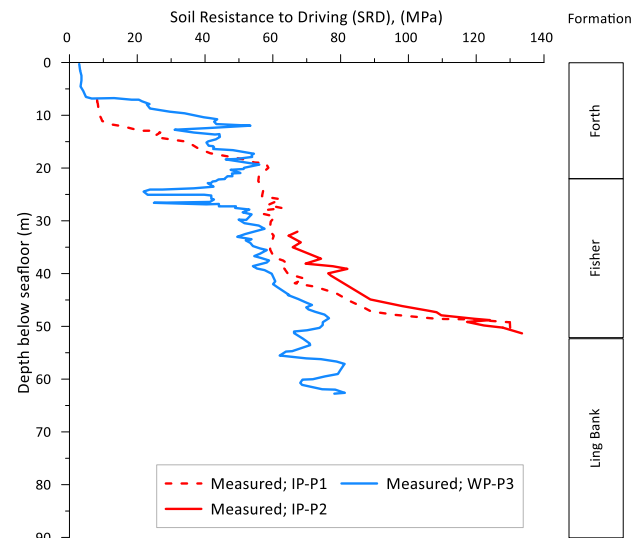


Figure 29 SRD at IP-P1, IP-P2, and WP-P3 pile located less than 10m away

Again, using the Alm and Hamre (2001) method, the CPT profile required to match the SRD at IP had to be significantly increased in the lower Fisher formation (Figure 30). Within the depth interval between 40m and 60m, the CPT values had to be increased by a factor of about three to match the measured SRD (Figure 31).

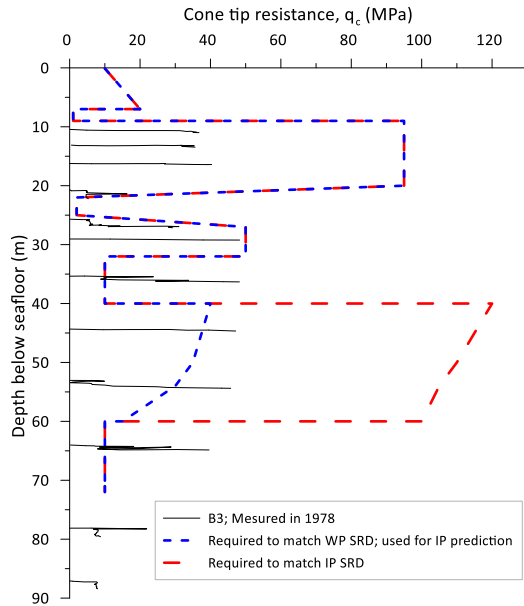


Figure 30 Re-calibration of Alm & Hamre method with increased CPT resistance between 40m and 60m BSF

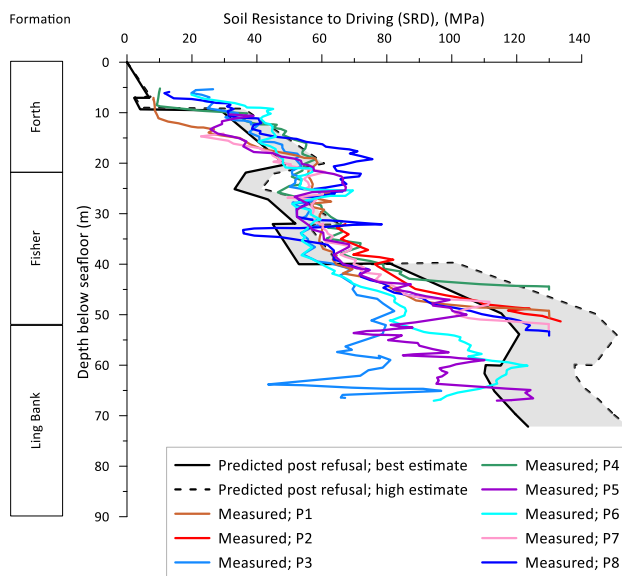


Figure 31 Hindcast of IP pile SRD with increased CPT resistance between 40m and 60m BSF

3.8 Post-refusal site investigation

Investigations and remediation activities started and a drilling jack-up was mobilized to the site. In October 2002, the Rowan Gorilla VII performed three boreholes on the Southwest corner of the IP jacket. Two borings were collected inside refused Pile P7 to 62.15m BSF, inside refused Pile P8 to 51.2m BSF, and one boring, BH3, was collected immediately outside the piles to 62.14m BSF (Figure 32).

The drilling techniques used did not allow for the collection of CPT data and only core and hammer

samples were collected. The core samples used a triple-barrel wireline Geobor S sampler with plastic liners of 102mm internal diameter. Split spoon 75mm hammer samples were also obtained when the Geobor S sampler achieved no recovery.

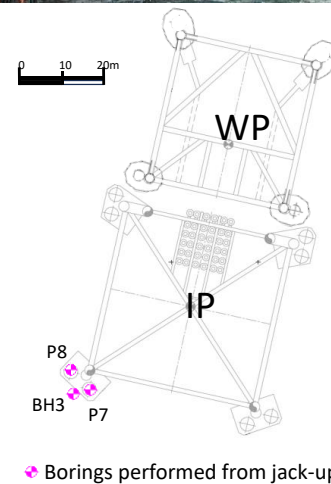


Figure 32 Jack-up-based post-refusal geotechnical site investigation

The stratigraphy from the P7 and P8 borings inside the piles is not presented as it was deemed to have been potentially affected by the driving and buckling of the piles and was therefore unreliable. During the initial driving analysis, the sand layer in the Fisher formation was assumed to extend between 40m and 60m. The findings of BH3 are therefore broadly aligned with these assumptions although the unit starts at 36m BSF (Figure 33).

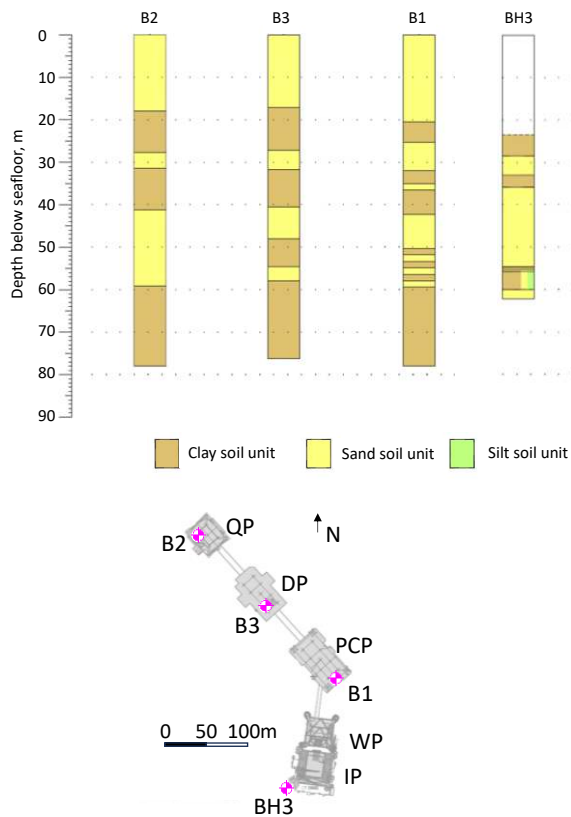


Figure 33 Inferred stratigraphy from Jack-up based post-refusal site investigation

During coring inside Pile P7, a 0.3m long piece of steel was recovered at 57.9m BSF (Figure 34). Prior to the steel being recovered, poor sample recovery had been experienced from 52.15m down to 57.1m. Drilling behavior indicates that the steel was probably pushed from higher in the borehole, from approximately 52.5m. Onshore laboratory metallurgical analyses confirmed the steel came from the pile. This was the first irrefutable evidence that the piles had buckled.

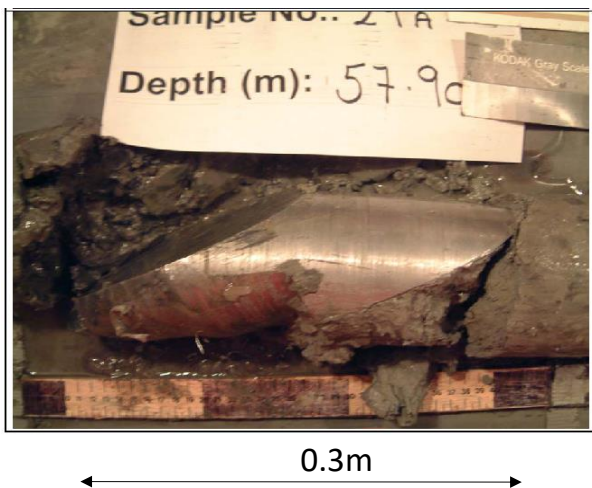


Figure 34 Portion of buckled pile steel wall recovered inside of Pile 7

Upon completion of the boreholes inside Piles P7 and P8, the piles were drilled out using a 2.2m diameter bit and air-lifting the cuttings up the drill string to a side discharge above the water line and subsequently cleaned out. During the drill out operation several very weak mudstone cobbles were recovered between 19m and 32.5m BSF in all three borings in the upper part of the Fisher formation (Figure 35). These clasts were up to 110mm in diameter and their roundness suggests deposition from a high energy fluvial environment.



Figure 35 Cobbles recovered in the drill out activities inside Piles P7 (left) and P8 (right)

A down-hole sonar tool was then used to image the inside of the piles (Figure 36). The sonar imagery indicated that the P7 cross section suffered significant changes starting about 8m above the pile tip and still had 87% of its full cross-sectional area at about 3.6m (1.5D) above the “notional” penetration. The data shows the pile cross section reducing rapidly below this depth so that it is closed off completely by about 1.65m (0.8D) above the notional pile penetration (Figure 37).

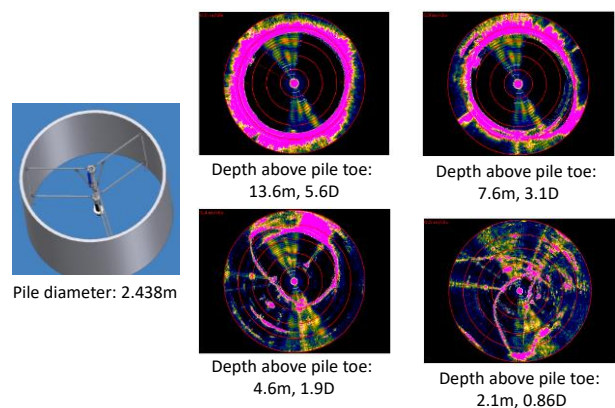


Figure 36 Schematic of downhole sonar with centralizers and measured shape of pile cross-sections at various depths.

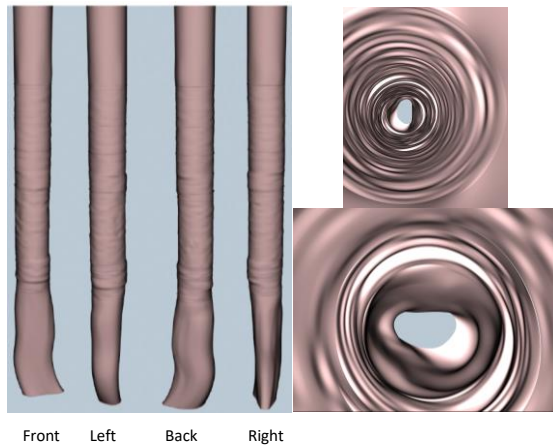


Figure 37 Deformed buckled shape of Pile P7

Pile P8 appears to have maintained essentially full diameter for longer than P7 and may have buckled only over the last 0.5D of its drive such that the last 0.5D of the pile is folded inwards all around (Figure 38). This conclusion was supported by camera image interpretation at the pile tip rather than by sonar measurements.

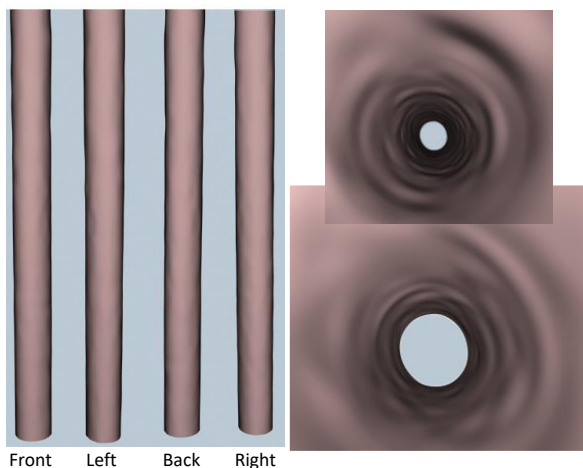


Figure 38 Deformed buckled shape of Pile P8

The key conclusions and observations from the boring program were:

- Confirmation that the piles had buckled by recovery of 0.3m long pile wall section and information on shape of buckles via sonar and camera imaging.
- Unexpected presence of coarse material in the upper Fisher formation between depths of 19m and 32.5m.
- No indication of cemented layers (their presence had been suggested as a cause for the refusal).
- The sands recovered in Borehole BH3 in the middle sequence of the Fisher formation (35.85m and 54.64m) were encountered 5m shallower than expected. The sands were described as very

dense and led to hard drilling conditions between 41m and 52m with extensive drill bit damage.

3.9 Potential causes for refusal and buckling

The key aspects that were investigated as potential causes of the pile refusal include:

- Unusual soil conditions,
- Pile manufacture,
- Pile handling and stabbing,
- Penetration into the seabed,
- Pile design.

3.9.1 Unusual soil conditions

The soils at Valhall were investigated to see if they fell outside the typical range of what should be expected in the North Sea. A database of site investigation in the North Sea (UK, Dutch, Danish, and Norwegian sectors), the Irish Sea, and the West of Shetlands was reviewed.

The measured maximum cone tip resistances, q_c , are summarized in Table 2. The cone resistances at Valhall are not unusual for very dense sand in the North Sea. However, the thickness observed at Valhall was at the high end of those observed in the database. Eighteen sites where q_c exceeded 100MPa were identified in this 2002 database.

Table 2 Summary of measured high cone resistances

Measured q_c values (MPa)	Number of sites
> 75	28
> 90	23
> 100	18
> 110	17
> 120	13
> 140	2

The cobbles present are believed to have contributed to local increases in SRD, but are not believed to have been a key factor in the refusal. Boulders have not been positively identified in the seismic data, perhaps due to the resolution of the data which may have been unable to resolve scattered boulders embedded in hard clays and very dense sands. They were not identified in the three borings and no issues were reported during the installation of conductors in the Valhall field. Although their presence cannot be completely discounted in these glaciogenic sediments, it is unlikely that the refusal of the piles was due to boulders. This view was further supported by the Measured While Drilling (MWD) data from conductor installations at the WP platform.

The refusal event cannot therefore be explained by the presence of unusual sediments.

3.9.2 Pile manufacture

All piles were manufactured within code and contractual tolerance. In particular, the pile ovalities (defined as the difference between the maximum and minimum diameter) were small and well within tolerances. Nevertheless, the pile ovality and its final penetration appear to be correlated (Figure 39). It is of interest that Pile P4 which was dropped to the seafloor during installation was the pile that refused at the shallowest depth. Although Pile P4 was visually inspected on deck after recovery, a small increase in ovality may not have been detected.

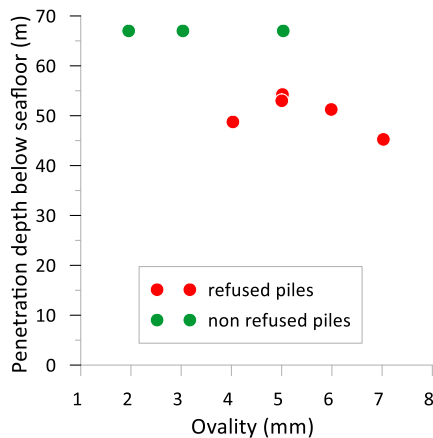


Figure 39 Pile ovality and refused depths

3.9.3 Pile handling and stabbing

Analyses indicated that it is unlikely that the pile tips were damaged during stabbing through the pile sleeve stabbing cones. This would have required the pile tip to hit the cone at a velocity in excess of 1m/s, which is not believed to have happened.

3.9.4 Pile self-weight penetration into the seabed

The pile self-weight penetration seems to be correlated to its final penetration depth (Figure 40). Piles P1 and P4 appear to have hung up within the sleeve above the seabed (i.e. penetrations less than zero). The refused piles are those with the lowest self-weight penetrations into the seabed which could have been the result of tip damage that happened before the piles penetrated the seabed, making the pile end area greater and therefore giving higher resistance to penetration.

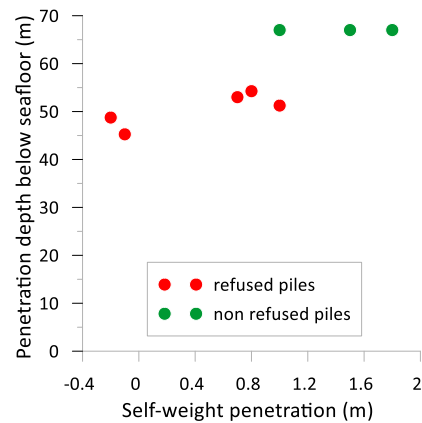


Figure 40 Pile self-weight penetrations and refused depths

The piles were left standing in the sleeves during the passage of a storm. Although this may have caused local yielding, this is not believed to have had any effect on subsequent driving.

Pile design: wall thickness and tip geometry

Table 3 summarizes the pile make up for all pile types installed in the Valhall complex.

Table 3 Summary of Valhall piles dimensions

	QP	DP	PCP	WP	IP original design
Leg No.	4	8	8	4	4
Pile No.	4 main piles 4 skirt piles	8 main piles 16 skirt piles	4 main piles 16 skirt piles	4 skirt piles	8 skirt piles
Diameter	1.4m (54")	1.4m (54")	Main: 1.2m (48"). Skirt: 1.4m (54")	2.438m (96")	2.438m (96")
Penetration (m)	43m to 44m	42m to 43m	42m to 44m except 1 skirt pile to 28m	63m (South piles) & 53m (North Piles)	Target penetration: 72m for pile P1 and P2, 67m for others
Wall thickness	50.8mm	Main: 50.8mm, 63.5mm Skirt: 63.5mm	Main: 50.8, 63.5, and 76.2mm at tip. Skirt: 50.8mm	75mm, 63.5mm, and 50mm at pile tip	9 changes (see Figure 41)
Tip details	Flat tip; 1.52m long, 63.5mm thick driving shoe	Flat tip. driving shoe unknown	Flat tip. driving shoe unknown	Flat tip. Shoe unknown	Steeply chamfered (1 in 4) tip (30mm over 120mm) (Figure 42)

Figure 41 and Figure 42 summarise the wall thickness schedule and tip geometry of the three types of piles used for the IP jacket. Although the IP piles had the same diameter as the WP piles, they had nine wall thickness changes, a much higher number than the three to four changes more typical of North Sea piles and the WP piles. In addition, the IP piles had a steep 76deg external chamfer at the tip whereas the WP piles had a flat tip.

Available material certificates indicate the pile steel to be S420M3Z grade with a design yield stress of 420MPa.

The stepwise reduction of the pile internal diameter in the lower 12m (Type 1) and 10m (Type 2 and 3) is believed to have had a detrimental effect on the pile driving behavior as it may have exacerbated plugging behavior.

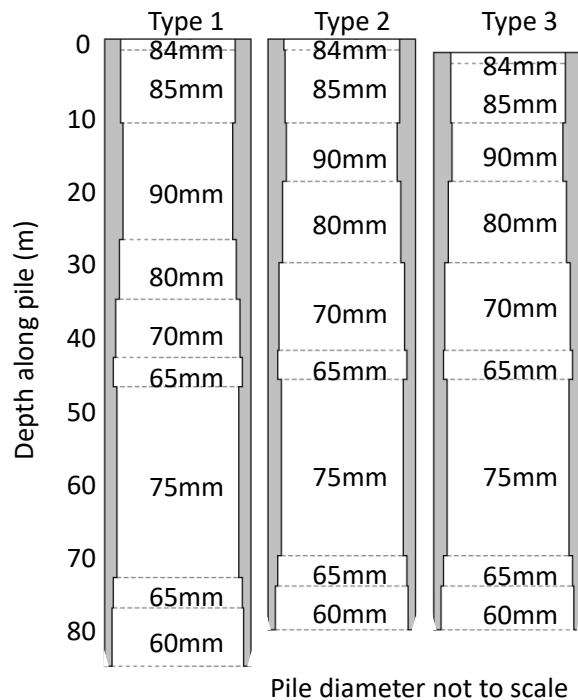


Figure 41 Wall thickness schedule for IP jacket piles original design

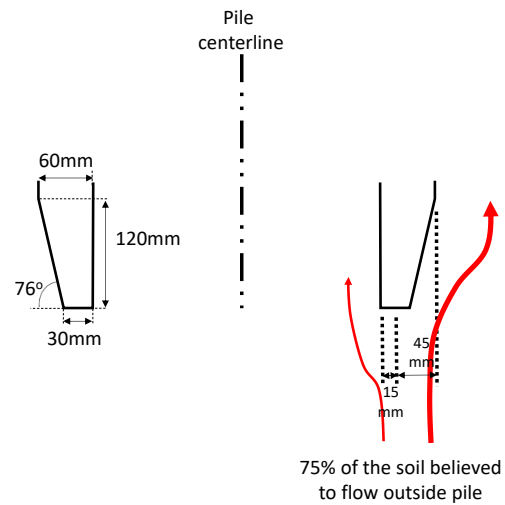



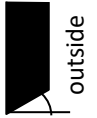


Figure 42 Details of pile tip chamfer for IP jacket original design (pile diameter not to scale)

3.9.5 Influence of external chamfer on risk of pile refusal

In 2003, a survey of pile installations in the North Sea was conducted with a focus on piles with diameters greater than 1372mm (54in) and with an impact energy greater than 1000kJ. A database of 188 platform case records was established with platforms from the UK, Dutch, Danish, and Norwegian sectors. The database was divided into four categories including piles with strong chamfers ($\alpha > 45^\circ$), weak chamfer ($\alpha < 45^\circ$), no chamfer ($\alpha = 0^\circ$), and piles with an inward chamfer ($\alpha < 0^\circ$).

The database indicated that, as of 2003, a strong chamfer was used at 50% of the platforms in the UK sector, 64% of the heavy platforms in the Norwegian sector, and 40% of the platforms in the North Sea overall. Details of the database are shown in Table 4.

Table 4 Statistics on the use of external chamfers

	 outside $\alpha > 45^\circ$ Strong chamfer	 outside $\alpha \leq 45^\circ$ Weak chamfer	 outside $\alpha = 0^\circ$ No chamfer	 outside $\alpha < 0^\circ$ Inward chamfer
Total case records: 188				
Per pile tip geometry	76	42	65	5
Pile tip in:				
Stiff clay	18	7	9	0
Hard clay	32	7	13	3
Dense sand	2	4	8	1
Very dense sand	16	20	35	1
Chalk & mudstone	8	4	0	0

For all platforms, the diameter, D , to wall thickness, t , slenderness ratio of the piles was taken at the tip, immediately above the chamfer. The D/t ratio shows no relationship with the target depth, drivability being more relevant than the target depth itself (Figure 43). The cases where pile refusal occurred are randomly distributed and show no relation with D/t . The D/t ratio for the IP piles is 41 and, while being higher than the database average of 33, falls within the range of industry practice.

Table 5 shows the statistics for the refused cases in very dense sands. A clear trend of increased occurrence of refusal can be established as the angle of the chamfer increases. The rate of occurrence increases from 9% for piles with no chamfer to 31% for piles with strong chamfer.

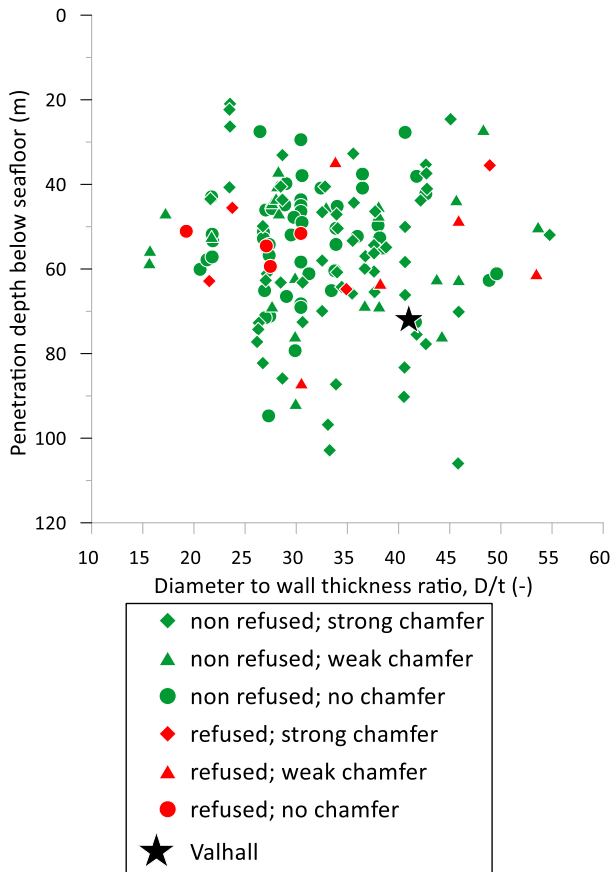






Figure 43 Case records of refused piles as a function of slenderness ratio and penetration depth

If the platforms with piles with weak and no chamfer are lumped together, for D/t ratios between 31 and 37, the strong chamfer statistically increased the risk of refusal from 11% to 31%, a factor of roughly three, as compared with piles with weak or no chamfer (Table 6).





Table 5 Statistics on refused piles in very dense sands

	 $\alpha > 45^\circ$ Strong chamfer	 $\alpha \leq 45^\circ$ Weak chamfer	 $\alpha = 0^\circ$ No chamfer	 $\alpha < 0^\circ$ Inward chamfer
No. of pile tip in very dense sand	16 ($D/t=31$)	20 ($D/t=39$)	35 ($D/t=32$)	1
Refusal ¹⁾	5 ($D/t=34$)	3 ($D/t=46$)	3 ($D/t=28$)	0
Percent refusal	31%	15%	9%	0

Notes:

- 1) "Refusal" refers to the number of platforms with at least one pile that refused early.
- 2) the D/t quoted are the average for each category.

Table 6 Simplified statistics on refused piles in sands

	 $\alpha > 45^\circ$ Strong chamfer	 $\alpha \leq 45^\circ$ Weak chamfer	 $\alpha = 0^\circ$ No chamfer	 $\alpha < 0^\circ$ Inward chamfer
No. of pile tip in very dense sand	16 ($D/t=31$)	55 ($D/t=35$)		1
Refusal ¹⁾	5 ($D/t=34$)	6 ($D/t=37$)		0
Percent refusal	31%	11%		0

Note 1): "Refusal" refers to the number of platforms with at least one pile that refused early.

As of 2003, the pile tip strong chamfer detail was often recommended for the following reasons:

- to aid pile stabbing into the pile sleeve,
- to preserve pile verticality when the pile encountered sloping strata,
- to ease penetration into dense soil, as compared to a flat tip,
- to push more soil to the outside of the pile thereby reducing the risk of plugging (Figure 42).

This last potentially beneficial effect could not however be rigorously supported by installation records and industry experience. No significant differences in measured blow counts, plugging and final internal plug elevation had ever been observed between piles with chamfered and non-chamfered tips.

Although the theoretical benefits of a strong chamfer had not been verified in the field, as of 2003, a strong chamfer had not been recognized as a factor that would increase the likelihood of pile refusal during driving in dense sands.

Given the above case records that showed an increased occurrence of refusal associated with piles with strong external chamfers, the distribution of stresses around the tip of such piles was investigated with empirical and FEA methods.

3.9.6 Stresses at the pile tip with chamfer: empirical approach

The soil properties required to propagate a potential initial damage were first assessed using the framework eventually published by Aldridge et al. (2005) using the damage geometry of Figure 44.

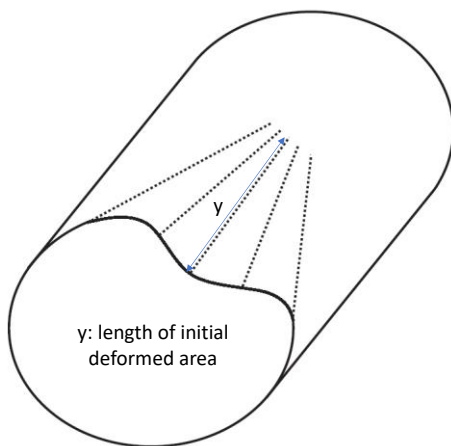


Figure 44 Shape of initial defect in the Aldridge et al. (2005) framework

The soil pressure, σ_{soil} , required to continue to progressively yield the pile wall as it penetrates the soil is (Aldridge et al., 2005):

$$\sigma_{soil} = \frac{3\sigma_y t^2}{y^2} \quad (1)$$

Where σ_y is the steel yield stress, t is the pile wall thickness, y is the length of the initial damage.

Taking an initial deformation length of $y = 0.15\text{m}$, a steel yield stress of 420MPa , and an average wall thickness around the pile tip of 45mm for the Valhall IP piles gives $\sigma_{soil} = 113\text{MPa}$. For sands, the most reliable estimate of the yield pressure would be the cone tip resistance, q_c . In clays, using bearing capacity theory, the yield pressure can be obtained as 9 to 12 times the undrained shear strength and this can be upgraded by 50% to account for dynamic effects. The soil pressure is then obtained as 15 to 20 times the shear strength, which is very similar to the cone resistance (Aldridge et al., 2005).

Therefore, either a clay with undrained shear strength of about 5670kPa or a sand with $q_c = 113\text{MPa}$ could have been sufficient to propagate a 0.15m long initial damage. The above value of undrained shear strength is well above what is measured in uncemented clays, even in glacial tills, indicating that initial damages are unlikely to propagate in these soils. However, the cone resistance of 113MPa is close to the values required to match the IP piles SRD (Figure 31), indicating that an initial defect could have propagated in the upper sands between 10m and 20m and the lower sands between 40m and 60m BSF.

3.9.7 Stresses at the pile tip with chamfer: Finite Element Analyses

FEA were also performed to estimate the cone resistance that would have been required to initiate yield and propagate failure in the pile. Software including ABAQUS (with and without the user element BASIL), LS-DYNA, Plaxis, ICFEP (Imperial College Finite Element Program) were used. The mean axial stress acting on the flat part of the chamfered tip, P , was estimated to be about 60% of the CPT resistance, q_c . A large differential normal pressure imbalance develops over the lowest part of the chamfered pile, giving an approximate triangular distribution with the maximum value of 35% q_c at the pile tip elevation and decreasing to zero at 180mm above the pile tip (Figure 45). No such imbalance was seen over the end of plain flat tip piles, which were also modelled.

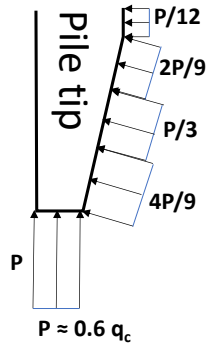


Figure 45 Assumed stress distribution around chamfered region of pile tip in sand in FEA.

An axisymmetric load case was first analysed where the pressure P applies uniformly over the pile tip. The pile develops the failure mode of Figure 46. Initial yield developed around the entire circumference close to the tip at a load corresponding to a CPT tip resistance of 105MPa and failure occurred by inward buckling at a load corresponding to a CPT value of 204MPa.

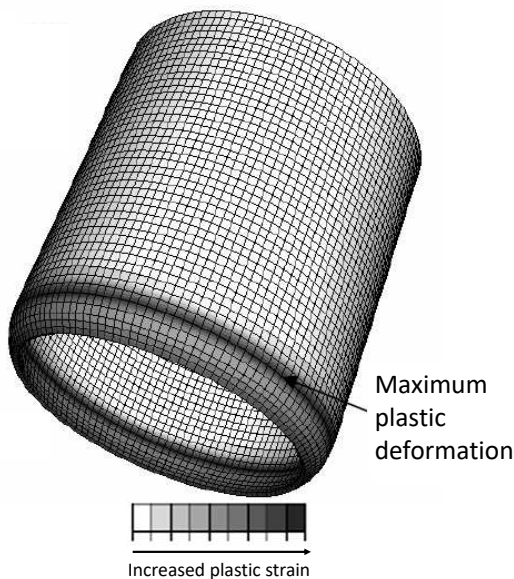


Figure 46 Stress distribution at failure for axisymmetric loading (displacements magnified by a factor of 4)

Recognizing that actual conditions around the piles are likely non-axisymmetric, (e.g. due to sloping strata, local variation in soil properties), a non-axisymmetric load case was run where the pressure P was double over half the pile base (Figure 47). Initial yield developed at a load corresponding to a CPT tip resistance of 70 MPa and failure occurred at a load corresponding to a CPT value of 137MPa.

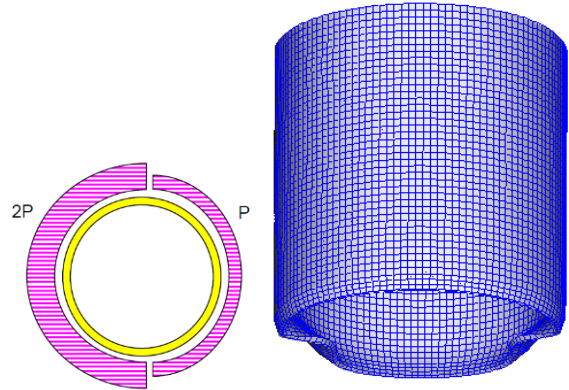


Figure 47 Illustration of non-axisymmetric load case simulating a sloping stratum and resulting failure mode (displacements magnified by a factor of 4)

Factors not addressed in these analyses include dynamic effects, non-axisymmetric initial geometry defects, and residual stresses due to pile fabrication. The CPT q_c values for yield and collapse of around 70MPa and 137MPa should therefore be interpreted as upper bounds.

Additional analyses were performed using the BASIL (Bucket Adjusted Soil Installation Loading) soil element (Barbour and Erbrich, 1995) in ABAQUS. The assumed stress distribution at the pile tip is shown on Figure 48. The stress q_1 is typically taken as $q_c/2$. The values adopted in the lower sand strata between 37m and 50m are $q_1 = 45\text{MPa}$ and $q_2 = 15\text{MPa}$ and the distribution therefore implies a cone resistance q_c of about 90MPa.

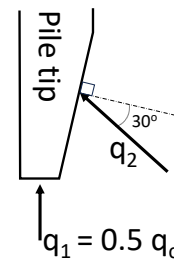


Figure 48 Assumed stress distribution around chamfered region of pile tip in Abaqus/BASIL in sand strata

For an assumed initial imperfection of 10mm on the horizontal axis, Figure 49 shows how the imperfection grows as the pile penetrates the soil. By the end of the analysis at 50m of penetration, the inward pile displacement on the vertical axis is 120mm and the outward displacement on the horizontal axis is 95mm. The analysis shows how an initial imperfection of 10mm can amplify with penetration.

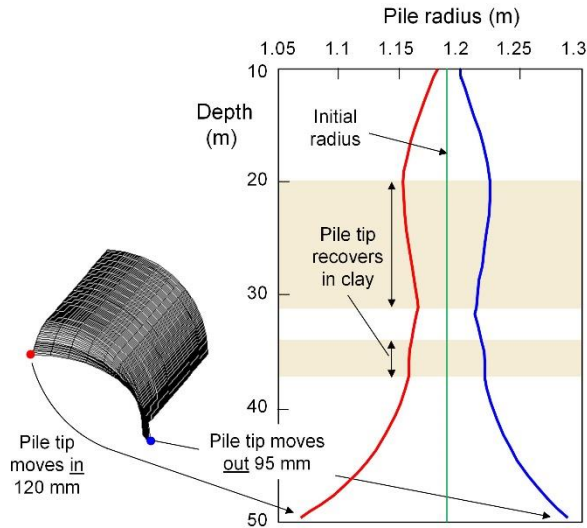


Figure 49 Predicted progression of pile distortion with increased penetration with BASIL analyses (from Randolph, 2018, used with permission)

Figure 50 shows the predicted yield zone for a total pile penetration of 50m. The von Mises stress in the bottom 10m of the pile exceeds the nominal yield stress of 420MPa.

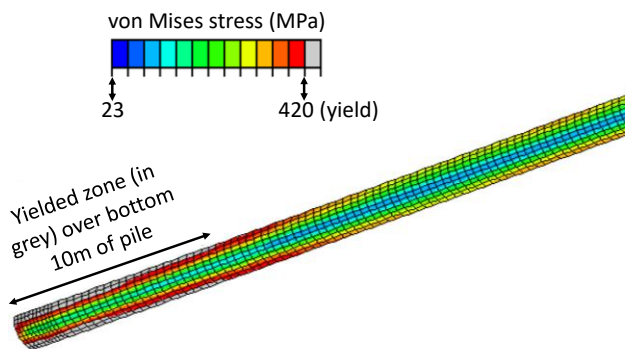


Figure 50 ABAQUS/BASIL analysis showing predicted von Mises stresses and yielding in the pile at 50m penetration

However, the 10mm initial imperfection in BASIL required to propagate the initial defect corresponds to an ovality of 40mm, which is greater than the maximum measured value of 7mm. Therefore, another mechanism is required to create a large enough initial imperfection. Perhaps, the model requires higher-than-measured imperfections because the dynamic behavior of the pile during driving is not captured by the model.

3.9.8 Pile remediation: the “Piggyback” system

The refusal event had three consequences (Alm et al., 2004):

- For the refused piles, proper connections to the jacket could not be made as there were no pile

weld beads on the piles to match with the pile sleeves.

- Since the piles had a variable wall thickness along their depths, the pile bending properties in some depths were now inadequate, particularly at the seafloor elevation.
- Due to the shorter pile penetrations, axial pile capacities were insufficient to support the design loads, particularly in tension.

A “piggyback” system was designed and installed at the two corners of the platform where both piles refused (Alm et al. 2004) to remediate the above issues (Figure 51). The refused piles were cut at the seafloor and two piggyback insert piles with adequate wall thickness and weld beads were installed inside the refused piles, along with a new pile sleeve. A new 2.438m diameter pile with a uniform 70mm wall thickness (apart from a driving head which had a wall thickness of 84mm), was driven into the piggyback sleeve to a depth of 41m. Details of the structural and grouted connection design can be found in Alm et al. (2004).

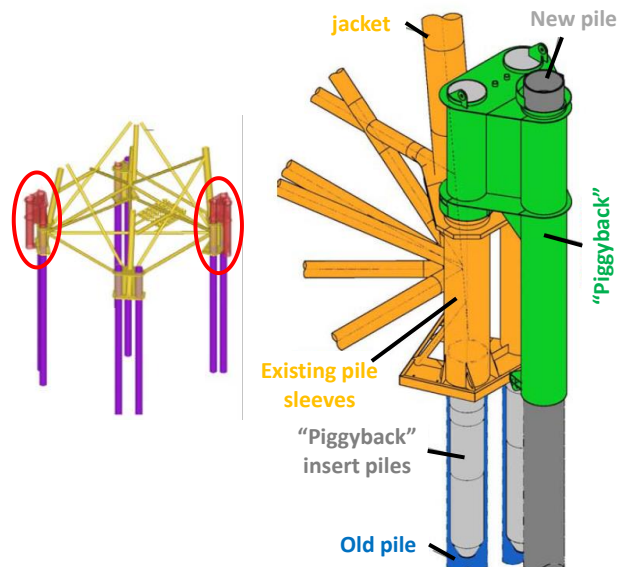


Figure 51 The piggyback repair system (modified from Alm et al., 2004)

At the corner where only one pile (Pile IP-P4) refused (Figure 26), a single insert pile with adequate wall thickness and weld beads was installed and grouted inside the refused pile as it could be demonstrated that the pile group at that corner had enough axial capacity without further driving.

The P4 insert pile, the two piggyback systems, and the platform topsides were installed in August 2003 (Figure 52).



Figure 52 The piggyback repair system (from Alm et al., 2004) and IP jacket topside installation

3.10 The 2004 site investigation for the PH platform

The 2004 site investigation for the design of the PH platform foundation comprised seven shallow boreholes, up to 20.4m BSF, sixteen shallow CPT up to 21.5m BSF, and two deep boreholes, up to 109.7m BSF (Figure 53).

The data revealed cone resistances in excess of 100MPa, both in the Forth and Fisher formations (Figure 54). Most of the CPT records in the lower Fisher formation where the piles refused exceeded the limit of the tools and refused between 100MPa and 120MPa.

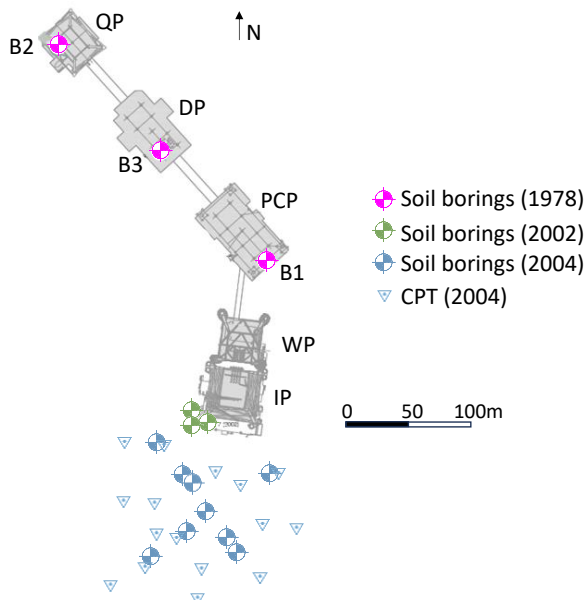
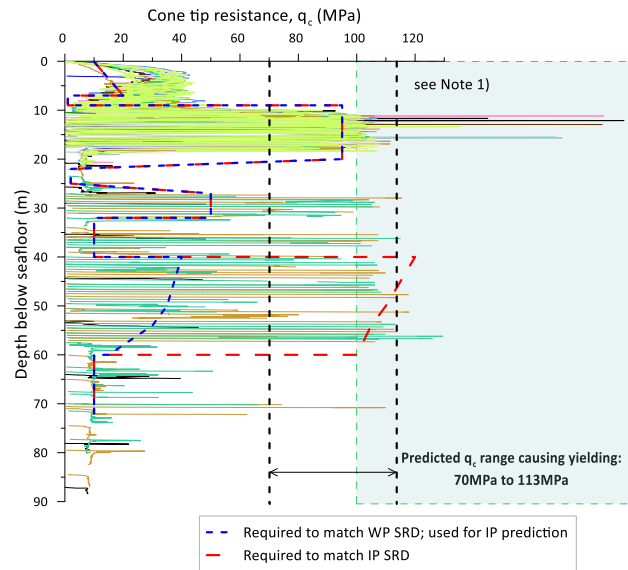


Figure 53 Base map of the 2004 site investigation used to design the PH jacket piles



Note: 1) All q_c values greater than 100 MPa were measured at CPT refusal. They do not represent actual in-situ values.

Figure 54 CPT records from the 2004 site investigation used to design the PH jacket piles

These measured values are consistent with the ones that had to be assumed to hindcast the SRD of the IP piles and the ones required to propagate an initial defect using the Aldridge et al. (2005) framework and the FEA analyses. They confirm that indeed an initial defect could have propagated in the sand layers.

3.11 Overall learnings on the pile refusals

Numerical displacement-controlled analyses generated a progressive failure mechanism that matched the observed deformations in the P7 and P8 piles. A slight imperfection grows as the pile advances in the high cone resistance strata. Yielding initiates due to hoop bending and causes extensive radial tip deformation which leads to collapse. The key factors required to generate the observed failures were (not in order of importance):

- A steeply chamfered pile tip.
- A sand stratum of sufficient density and stiffness.
- A sand stratum of sufficient thickness to propagate the initial deformation to the point of collapse.
- An initial out-of-roundness or tip deformation upon entering the very dense sand stratum in which the pile refused.

The analyses showed that initial yielding could take place if the cone resistance was in the range of 70MPa to 113MPa (70MPa with FEA with non-axisymmetric pressures, 90MPa with Abaqus/BASIL FEA, 105MPa with FEA with axisymmetric pressures, and 113MPa with Aldridge et al. 2005). This suggests that some initial yielding could have

occurred in the top sand between depths of 10m and 20m BSF and further propagated in the deeper sands between depths of 40m and 60m BSF.

However, all models required initial defects or imperfections more severe than those measured prior to the pile being lowered through the water column. Additional damage could have happened during pile stabbing, during lowering through the pile sleeve, or while the piles were left in the sleeves during the passage of a storm.

These analyses indicate that whether the piles collapsed or not was marginal, since the measured cone resistances were higher than the required level to propagate a defect and close to the level above which collapse would occur. This is consistent with the fact that some of the piles collapsed, and some did not. This also suggests that small differences in ovality and tip damage between the piles could have made just enough difference to the stresses at the pile tip to cause collapse.

One of the key learnings is that SRD in dense sands can be greatly influenced by the details of the pile tip, particularly the presence of an external chamfer. When developing and publishing pile driving prediction methods, these details should be included. Hamre (2024) confirmed that at least 11 out of the 15 pile driving records that were used to develop the Alm and Hamre (2001) method had piles with steep external chamfers (1:4 to 1:5), which designers should be aware of when applying the method to flat-tipped piles.

4 THE SCIENTIFIC METHOD

Once the foundation is successfully installed, its field performance under environmental loads is arguably the ultimate test by which industry design methods can be judged.

It is legitimate to ask ourselves: does the field performance of offshore foundations prove that our design methods are right?

Prof. Feynman (1964) provided an interesting perspective and described the scientific method of discovering new laws of physics as a process involving three steps:

- Develop the theory,
- Compute the consequences of the theory to see what it would imply,
- Compare the computed consequences with nature, experiments, experience, or observations to see if it works.

If the predicted consequences of the theory disagree with experiments, the theory is wrong. But Feynman argues that we cannot prove any theory right:

“Suppose that any calculated consequence from a theory agrees with experiment, is the theory then right? No, it has simply not been proved wrong. Because in the future, there could be a wider range of experience or experiment available and we may discover that the theory is wrong (...). We never are right, we can only be sure we are wrong.”

In this spirit, the performance of MODUs and fixed structures in the Gulf of Mexico during hurricanes is analysed to document that the performance of these structures (i.e. the experiment) has not proved our geotechnical design methods to be wrong, if the latest international code recommendations are followed.

5 ANCHOR PERFORMANCE DURING GULF OF MEXICO HURRICANES

The paper now summarizes selected field performances of temporary foundations used in the mooring of drilling rigs.

5.1 Introduction

Hurricanes Ivan (2004), Katrina (2005), Rita (2005), Gustav (2008), and Ike (2008) impacted the Gulf of Mexico offshore infrastructures and caused extensive damages to fixed and floating structures, as well as pipelines. In particular, floating MODUs were exposed to environmental events well beyond the 10yr return period events for which they were designed as the rigs experienced hurricanes of Category H4 and H5 on the SSHS (Saffir-Simpson Hurricane Scale) (Figure 55).

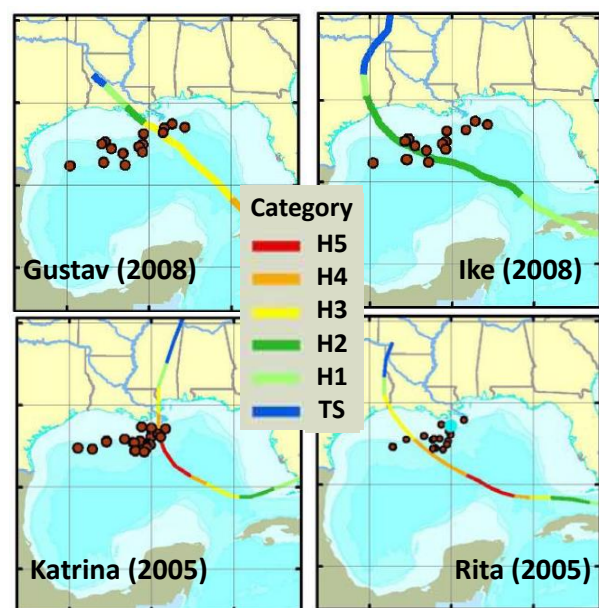


Figure 55 Rig locations with selected hurricanes path and category (modified from ABS, 2012)

Five MODUs broke mooring lines during Hurricane Ivan (Sharples, 2006), eight rigs suffered some level of mooring system failures during Hurricane Katrina, twelve during Hurricane Rita, one during Hurricane Gustav, and five during Hurricane Ike. Some of the units remained in the vicinity of their location with a reduced number of lines holding while others experienced complete mooring failure and drifted more than 160km (ABS, 2012).

During Hurricane Ivan (Figure 56), the Jim Thompson rig drilling in Block MC383 was subjected to wind intensity with a return period of 50yr to 100yr, while the maximum wave height had a return period ranging from 100yr to more than 1,000yr (Petruska, 2005) as per Figure 57.



Figure 56 Hurricane Ivan, September 15, 2004 (from NOAA)

Table 7 Statistics of anchor types for failed mooring lines

Anchor type	Number of failed mooring line with this anchor	Number of anchors that dragged
Conventional drag embedment anchors (DEA), mostly Vryhof Stevpris [®] Mk5, and Bruce FFTS anchors	116	31
Vertically Loaded anchors (VLAs), a.k.a drag-embedded plate anchors, normally loaded anchors, or near normally loaded anchors (Vryhof Stevmanta [®])	16	8
Suction piles, a.k.a suction anchors	18	0
Gravity anchors (i.e. Omni-Max [®] anchors)	7	0

The lessons learned from the performance of the moorings systems are now analysed, with a focus on anchor performance.

The most striking factor is the fact that, for the 157 No. mooring lines that failed, 75% of the line failures occurred at, or close to, the fairlead without resulting in a dragged mooring component on the seafloor (ABS, 2012).

In most cases the anchors held and managed to resist a load greater than the mooring line strength.

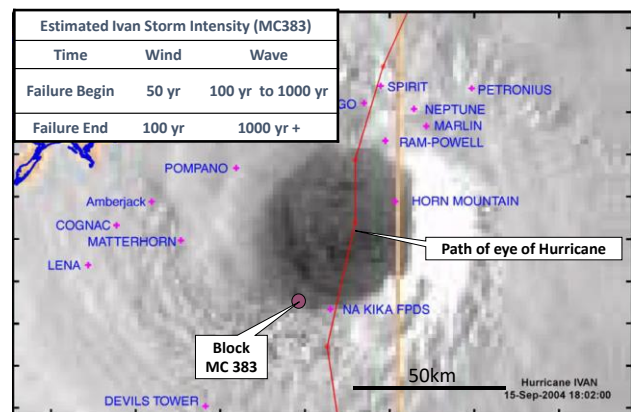


Figure 57 Hurricane Ivan storm intensity in Block MC383 (from Sharples, 2006, and Petruska, 2005)

The details of the MODUs mooring and anchors performance was well documented except for three rigs which broke moorings and potentially dragged anchors during Hurricane Ike and for which such details were not released.

Four types of failure were observed:

- Failure of the line at or close to the fairlead (a device attached to the hull to guide the rig wire line),
- Failure in the intermediate mooring wire,
- Dragged anchor,
- Structural failure of the anchor.

Four types of anchors were used on the mooring lines that failed, as summarized in Table 7.

This is consistent with the assertion by Ward et al. (2008) that it is unlikely that an anchor will pull out in in-plane loading before the line breaks. Indeed, reliability analyses on mooring systems for permanent floating production facilities have shown that the probability of an anchor failure is more than one hundred times smaller than that for a line or chain break (Gilbert et al., 2005).

The details of the performance of each type of anchor are now summarised.

5.2 Performance of VLAs during hurricanes

Two rigs that used VLAs were tested during hurricanes. The Noble Therald Martin was affected by Hurricane Rita and the Noble Lorris Bouzigard rig was affected by both Hurricanes Rita and Ike.

5.2.1 Installation and retrieval of VLAs

Before analysing the performance of the anchors, it is important to understand how VLAs are installed and retrieved for temporary mooring systems.

The typical installation of VLAs first starts by increasing the rig wire load causing the anchor to penetrate into the seabed. When the load reaches a pre-determined installation value, a further increase in load tension activates a shear pin and increases the angle between the fluke and the shank. The anchor switches from installation mode to a “near-normal” load configuration where the load angle is almost perpendicular to the fluke plane (Figure 58). The degree to which this near-normal configuration is reached depends on the available bollard pull from either the anchor installation vessel or the rig winches and on the achieved proof tension load.

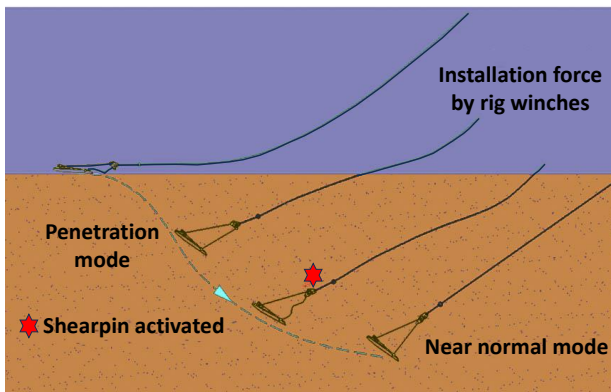


Figure 58 Installation of a VLA (courtesy of Vryhof, 2024, used with permission)

During retrieval, the load direction is reversed. The two wires that were at the front of the anchor during penetration are attached to the fluke with one-way claw sockets that only engage when the load is in the direction that it is during embedment. When the load is reversed during retrieval the two front claw sockets disconnect and the two front wires are released. The load becomes in-line with the fluke plane, minimising the retrieval load (Figure 59).

VLAs such as Stevmanta[®] anchors used for temporary mooring are therefore designed to have greatly reduced capacity when loaded in the direction opposite of embedment to ease retrieval. Such disconnectable claw sockets are not present when the anchor is used for permanent mooring systems.

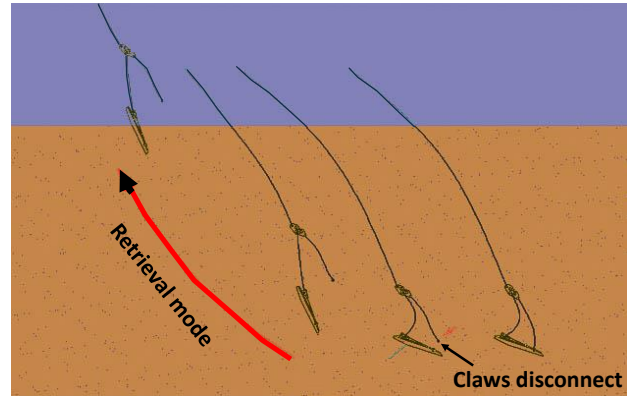


Figure 59 Retrieval of a VLA (courtesy of Vryhof, 2024, used with permission)

5.2.2 Performance of VLAs during hurricanes

The Noble Therald Martin rig used eight 9mT Vryhof VLAs and one suction pile, during Hurricane Rita (ABS, 2012). It is unusual to refer to a VLA by its weight as they are usually referred to by the area of their fluke. Details of how the anchors were set-up are not available. Six lines broke at the fairlead, including the one with the suction pile, but three lines dragged their anchors for 205km (ABS, 2012).

The Noble Lorris Bouzigard rig was affected by both Hurricanes Rita and Ike. The performance during Ike was kept confidential and is not in the public domain. Before Hurricane Rita, two out of ten legs used 8mT Stevpris[®] anchors and the remaining eight legs used 13m² Stevmanta[®] (Vryhof, 2024). No soil data were available, and the installation experience suggests the soils consist of hard clays and sands.

All Stevmanta[®] VLA were installed with non-shearable solid pins and therefore would have behaved like conventional fluke anchors (e.g. Stevpris[®] anchor) (Vryhof, 2024). They could not be set to near-normal load conditions. All anchors were successfully installed with anchor tensions of 73mT to 77mT out of the required capacity of 210mT.

The performance of the mooring system reported by Vryhof (2024) differs from the account of ABS (2012) and is shown on Figure 60:

- Line 7 broke at the fairlead,
- Line 1 broke at a socket location,
- Line 2, 3, and 4 were recovered intact,
- Line 5, and 6 anchors dragged and could not be recovered as they had penetrated too deep,
- Line 8, 9, 10 were recovered successfully.

Therefore, Lines 1, 8, 9, and 10 did not fail at the anchor, contrary to the account of ABS (2012). The rig was moored in 744m of water and drifted 1.4km (ABS, 2012), presumably held by Lines 5 and 6.

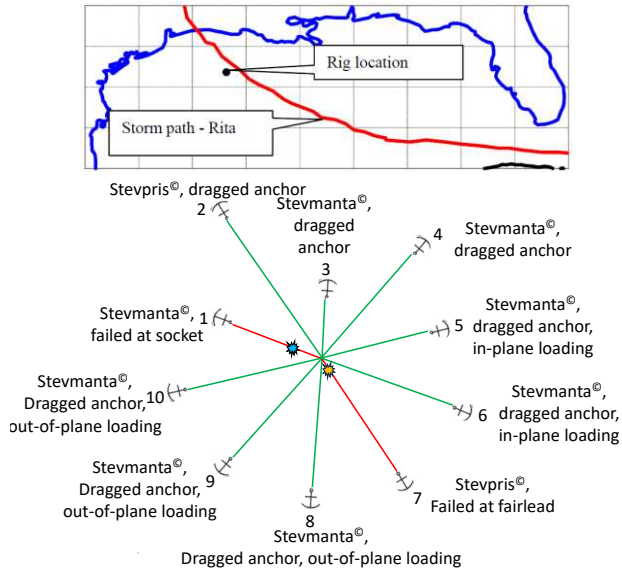


Figure 60 Details of mooring failure of the Noble Lorriss Bouzigard rig during Hurricane Rita (Vryhof, 2024, modified from ABS, 2012)

5.2.3 Learning

Even though some rigs were reported to have used VLAs, the performance record of such anchors is simply not available. Either the details of the mooring performance were not released or the VLAs were installed with solid pins in conventional drag anchor mode. When installed in such a manner, the anchors performed as expected, achieving deeper penetration when loaded in-plane but not being able to mobilise large capacities when loaded out-of-plane.

5.3 Performance of conventional DEA

Only 9 cases of rig dragging at least one conventional DEA were recorded, as summarized in Table 8. Drag distances ranged from 150m to 205km.

The performance of the Transocean Marianas rig during Hurricane Rita is now examined. Hurricane Rita caused the rig to break free of all its mooring and drift from Block GC821. The rig was set out on a wire and chain mooring system with 18mT Stevpris® MK5 anchors. The breaking strength of the chain and wire was 7.03MN and 7.0MN, respectively. Six lines broke at the fairlead and two in the intermediate wire (ABS, 2012). The details of the mooring failure locations, anchor drag distances and rotation from in-line loading are shown on Figure 61.

Time domain analyses were performed to hindcast the line breaking sequence and the expected locations of the broken lines on the seafloor post-hurricane. The in-line Ultimate Holding Capacity (UHC) of the anchors in the very soft to medium clays at the site was estimated as 7.66MN. Like all drag anchors, the holding capacity can be significantly reduced if an uplift angle or azimuth change is incurred in the mooring line as the line experiences tension at the anchor and the analyses used the assumed reduction in capacity as a function of the uplift and out-of-plane angles as per Figure 62 (Delmar, 2005b).

Table 8 Summary of conventional drag anchor (DEA) performance (modified from ABS, 2012, and Sharples, 2006)

Anchor Type	Size	Rig	Hurricane	Anchor drag information
Vryhof Stevpris® MK5	8mT	Noble Lorriss Bouzigard	Ivan	4 No. anchors dragged 915m and stopped the rig movement (Line #2 broke after anchor dragged)
	9mT	Noble Therald Martin	Rita	3 No. anchors dragged for 205km
	15mT	GSF Celtic Sea	Katrina	1 No. windward anchor dragged for 8km but line did not break.
		GSF DDII	Katrina	5 No. anchors dragged 150m to 450m
		GSF DDI	Katrina	5 No. anchors dragged 670m to 915m
		GSF Celtic Sea	Rita	4 No. anchors dragged less than 1.6km
		Transocean Falcon F-100	Rita	3 No. anchors dragged up to 350m
	18mT	Transocean Marianas	Rita	2 No. anchors slipped less than 900m
Bruce FFTS (?) MK4	12mT	Noble Jim Thompson,	Katrina	4 No. out 9 No. anchors (2 windward, 2 leeward) dragged 40km

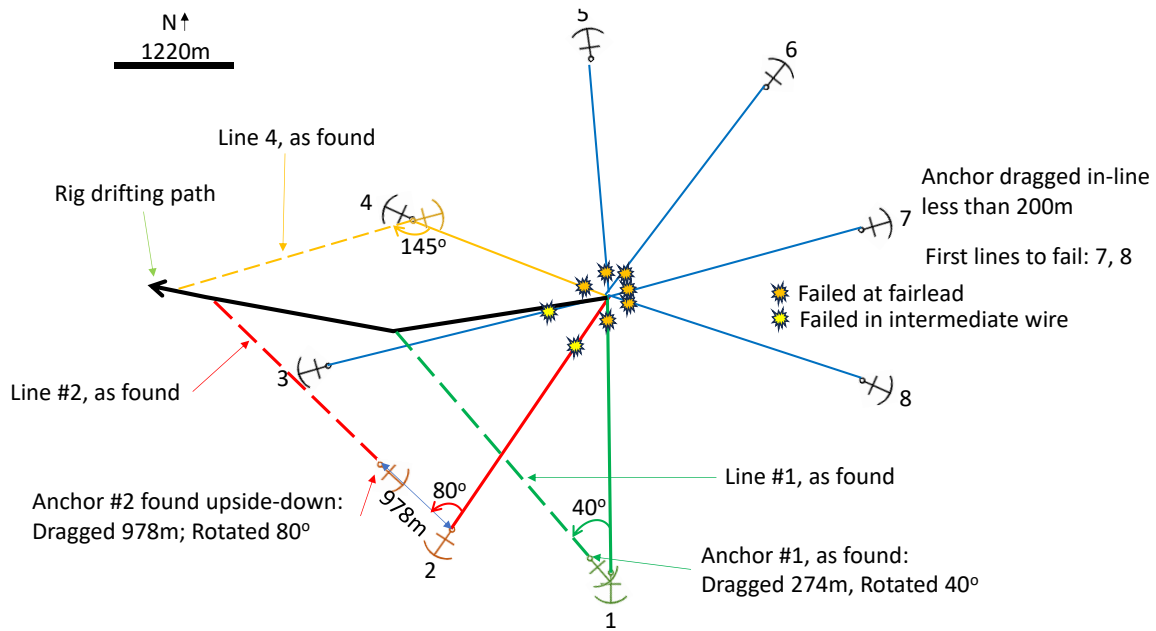


Figure 61 Details of mooring failure of the Marianas rig during Hurricane Rita (modified from Delmar, 2005b)

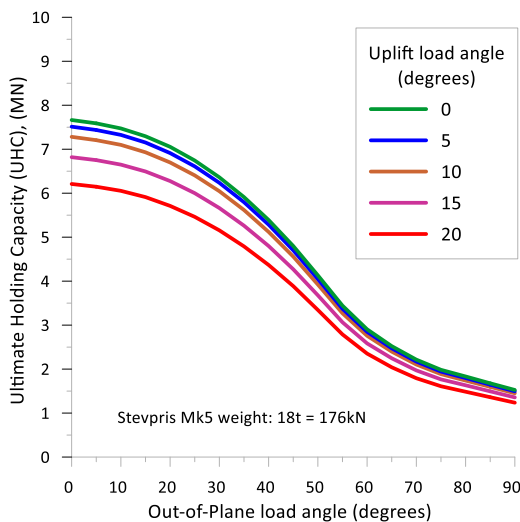


Figure 62 UHC of 18mT Stevpris[®] Mk5 anchor as a function of uplift and out-of-plane load angles (Delmar, 2005b)

The predicted recovery zones for the lines were accurately estimated, except for line #4 which laid outside the predicted zone. The out-of-plane angle for Line 4 was in excess of 145deg when estimated failure occurred, making it difficult to accurately predict its location on the seafloor.

Anchor #2 dragged 978m and experienced out-of-plane loads angle of 80deg while the uplift angle was estimated to be as much as 20deg (Delmar, 2005b). Consequently, as per Figure 62, its capacity was reduced to 1.46MN, which caused the anchor to drag. A typical 18mT Stevpris[®] Mk5 anchor is shown on Figure 63 and a photo of Anchor #2, as it was found laying upside down on the seafloor is shown on Figure 64.



Figure 63 Typical 18mT Stevpris[®] Mk5 anchor (from Delmar)



Figure 64 Anchor #2 as-found upside down after Hurricane Rita

5.3.1 Learning

The recorded performance of the Stevpris® Mk5 drag anchors (Figure 63) was globally consistent with expected behavior. They developed enough in-line capacity with minimum drag to force the breaking point of the line to be at the fairlead for the first lines to fail.

Once the first line had failed, high out-of-plane load angles of 40deg, 80deg, and 145deg were recorded, causing severe loss of capacity (Figure 62). One anchor dragged a moderate distance (about 1km) nevertheless eventually developing enough capacity to cause line failure in the wire.

5.4 Performance of suction piles

A total of 18 No. mooring lines anchored with suction piles experienced hurricane loads. Eight suction piles were used on the Deepwater Nautilus rig during Hurricane Ivan and on one line of the Noble Therald

Martin during Hurricane Rita, but all lines failed either at the fairlead or in the intermediate wire, giving limited insight into the anchor performance.

5.4.1 Performance during Hurricane Ivan

However, suction piles experienced failures for the Noble Jim Thompson during Hurricane Ivan. The rig was positioned in Block MC383 drilling a well in the Kepler field which is part of the greater NaKika development.

Details of the mooring performance were reported by Delmar (2005a) and Petruska (2005). Four anchors, both windward and leeward, broke at the anchor padeye. The condition of each pile post Ivan is given in Table 9. The failed component of the semi-taut mooring system for each of the nine lines is shown on Figure 65 and pictures of the broken missing padeyes are given on Figure 66.

Table 9 Summary of suction pile performance on the Jim Thompson rig during Hurricane Ivan

Pile #	Dimensions	Embedment (m)	Comments
	Diameter (m) x length (m)		
1	3.65x18.3	17.1	Rotation clockwise
2	3.65x18.3	16.8	Soil disturbance around the pile, padeye failure
3	3.65x18.3	16.8	Pile appeared normal
4	2.91x21.3	20.1	Soil depression reported on back side of pile
5	3.65x18.3	17.1	Pile appeared normal
6	2.91x21.3	19.8	Pile appeared normal
7	3.65x18.3	16.5	Padeye failure
8	3.65x18.3	16.8	Rotation counterclockwise, padeye failure
9	3.65x18.3	17.4	Rotation counterclockwise, padeye failure

Notes for the 3.65m x 18.3m piles: 1) embedment: 16.8m below seafloor; 2) L/D: 4.5 to 4.75; 3) padeye located 10.67m below seafloor; 4) anchor weight: 756 kN

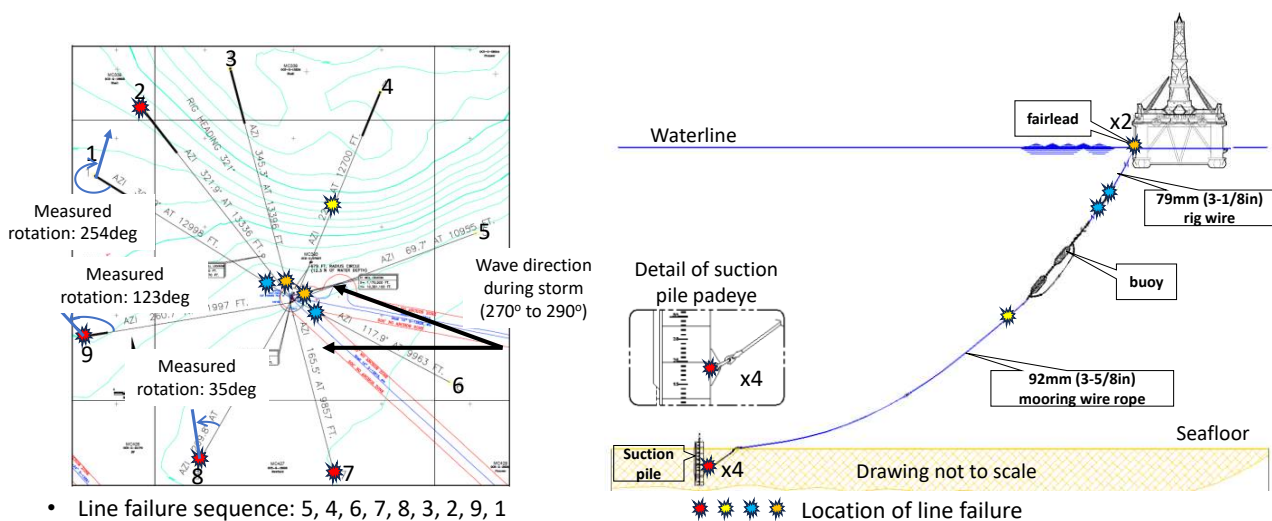


Figure 65 Details of mooring failure of the Jim Thompson rig during Hurricane Ivan (modified from Delmar, 2005a)

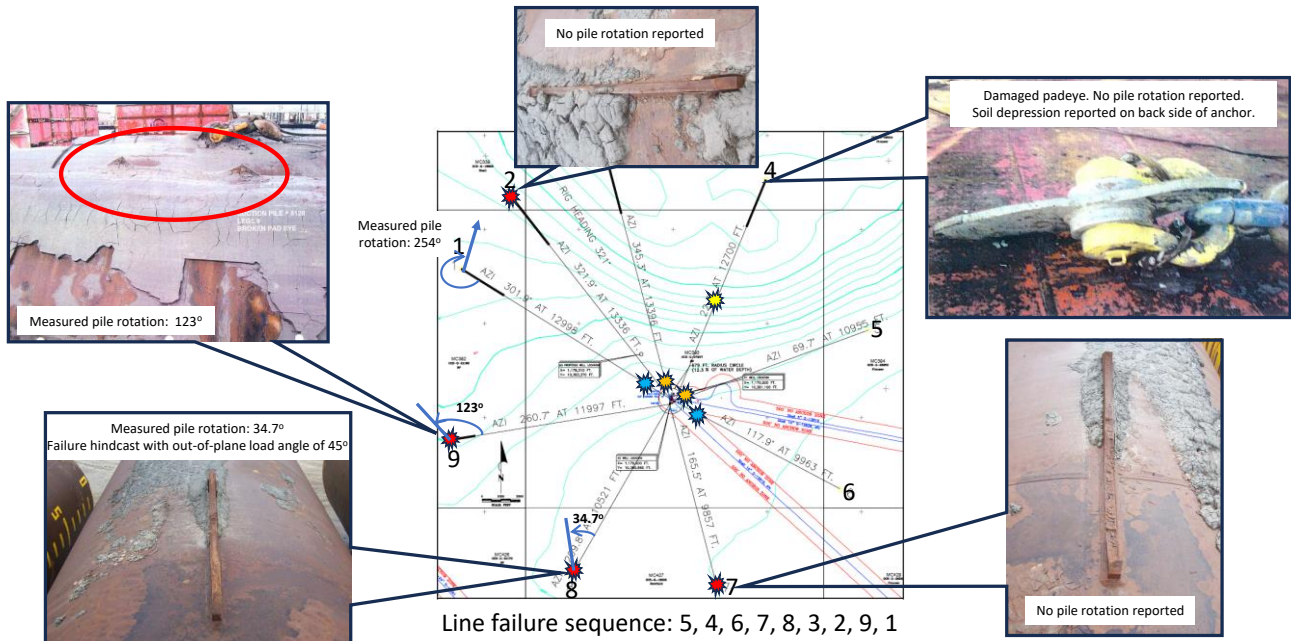


Figure 66 Details of suction piles padeye failures on the Jim Thompson rig during Hurricane Ivan (modified from Delmar, 2005a)

The piles were installed between July 27th and August 5th 2004, about 40 days before Hurricane Ivan hit the rig on Sept. 15th 2004.

The DSS cyclic shear strength profile of Newlin (2003) (Figure 67), which was developed for the Greater NaKika field, formed the basis of the hindcast analyses.

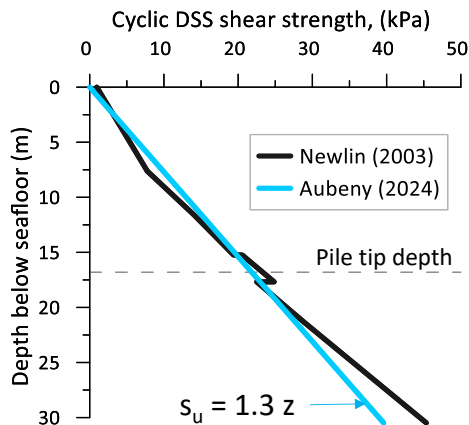


Figure 67 Soil profiles used for Jim Thompson suction pile performance

A soil-pile adhesion factor $\alpha = 0.75$ was used and represents a best-estimate value for GoM conditions after 40 days of set-up as per Jeanjean (2006).

Aubeny (2024) derived the horizontal-vertical load failure interaction diagram for the 3.65mx18.3m anchors using the simplified linear profile of Figure 67 with the model of Aubeny et al. (2003) (Figure 68).

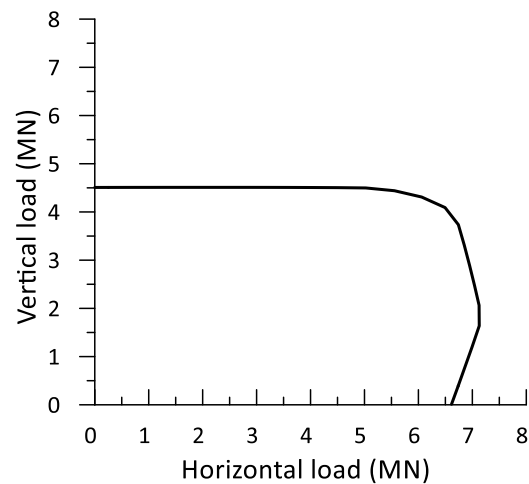


Figure 68 H-V failure interaction diagram for the 3.65m diameter suction piles (Aubeny, 2024)

It can be seen that the horizontal capacity is not maximum for the purely horizontal load because, for this case record, the padeye is located above the optimum point that would maximize the horizontal capacity.

In the model of Aubeny et al. (2003), the loads are assumed to act on the centreline of the pile. Therefore, when calculating the horizontal capacity, the inclined load applied at the padeye is first projected onto the centreline, giving a deeper virtual attachment point which results in an increased horizontal capacity. This is illustrated in Figure 69 which shows that a load applied at 13deg from the horizontal will result, for this case record, in a greater horizontal capacity than when the load is purely horizontal

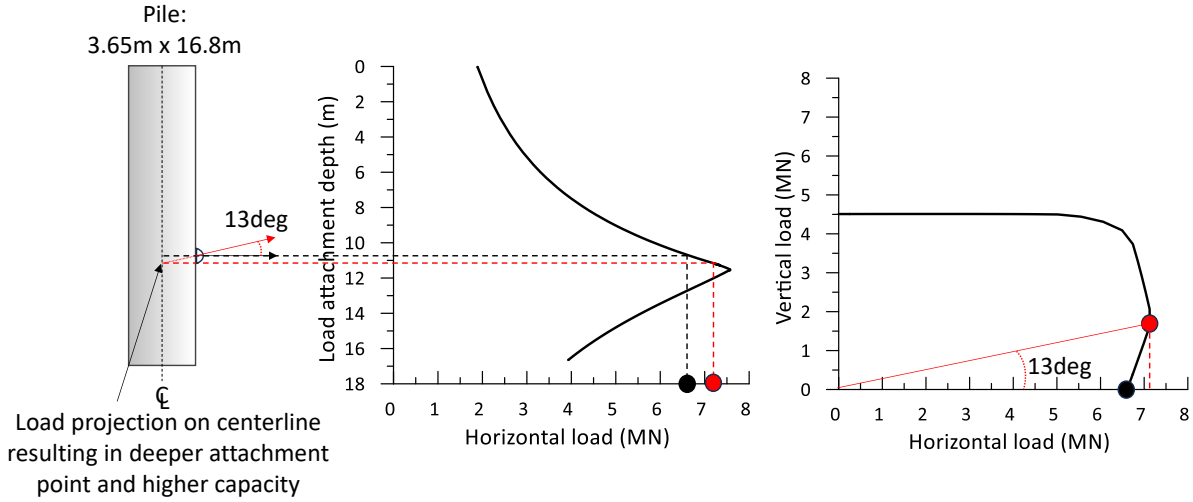


Figure 69 H-V failure interaction diagram and horizontal capacity vs padeye depth for the 3.65m suction piles (Aubeny, 2024)

Failure interaction diagrams were developed by Aubeny (2024) for various adhesion factors ranging from 0.75 to 0.0 for the 3.68m anchors and the 2.91m diameter anchors. The value of $\alpha = 0.0$ simulates a case where the anchor is under a moment load equal to the moment capacity of the anchor and all the side friction is mobilised in the torsional load direction, leaving no friction left to resist the vertical and horizontal loads.

The breaking strength of the rig wire was 5.09 MN and is a limiting condition in any load direction.

Time histories of the dynamic line loading at the fairleads and at the anchors were hindcast using the Orcaflex software (Delmar, 2005a).

The interaction diagrams and line loading paths are shown on Figure 70 and Figure 71.

The peak torsional moment capacity, M_{ult} , was calculated to be 3.11 MNm for the 3.68m anchors and 2.7 MNm for the 2.91m anchors using Eq (2) with the strength profile of Figure 67 and an adhesion factor of 0.75.

$$M_{ult} = \int_0^L \frac{D}{2} \pi D \alpha s_u(z) dz + \frac{\pi}{12} D^3 s_{u_tip} \quad (2)$$

where L is the pile embedded length, D is the pile diameter, α is the adhesion factor = 0.75, $s_u(z)$ is the shear strength at depth z , and s_{u_tip} is the shear strength at the pile tip.

Results show that Line 3, 4, 5, and 6 were loaded mostly in-plane with the torsional moment less than 36% of the moment capacity. This results in a modest reduction of the adhesion factor, R , of 7% using Eq. (3):

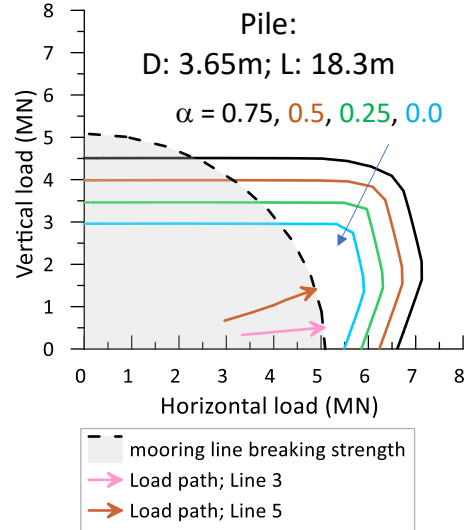


Figure 70 Failure interaction diagrams and load path for Lines 3 and 5.

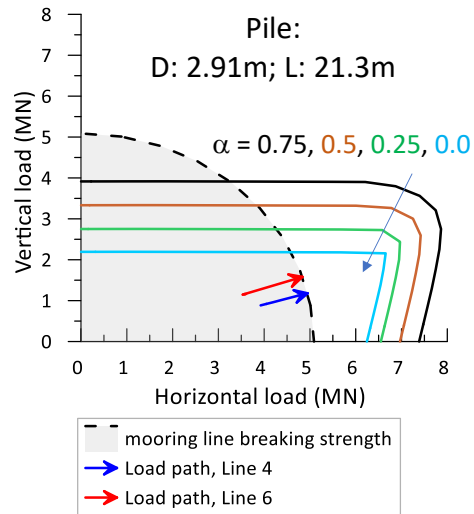


Figure 71 Failure interaction diagrams and load path for Lines 4 and 6.

$$R = \left[1 - \left(\frac{M}{M_{ult}} \right)^2 \right]^{0.5} \quad (3)$$

where M is the mobilised moment

For Lines 3, 4, 5, 6, results indicate that the line load reached the line breaking strength before exceeding the anchor capacity. The vertical load angles were between 6deg and 18deg, which is typical of semi-taut mooring systems. These results show that even if the anchor was under large torsional loads (e.g. $\alpha = 0.0$), the line wire would still be expected to fail before the anchor for these load angles less than 18deg.

The above results are consistent with the fact that these anchors did not experience pull-out and the Lines 3, 4, 5, and 6 broke close to the fairlead or in the wire.

An anecdotal observation of a “*soil depression on the back side of the pile*” was reported for Line 4 but unfortunately not rigorously documented with photographs. It is acknowledged but not relied upon for any conclusions.

For Lines 2, 7, 8, and 9, which broke at the padeye, the moment vs in-line load during the storm is plotted on Figure 72 with the pile moment capacity and the line breaking strength.

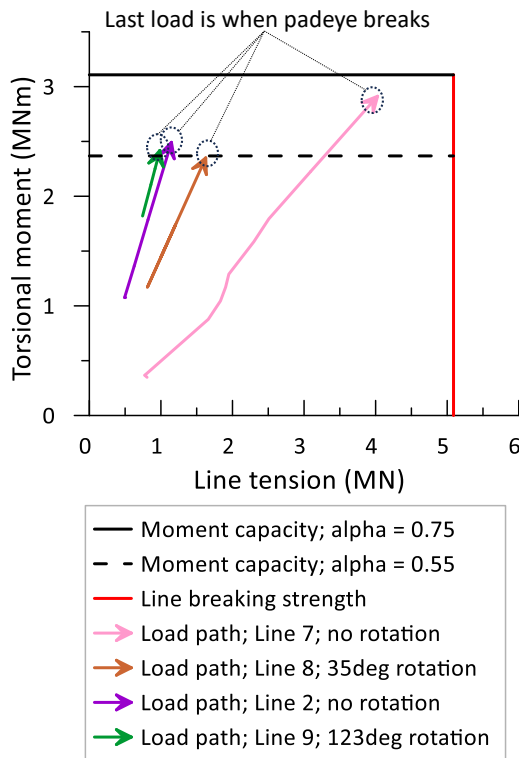


Figure 72 Moment and line tension load path at anchor during Hurricane Ivan for Lines 2, 7, 8, and 9.

Because the four lines broke at the padeye, the structural capacity of the padeyes were evaluated

with the Ansys software using the loads magnitudes and directions obtained from the Orcaflex analyses.

For each loading step, an FEA of the padeye was performed. Figure 73 shows that the padeye for Pile 7 failed for an in-line anchor load of 4.03MN applied with a vertical angle of 12.1deg and an out-of-plane angle of 16.8deg because the stresses in most of the padeye exceeds the yield value of 34.5MPa. Similar results were obtained for the padeyes of Lines 2, 8, and 9. The padeye breaking loads are the final points in the load paths of Figure 72.

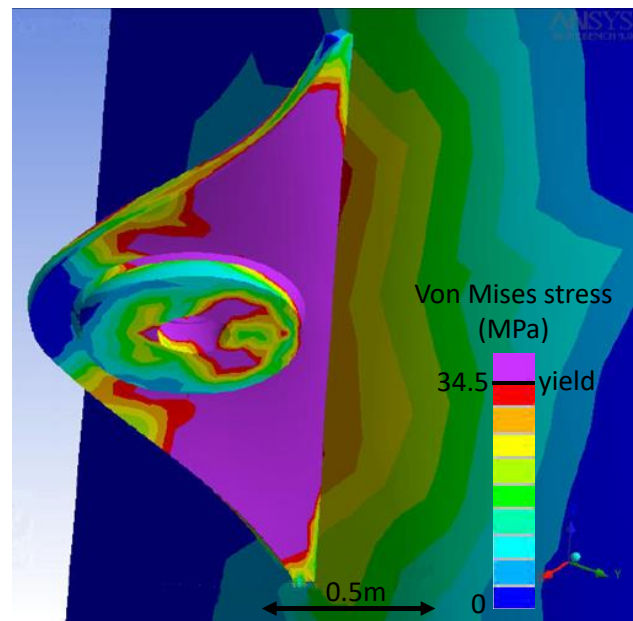


Figure 73 Stresses in padeye for Line 7 at failure (modified from Delmar, 2005).

Figure 72 shows that the padeyes broke for in-line loads well below the line breaking strength and for moment loads at or near the moment capacity of the anchor. The anchors of Lines 2 and 7 did not rotate before the padeye broke but those of Lines 8 and 9 experienced rotations of 35deg and 123deg respectively before the padeyes broke. This suggests that the moment capacity of these anchors was close to the padeye structural capacity and whether the pile rotated or not before the padeye broke may have depended on the difference in moment load paths and local shear strength variations, or other factors not included in the analyses.

For Line 1, which was the last to break, the hindcast which was carried up to a duration of 8100s shows low level of loading on the line. This suggests that the high loads and line failure occurred after the end of the numerical simulation.

The fact that the line broke at the fairlead, even after the anchor having experienced a 254deg rotation is consistent with the fact that failure is not

expected in the anchor, even with full moment capacity mobilisation with a resulting adhesion factor equal to 0.0 (Figure 70).

5.4.2 Learnings

No suction pile anchor used for MODU mooring in the Gulf of Mexico has ever been documented to fail geotechnically under in-line loading. For the case records analysed, the line breaking strength was the weak point for in-line loading conditions (Figure 70).

When the mooring load applied to these anchors is significantly out-of-plane, anchors can fail in torsional loading mode and experience large rotations up to 254deg. Torsional load can cause geotechnical rotational failures and/or padeye structural failures and four such failures were recorded.

For the Jim Thompson rig case record, the hindcast results are consistent with the failure mechanisms observed. It is consistent with Figure 70 and interesting to note that the anchor on Line 1 still retained enough inline capacity to cause the failure of the line at the fairlead although it had experienced a rotation of 254deg and the moment capacity of the anchor had been fully mobilised.

Improving the performance of suction piles therefore involves increasing the structural capacity of the padeye. On permanent mooring systems, the structural capacity of the padeye is much improved from that for temporary mooring systems by having a thicker cast pad-eye instead of the thinner fabricated pad-eye used in temporary moorings. Typical examples are shown on Figure 74. Therefore, all the lessons learned from pile performance on temporary moorings may not be directly applicable to permanent oil and gas mooring applications.



Figure 74 left) fabricated pad-eye for temporary moorings and right) typical cast pad-eye for permanent moorings.

Globally, the industry methods to analyse mooring line and suction anchor performance during extreme loading conditions have therefore not been proved wrong by the Jim Thompson rig mooring performance during Hurricane Ivan.

5.5 Performance of gravity anchors, OMNI-Max[®] Mk1

OMNI-Max[®] Mk1 anchors were put to the test during Hurricane Gustav on the Transocean Amirante rig (ABS, 2012). These anchors are omni-directional gravity-installed plate anchors. They are released about 50m above the seafloor and self-embed into the seabed (Figure 75) (Shelton, 2007).

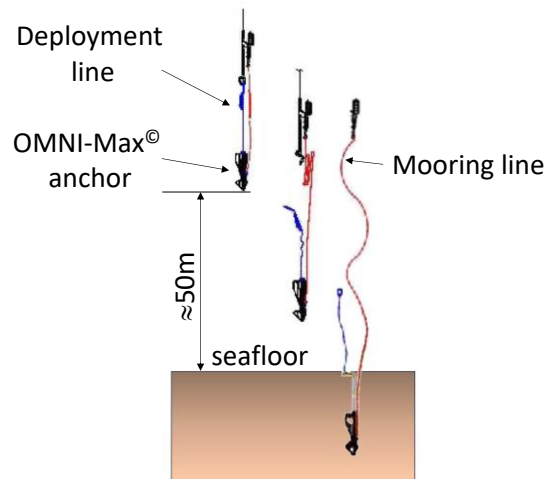


Figure 75 Simplified OMNI-Max[®] installation sequence (Modified from Shelton, 2007)

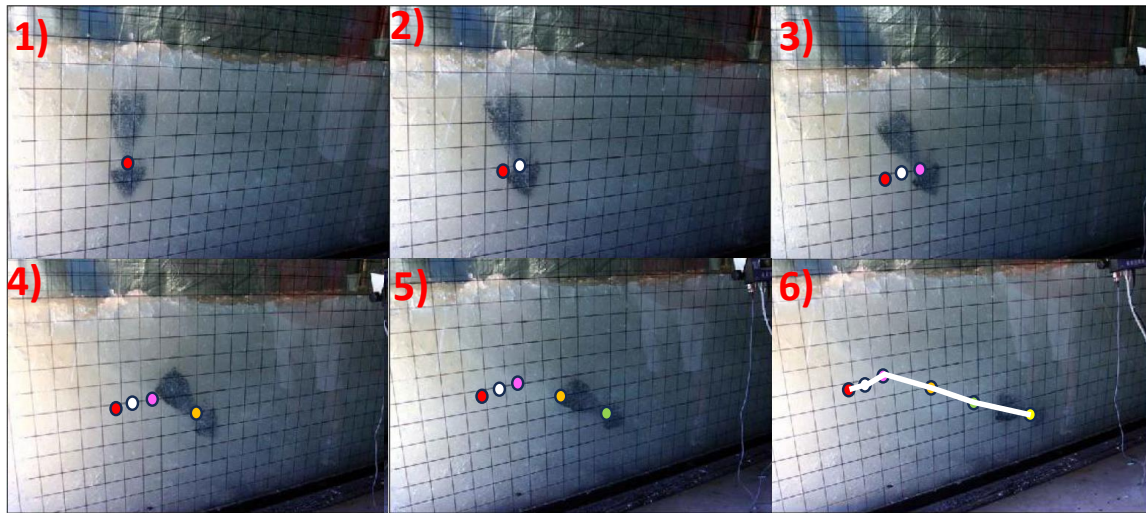
The padeye is attached to a swivelling mooring arm which can freely rotate along the axis of the anchor and re-align itself with the load direction (Figure 76).

By proper sizing of the top fin, bottom fin, and the mooring arm length, the anchor will dive deeper into the seabed once its capacity has been exceeded, as confirmed by laboratory tests in laponite (Figure 77, Shelton, 2007).



Typical length overall: $\approx 9.1\text{m}$; Weight (dry): $\approx 39\text{t}$

Figure 76 Typical OMNI-Max[®] Mk2 anchor (picture from <https://delmarsystems.com/products/anchors/omni-max/>).



● ○ ● ● ● ● Trajectory of load attachment point with load sequence 1 to 6

Figure 77 Illustration of OMNI-Max[®] anchor keying and diving behavior upon loading (modified from Shelton (2007)).

The omni-directional loading capability allows the foundation to withstand loading from nearly any direction which, in theory, allows for damaged mooring systems to survive longer during an extreme event.

The pre and post Hurricane Gustav rig mooring pattern is shown on Figure 78.

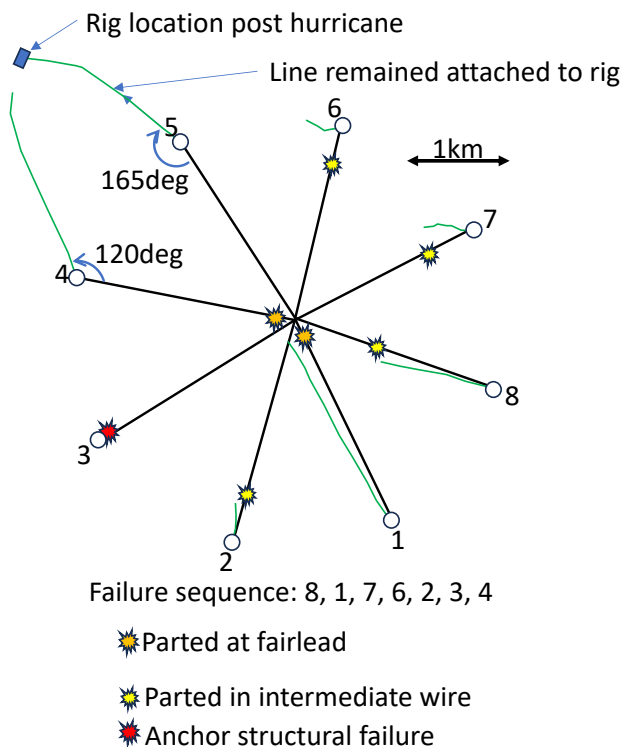


Figure 78 Installed (black) vs post Hurricane Gustav (green) mooring pattern (modified from Zimmerman et al. (2009)).

The rig was found about 3.7km northwest of its original location attached to only one of the eight anchors (Line #5) (Zimmerman et al., 2009). The first lines to fail (Lines #8, #1, #7) broke at the fairlead or in the intermediate wire as the anchors were loaded close to in-line conditions. It is noteworthy that Line #4 broke at the fairlead even after it had sustained a 120deg rotation (i.e. out-of-plane anchor loading) and that Line #5 remained attached to the anchor even after a rotation of 165deg.

Once the first four lines broke, the rig left its original pattern and the inertia of the rig could have shocked load one or more of the anchors (Zimmerman et al., 2009), including Line #3 where the anchor is suspected to have failed under such high shock loading (ABS, 2012).

The anchors pre and post event penetration below seafloor were included in Zimmerman et al. (2009), along with the loads calculated from hindcast analyses, as per Table 10.

The hindcast and field data suggest that the anchors were over-loaded by 36% to 44% above their initial capacity, which caused them to dive and embed an additional 7.0m to 19.2m, or roughly 0.75 to 1.1 times their length.

Table 10 Summary of OMNI-Max[®] anchors performance during Hurricane Gustav (modified from Zimmerman et al. 2009).

Anchor	Installed penetration (m)	Post hurricane penetration (m)	Estimated capacity (MN)	Estimated maximum anchor load (MN)	Ratio maximum Load/Capacity	Additional embedment during hurricane (m)
1	16.5	23.5	2.5	3.6	144%	7.0
2	16.5	32.9	3.4	4.9	144%	16.4
3	15.9	35.1	3.9	5.5	141%	19.2
4	17.7	36.6	3.4	4.8	141%	18.9
5	16.5	19.2	2.2	3.0	136%	2.7
6	16.8	26.5	2.7	3.9	144%	9.7
7	18.3	31.1	2.8	4.0	143%	12.8
8	16.8	29.0	3.0	4.2	140%	12.2

5.5.1 Learnings

The OMNI-Max[®] Mk1 anchors performed as designed, by embedding deeper once their initial capacity was exceeded. Two anchors experienced changes in load direction of about 120deg and 165deg without losing significant capacity.

The failure mechanism of Anchor #3 has not been released. The structural design of the Mk1 anchors has been modified in the subsequent Mk2 and Mk3 versions, including a cast core and arm, an increased weight, and a structural capacity in line with the geotechnical capacity in typical GoM soils, as shown on Figure 79 (Delmar, 2024). The Mk1 version is no longer available



Figure 79 Comparison of OMNI-Max[®] Mk2 and Mk3 anchors (from Delmar, 2024).

5.6 Overall learnings and conclusions

Prior to 2004, temporary MODU mooring systems in the GoM needed only to be designed to 10-year environmental load conditions. As a result of the mooring performance described in this paper, this requirement has been updated and the return period of the hurricanes for mooring survival conditions is now determined through a mooring-specific risk assessment and ranges between 5 years and 25 years for rigs operating during the hurricane season (API 2SK, 2024).

The most striking conclusion when analysing the mooring failures is the fact that, for the 157 No. mooring lines that failed, failure of the mooring system typically initiates with failure of the first line at the fairlead under anchor in-line loading conditions. About 75% of the line failures occurred at, or close to, the fairlead without resulting in a dragged mooring component on the seafloor (ABS, 2012).

Overall, conventional DEA anchors behaved as expected. They experienced in-plane failures (i.e. they dragged) but no suction caissons failed in this manner:

- 27% of the conventional DEA dragged but the anchors eventually regained enough capacity to stop the rig or break the mooring line.
- 2 No. suction piles had indications that the geotechnical capacity was almost entirely mobilized as evidenced from soil disturbance around the anchors and soil depression on the back side of the anchors.

OMNI-Max[®] Mk1 anchors also behaved as expected, experiencing increased penetration as they were loaded beyond their capacity. They also retained enough capacity under severe out-of-plane loading (up to 120deg) to force the failure in the mooring line, except for one anchor which failed structurally.

Structural failures were also experienced at the padeye by 4 No. suction piles under out-of-plane loading angles up to 45 degrees.

Last, none of the Stevmanta[®] anchors used were installed in VLA mode and all had non-shearable pins which made them behave as conventional DEA. Four of them had their shank chains disconnected under reverse loading, as designed for these temporary mooring applications.

Consequently, increasing the capacity of anchors under in-line loading conditions will have very little

effect on reducing the probability of a mooring failure. However, once several lines in the mooring system break and the rig begins to move off station, the remaining lines start loading the anchors at an angle to the plane of the intended loading.

With a focus on anchor design, the most effective way to reduce the likelihood of the rig losing all its mooring is to improve the geotechnical and structural capacity of the anchors under out-of-plane loading conditions.

6 FIXED STRUCTURES PERFORMANCE IN GULF OF MEXICO HURRICANES

Sixty fixed platforms were destroyed in 2008 by Hurricanes Gustav and Ike (1 in Gustav, 59 in Ike), as officially tallied by MMS (2008). Destroyed platforms included jackets and free-standing caissons that were completely toppled with no part of the structure remaining above the waterline or severely leaning or damaged platforms which, although still standing, were considered beyond repair and destroyed. An additional 31 platforms sustained extensive damage and another 93 sustained moderate damage (MMS, 2008).

Over 300 platforms in total have been destroyed by hurricanes since 1948 (Energo, 2010). The reported damage in almost every case was failure in the jacket tubular structure with only a few cases where the foundation was suspected to contribute to the failure.

Learnings from the performance of the pile foundations and the structures are now detailed.

6.1 Jacket piles performance

6.1.1 The OTRC (2009) study

OTRC (2009) analysed 13 platforms where the foundation was most likely to have been loaded beyond its capacity during Hurricanes Katrina, Rita, and Ike. The simplified plasticity model used to develop the foundation system capacity is shown on Figure 80. The model provides an upper-bound plastic collapse mechanism which occurs for the system when two hinges form in each of the piles and conductors due to translation and rotation of the platform base (Chen, 2011).

The platform fails in a shear, overturning, or combines shear/overturning mode depending on the relative magnitude of the shear and overturning moment experienced by the foundation (Figure 81). The shallower the water depth, the more likely the shear failure mechanism is.

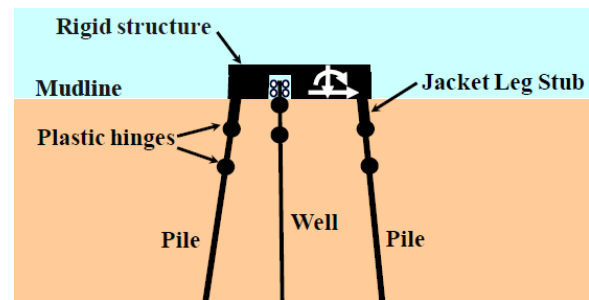


Figure 80 Simplified foundation collapse model (OTRC, 2009).

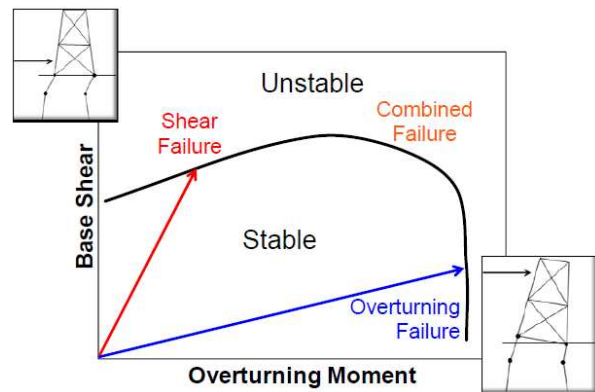


Figure 81 Simplified foundation collapse model (Chen, 2011).

The hindcast analyses showed that:

- For 5 out of 13 cases, foundation failure was neither observed nor predicted, even when the foundation capacity calculations did not include the well conductors.
- For 3 out of 13 cases, foundation failure was neither observed nor predicted, when the foundation capacity did include the well conductors. Failure was predicted without modelling the conductors.
- For 1 out of 13 cases, overturning failure was observed and predicted. The failure consisted of a pile axial pull-out of less than about 1m due to tension loads. When standard API RP 2GEO:2014 axial t-z springs with a residual factor of 0.8 are used, the calculated axial capacity is approximately equal to the hindcast hurricane load.
- For 2 out of 13 cases, no overturning foundation failure was observed although it was predicted. This discrepancy is most likely explained by the lack of site-specific soil boring for these two adjacent 1960 era jackets. The analysis was done using a 1979 boring about 900m away. The geological setting is complex with interbedded sands and clays strata being present and the stratigraphy at the boring may not be representative of that at the platforms. Additionally, the sand strata were characterised

only with driven penetration test and no CPT data are available, which precludes the use of modern CPT-based design methods. The capacity is therefore most likely underestimated, although conservatism in the design cannot be formally ruled out without acquiring a site-specific soil boring with modern techniques and using modern design methods.

- For the last 2 out of 13 cases, including Platform 31, no foundation failure was observed nor predicted, when the foundation was modelled realistically by:
 1. increasing the yield stress of the A36 steel pipe piles by 15% beyond the nominal values of 248 MPa,
 2. including the jacket leg stubs that extend below the seafloor in the structural model,
 3. and by using more realistic p-y curves than the cyclic curves of API RP 2GEO:2014.

The foundation system capacity diagram of Platform 31 in Gilbert et al. (2010) is reproduced in Figure 82 with additional data from Chen (2011). Note that the Ike hindcast maximum load is as per Chen (2011) and differs from the one plotted by Gilbert et al. (2010) due to updated load calculations post 2010.

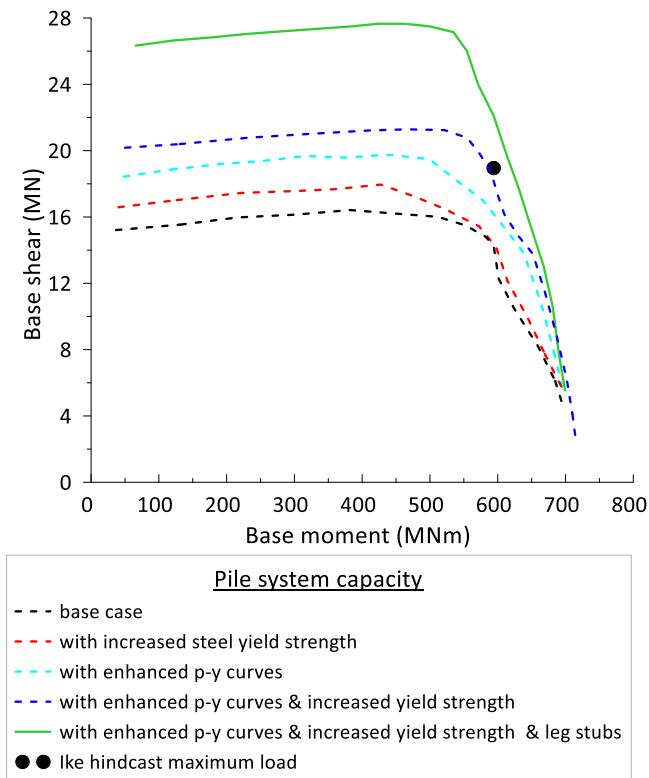


Figure 82 Pile system capacity and hindcast maximum load for Platform 31 during Hurricane Ike (modified from Gilbert et al., 2010, and Chen, 2011)

Figure 82 shows that leg stubs can greatly increase the lateral foundation capacity. They provide an enhanced connection with a much higher moment capacity between the leg and the pile and this does not allow the first plastic hinge in the simplified foundation collapse model to form at the seafloor. The first plastic hinge will typically form at the bottom of the leg stub, where the moment capacity reduces suddenly to the value of a regular pile section. As a result, the second plastic hinge will be pushed to a greater depth below the seafloor, thereby allowing the pile to mobilize more lateral soil resistance (Chen, 2011).

Platform 31 experienced a combined shear/overturning loading condition, and its survival can only be explained if the three above foundation model assumptions are made.

6.1.2 Learnings

The axial performance for the one case of predicted and observed overturning jacket piles failure under hurricane loads has therefore not shown the API RP 2GEO:2014 method for axial capacity in clays to be wrong. This is consistent with the fact that the soil properties at these platform sites (e.g. plasticity, OCR, strength) are within the range for which the method was originally calibrated (Jeanjean, 2012).

The following findings from OTRC (2009) were also reported in Gilbert et al. (2010) and are now included in ISO 19901-4:2025:

- When performing assessment, include all tubular members below seafloor (i.e. piles, conductors, and jacket leg stubs)
- Use unbiased values rather than low estimates of steel yield strength (e.g. increase nominal yield value by 15%).
- Do not use the API RP 2GEO:2014 cyclic curves and use enhanced p-y curves for the lateral pile-soil modelling. Such curves were developed in the years after the OTRC (2009) publication and are now included in ISO 19901-4:2025.

The assessment of existing platforms should not therefore be performed using the same assumptions and input parameters used in design. Design activities focus on ensuring that every structural component remains within its elastic range whereas assessment activities aim to estimate the ultimate capacity of the structure system with an understanding of its failure mechanism and its weakest link so that effective remediation measures can be implemented, if necessary.

The above discussion focused solely on the performance of the foundation and examples of the

combined performance of the jacket tubular truss and piles are now analysed.

6.2 Jacket structural performance in Hurricane Ike

The SS-Platform is located in 31.4m of waters in the West-Central region of the GoM and was damaged during Hurricane Ike. It comprises two (2) 4-pile jackets, connected above the waterline, which were installed in 1969 and 1972. The foundation includes 0.9m and 1.07m diameter piles penetrating 54.8m into the seabed (Figure 83).

EnergO (2019) performed structural analyses using computer models developed in CAP (Capacity Analysis Program, CAPFOS Inc.) using available platform data. CAP is an advanced offshore structural analysis program developed for nonlinear static and dynamic pushover analyses under the effect of wave, earthquake, and wind loadings. Compared to other industry software packages, CAP provides more options for special analysis elements, especially for pile-soil interaction, and modelling techniques tailored for more advanced users

6.2.1 Damages after Hurricane Ike

The platform was surveyed after Hurricane Ike and damages were concentrated on the 1969 jacket truss

structure, including joint failures, and damaged and buckled members (Figure 84). The 1972 jacket included improved structural design, and no damage was observed on that side of the platform (EnergO, 2019).

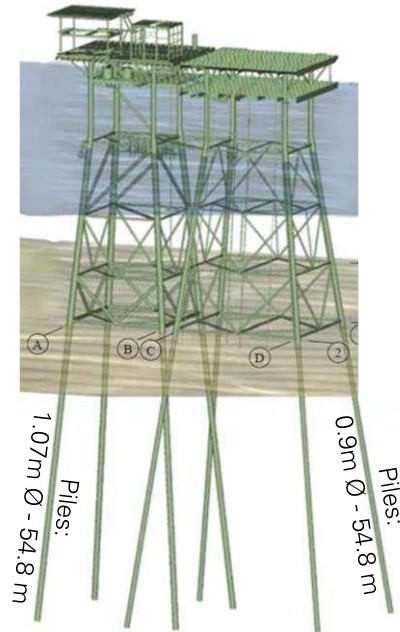


Figure 83 Schematic of SS-Platform. Left jacket installed in 1972, right jacket installed in 1969. (modified from EnergO, 2019)

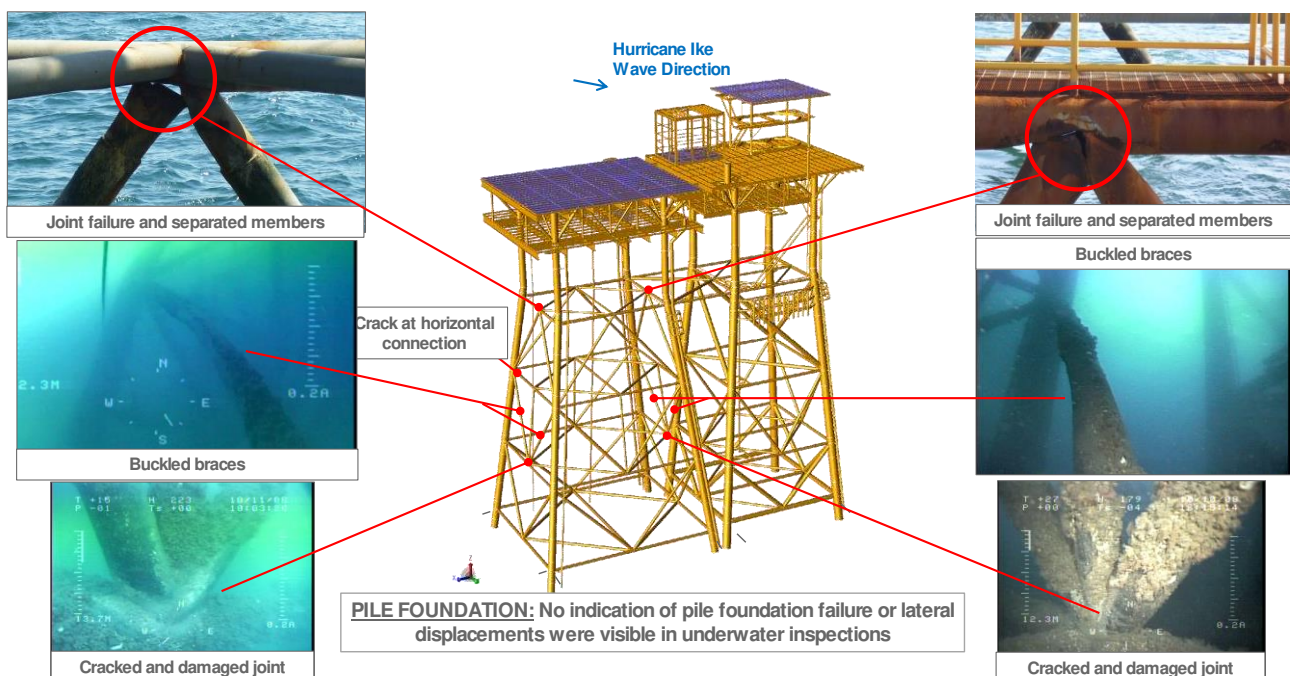


Figure 84 Summary of SS-Platform damages after Hurricane Ike (modified from EnergO, 2010, 2019)

6.2.2 Soil properties

No site-specific boreholes are available and a borehole approximately 610m away from the

platform location was used in the original design. It was collected in 1979 and included 63.5mm diameter percussion samples, on which UU and MV tests were performed. ISO 19901-4:2025 requires the use of

shear strengths measured in DSS testing on modern samples, 75mm in diameter, acquired by push or piston sampling.

The original tests results were converted to DSS values as follows. The UU and MV strengths on 63.5mm percussion samples were first converted to equivalent UU strength values that would have been obtained on 75mm pushed samples using the recommendations of Young (1919) and Young et al. (1983). These values were then converted to DSS values using the recommendations of Cheon et al. (2015). The strength measured on 63.5mm percussion samples were therefore converted to equivalent DSS strength on 75mm pushed samples using the combined multiplication factors of Table 11.

Table 11 Strength conversion factors for 1979 soil boring.

Test type	Factor to convert from 63.5mm percussion sample to UU on 75mm pushed sample	Factor to convert to DSS strength	Combined conversion factor
UU	1.4 ¹⁾	1.2	1.68
MV	1.1	1.2	1.32

Note 1) For samples with a blow count less than 3, a percussion to push sample factor of 1.2 was used due to their potentially lower sample disturbance.

The best-estimate strength profile used in the hindcast is shown on Figure 85.

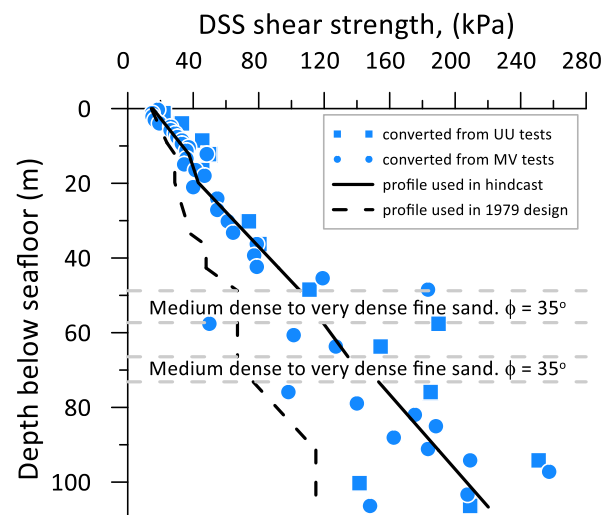


Figure 85 Best-estimate soil profile used in hindcast of SS-platform

Figure 86 compares the re-interpreted soil boring data and best-estimate DSS profile with 3 other available soil borings collected with push samplers within 5km of the platform. It confirms that, although

no site-specific data are available, the strength properties in the top 25 pile diameters over the area of interest are consistent with the soil strengths used in the hindcast.

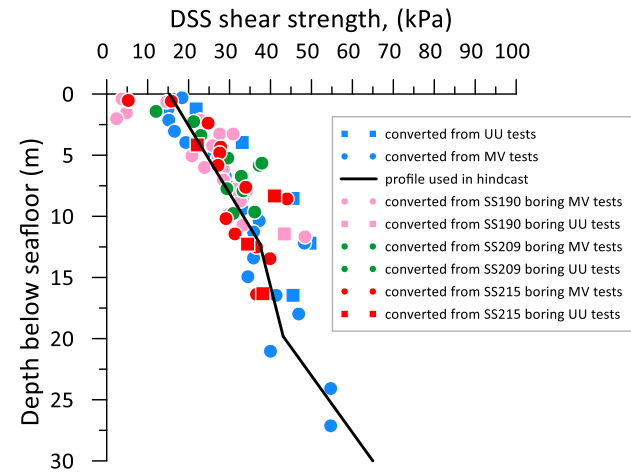


Figure 86 Best-estimate soil profile used in hindcast of SS-platform with data from nearby borings

Because the analyses are performed in the time domain, the unload-reload behavior of the soil needs to be defined. The hysteretic behavior of the soil adopted by the CAP program is illustrated on Figure 87. The first quarter cycle is defined by the ISO 19901-4:2025 backbone p-y curves. The unload-reload loop follows the first Masing rule (Masing, 1926) which states that the unload modulus is initially equal to the virgin load modulus, but it does not follow the second Masing rule which states that the first quarter cycle is then scaled by a factor of 2 on both the horizontal and vertical axes. It is well known that such a loop overpredicts hysteretic damping in soils. The loop in CAP roughly follows a modified second Masing rule with a scaling factor of 2 on the Y-axis and a scaling factor of 1.15 on the X-axis (Figure 87).

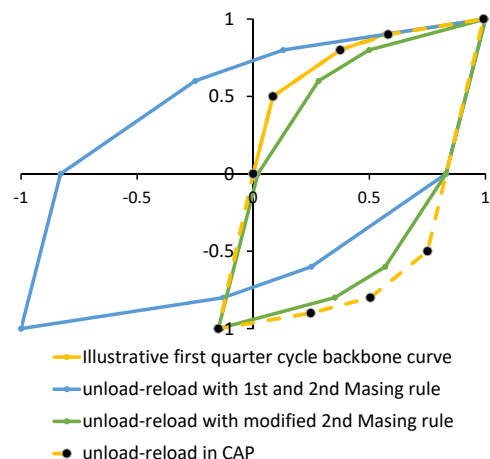


Figure 87 Soil unload-reload behavior in CAP software

6.2.3 Results and learnings

The hurricane maximum wave, including wave-in-deck loads, was run dynamically through the platform for multiple wave cycles. The expected jacket performance was believed to be close to the condition at the end of wave cycle #2 (Energo, 2019).

The hindcast was run with two foundation models: the first one used the static p-y curves of ISO 19901-4:2016, which are the same as those of API RP 2GEO:2014, and the second one used the stiffer cyclic p-y curves of ISO 19901-4:2025.

A noteworthy difference between the two hindcasts is the predicted pile head lateral displacements vs time for the 1969 East jacket piles (Figure 88). At the end of Cycle 2, the hindcast with the ISO 19901-4:2016 curves predicts a permanent displacement of 0.4m, whereas this displacement is only 0.12m with the ISO 19901-4:2025 curves, which is more consistent with the fact that no noticeable permanent displacements of the piles were noted during underwater inspections of the platform.

With the stronger ISO 19901-4:2025 p-y curve, the East jacket structure was predicted to experience more damage (three buckled struts vs two) (Figure 89). This additional buckled strut was indeed observed to be damaged (Figure 90), therefore

confirming that the use of these stronger p-y curves results in damages more consistent with observations, both in the jacket structure and the at the pile head. They therefore have not been proved wrong by the performance of this structure.

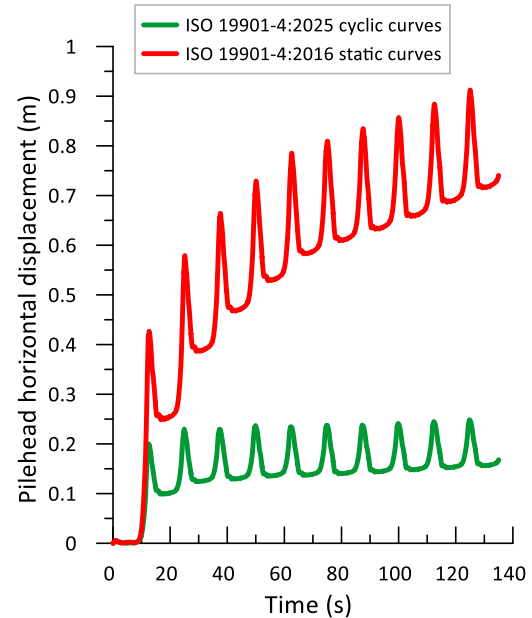


Figure 88 Pile head displacement vs time for two hindcasts

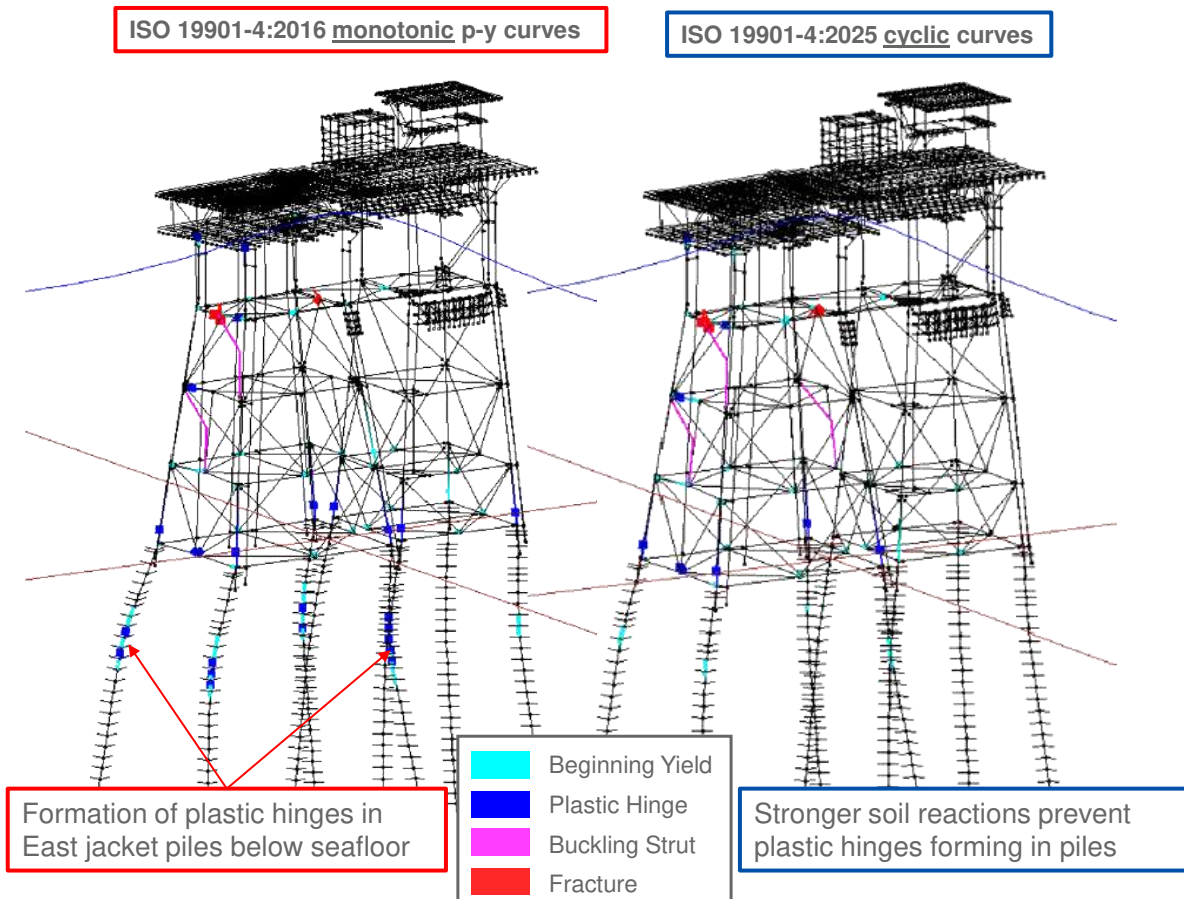


Figure 89 Comparison of hindcast damage for SS-platform for two sets of p-y curves (modified from Energo, 2019)

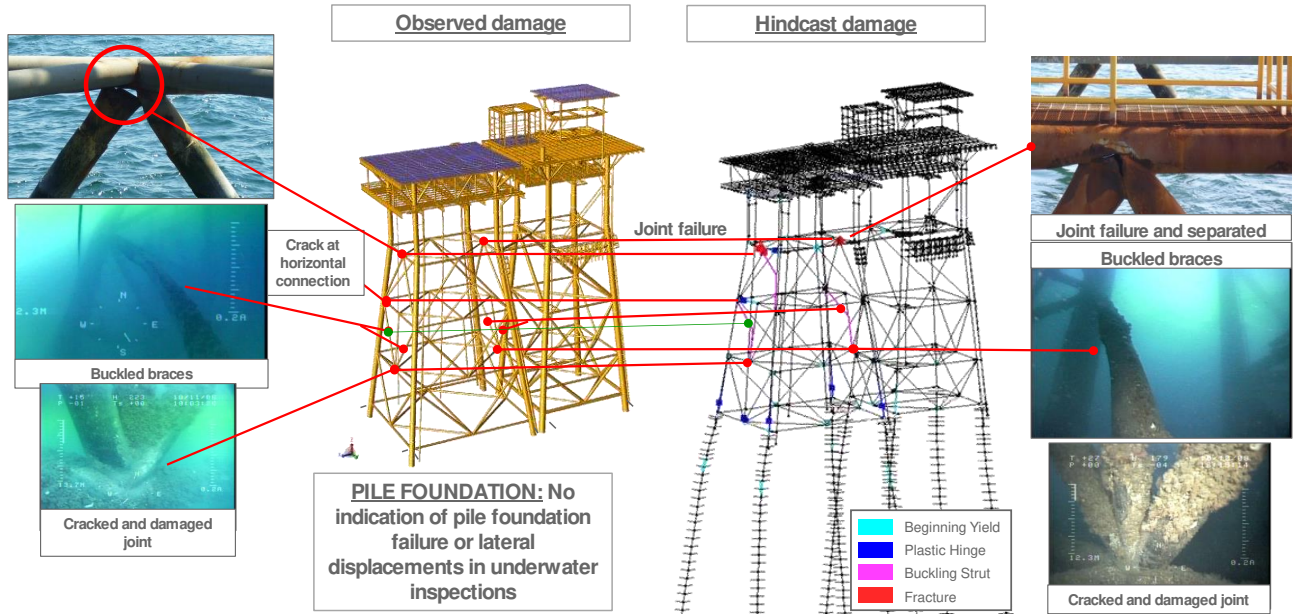


Figure 90 Comparison of SS-platform observed damage and damage hindcast with ISO 19901-4:2025 cyclic p-y curves

6.3 Free-standing caisson performance in Hurricane Andrew

A free-standing caisson is a minimum single column platform often used in the GoM to develop marginal fields. The topside is often limited to a single wellhead. The SS-caisson, installed in 1983, was damaged during Hurricane Andrew and was found leaning at an angle of 15deg at the waterline (Energo, 2019). The lateral performance of this caisson was again hindcast using the ISO 19901-4:2016 static p-y curves and the ISO 19901-4:2025 cyclic p-y curves.

The findings of the hindcast were published in Energo (2019), API 2PY (2020), and Wu et al. (2020).

The caisson sat in a water depth of 16.2m and was supported by a single 1.2m diameter pile penetrating 29m into the seabed (Figure 91).

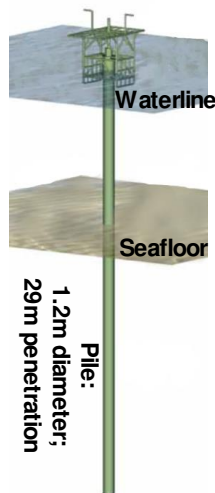


Figure 91 Schematic of free-standing SS-caisson (modified from Energo, 2019)

6.3.1 Soil conditions

The site lies on the continental shelf. During each glaciation period of the Pleistocene epoch (last 1.2 million years) great portions of the shelf were exposed, subjected to desiccation, oxidation, erosion, entrenchment of streams which crossed the exposed shelf, and subsequent burial of each older surface. Therefore, as many as four sequences of deltaic-marine deposition may lie of top of each other beneath the present continental shelf (McClelland Engineers, 1979).

The sediments consist of fined grained material. A site-specific soil boring was acquired in 1982 and 57mm percussion samples were collected on which UC, UU, and MV tests were performed. ISO 19901-4:2025 requires the use of shear strengths measured in DSS testing on modern samples, 75mm in diameter, acquired by push sampling. The original tests results were transformed to DSS values by first converting the UU, UC, and MV strengths on 57mm percussion samples to the equivalent UU strength values that would have been obtained on 75mm pushed samples using the recommendations of Young (2019) and Young et al. (1983). These values were then converted to DSS values using the recommendations of Cheon et al. (2015). The strength measured on 57mm percussion samples were therefore converted to equivalent DSS strength on 75mm pushed samples using the combined multiplication factors of Table 12.

Table 12 Strength conversion factors for 1982 soil boring.

Test type	Factor to convert from 57mm percussion sample to UU on 75mm pushed sample	Factor to convert to DSS strength	Combined conversion factor
UU	1.4	1.2	1.68
UC	1.5	1.2	1.8
MV	1.1	1.2	1.32

The best-estimate strength profile used in the hindcast is shown on Figure 92. The various strength measurements were converted to DSS strength values as per Table 12.

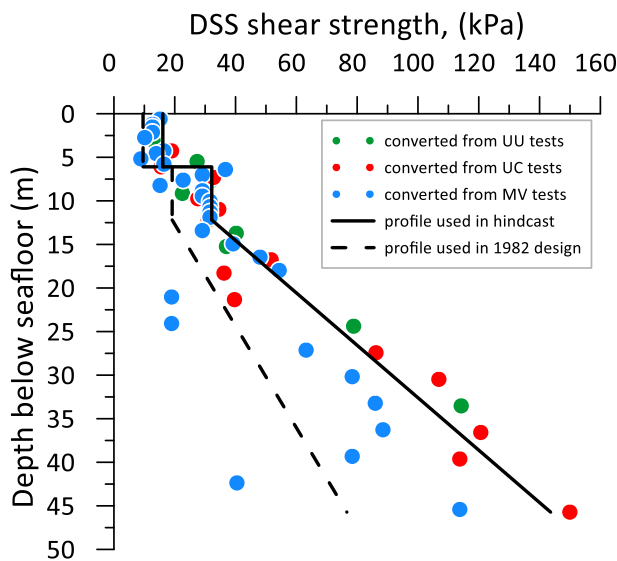


Figure 92 Best-estimate strength profile for caisson hindcast

6.3.2 Hindcast results

Details of the structural modelling and metocean hindcast can be found in Wu et al. (2020). The caisson elevation above the waterline was relatively low and its topside was fully inundated by waves larger than 6m. The maximum hindcast wave height of 13m at the site therefore resulted in multiple cycles of maximum loads on the platform.

A time domain dynamic push-over analysis was performed where twenty cycles of the maximum wave were run through the platform. The base shear and caisson rotation throughout the 20 cycles were calculated and shown on Figure 93.

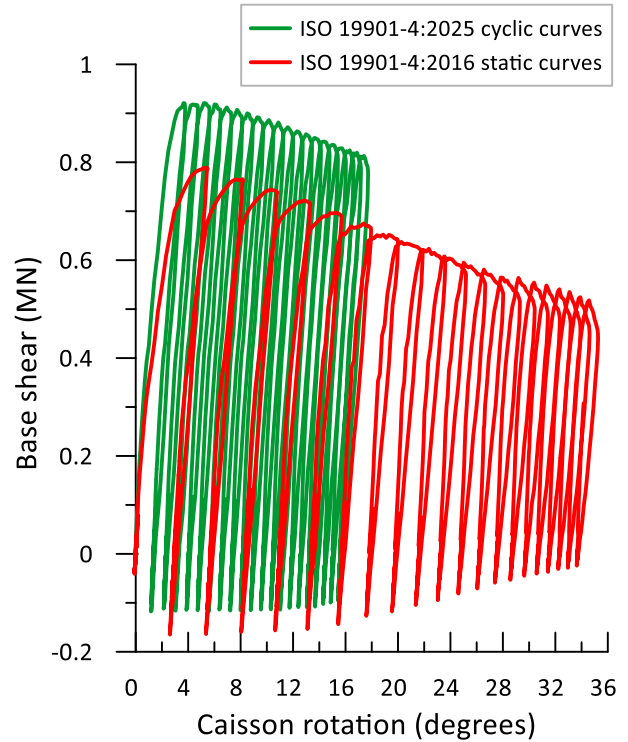


Figure 93 Hindcast of SS-caisson base shear and rotation during Hurricane Andrew (modified from Energo, 2019).

The deformation and plastic strains for the final cycle are shown on Figure 94. The model with the ISO 19901-4:2025 cyclic p-y curves predicts a final inclination of 16deg which is very close to the observed value of 15deg. The plastic hinge in the pile is higher than with the ISO 19901-4:2016 model because the predicted soil resistance is greater, and the maximum bending moment occurs at a shallower depth below the seafloor.

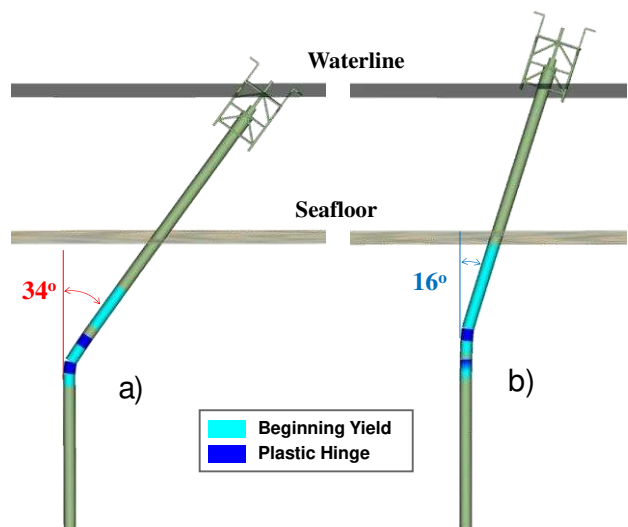


Figure 94 Hindcast of SS-caisson final inclination and plastic hinges with a) ISO 19901-4:2016 static p-y curves and b) ISO 19901-4:2025 cyclic p-y curves (modified from Energo, 2019).

6.4 Learnings

The performance of free-standing caissons and jacket structures and their foundation piles during GoM hurricanes can be accurately analysed if appropriate foundation models are used. The predicted foundation performance and jacket structural damage of these case records were consistent with and closely matched the observations

This experience has therefore not proved the latest soil models and guidance in ISO 19901-4:2025 to be wrong.

Managing the structural integrity of existing and aging platforms is critical to justify their life extension beyond the duration of the original design. It is crucial to not only accurately calculate the ultimate capacity of the structure but also predict the right failure mechanism and identify its weakest components so that, if the capacity of the platform needs to be enhanced, these critical components (e.g. members, joints, braces) can be effectively strengthened.

7 PERFORMANCE OF TRIPOD AT FATIGUE LIMIT STATE

The natural period of a tripod structure located in the West-Central region of the GoM in a water depth of 37m was measured under low sea states with wave heights less than 1.3m. The structure is supported by three 0.91m diameter piles embedded 84.1m in clay sediments (Figure 95).

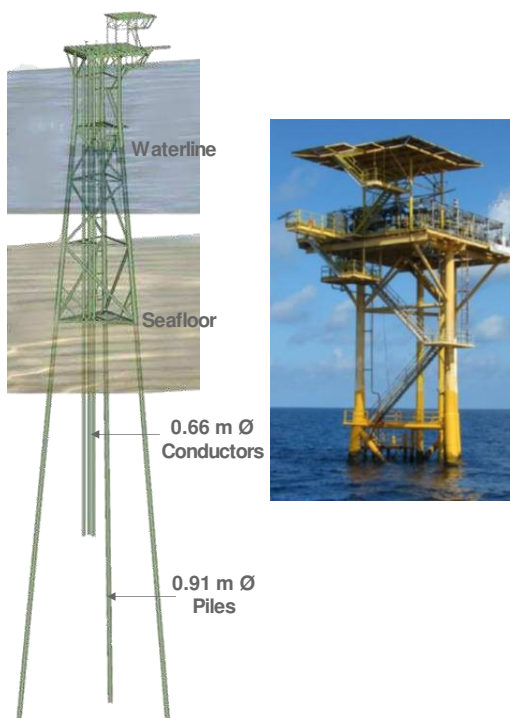
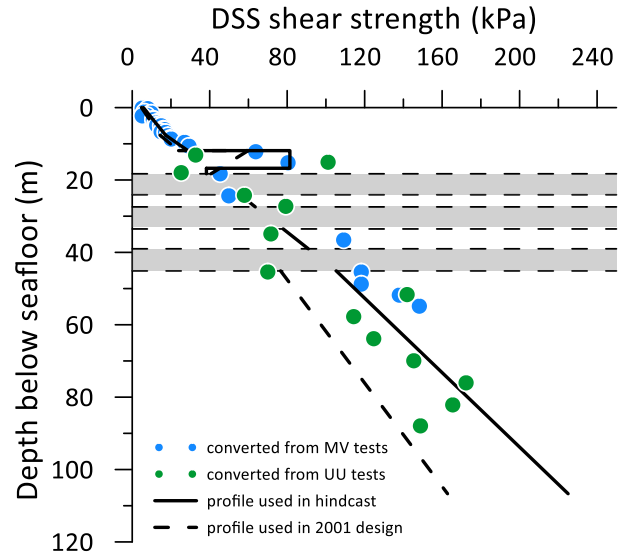


Figure 95 EI tripod structure and model (modified from Energo, 2019)

7.1 Soil profile

A site-specific boring was obtained for the original pile design and strength values measured in MV and UU test were converted to DSS strengths with a multiplication factor of 1.2. The profile used in the hindcast is shown on Figure 96



■ silty fine sand; $\phi = 30\text{deg}$; $\delta = 20\text{deg}$; $f_{\max} = 81\text{kPa}$

Figure 96 Soil profile for EI tripod

7.2 Hindcast results

A natural frequency analysis was performed to extract eigen values frequencies and mode shapes of the structures. The analysis was repeated twice with two different lateral p-y curves formulations. The ISO 19901-4:2016 static p-y curves were used for the first model because this code does not include recommendations for fatigue analyses. The second model used the ISO 19901-4:2025 curves specifically formulated for fatigue analyses. The springs in the axial direction were developed using ISO 19901-4:2016 for both models.

Three dominant vibration modes and natural periods in the X-sway, Y-sway, and torsional modes were extracted and compared to the measured values in the field as per Table 13 and Table 14.

Table 13 Hindcast and measured natural periods for EI tripod.

	Natural period (s)		
	X sway	Y-sway	Torsion
ISO 19901-4:2016 static p-y curves	1.13	1.13	0.83
ISO 19901-4:2025 fatigue p-y curves	1.08	1.07	0.75
Field measurements	1.07	1.00	0.76

Table 14 Difference between hindcast and measured natural periods for EI tripod.

	Difference from measurements (%)		
	X sway	Y-sway	Torsion
ISO 19901-4:2016 static p-y curves	12.1	13.0	9.2
ISO 19901-4:2025 fatigue p-y curves	1.0	7.0	-1.3

7.3 Learnings

The analyses show that the impact of the p-y curves is not constant and depends on the level of mobilisation of the piles in the lateral direction. The fatigue p-y curves of ISO 19901-4:2025 provide a much improved hindcast, within 1% of measurements in two out of three directions, when compared to those of ISO 19901-4:2016 which differed by more than 10% from the measurements. The fatigue p-y curves of ISO 19901-4:2025 have therefore not been proved wrong by these measurements.

8 PERFORMANCE OF DRILLING RISER AT FATIGUE LIMIT STATE

8.1 Introduction

A deepwater drilling riser system includes many sub-systems, as depicted on Figure 97 and its design includes the assessment of the fatigue life of each of these components. Although the geotechnical engineer can only be focused on the behavior of the conductor since it is the only component in direct contact with the soil, critical fatigue hot spots can occur at other locations above the seafloor such as BOP-to-wellhead and casing connectors or welds.

These hot spots can be affected by the soil-conductor interaction model. For these fatigue analyses, two models were developed by Zakeri et al. (2015) and are now included in ISO 19901-4:2025. The models use equivalent linear springs at steady-state, sometimes associated with dashpots (Figure 97).

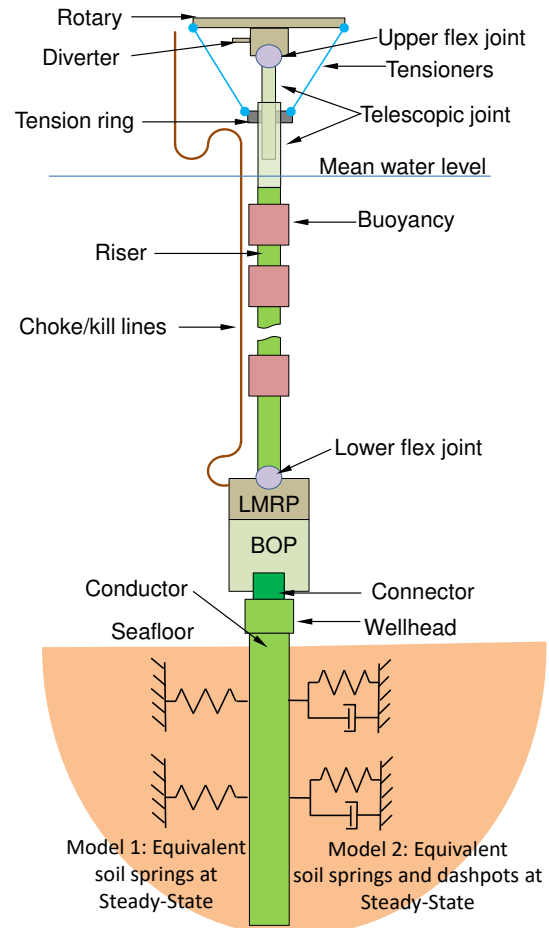


Figure 97 Schematic of deepwater drilling riser system and soil-structure modelling - not to scale (modified from Zakeri et al, 2015).

8.2 Fatigue analyses and field monitoring

Fatigue analyses first include a global analysis where each component of the system of Figure 97 is modelled with a series of sections characterized by their mass, axial stiffness, bending stiffness, torsional stiffness, and hydrodynamic properties. FE models then calculate forces and displacements along the entire system.

To verify fatigue calculations, LMRP and BOP are instrumented during drilling operations with accelerometers. Subsea data logger acquisition systems with acoustic modems transmit the data to the surface facility for processing and analysis (Kannala et al., 2016) (Figure 98).

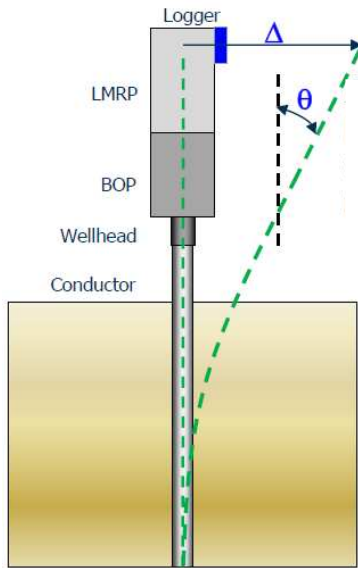


Figure 98 Schematic of deepwater drilling riser system instrumentation (from Kannala et al., 2016).

An example of such monitoring results is given for a deepwater well for which angle and displacement time traces at the top of the LMRP were derived from the acceleration data. They were also numerically extracted from pluck test FE analyses using the fatigue soil-conductor framework of ISO 19901-4:2025.

Figure 99 shows the comparison between measured and calculated displacements for a small amplitude event using a low estimate soil profile. The stiffness ratio, i.e. the ratio of lateral displacement, Δ , over rotation angle, θ , in the X-direction was predicted to be 0.41m/deg but was measured to be only 0.34 m/deg, thereby indicating that the measured response was stiffer than predicted.

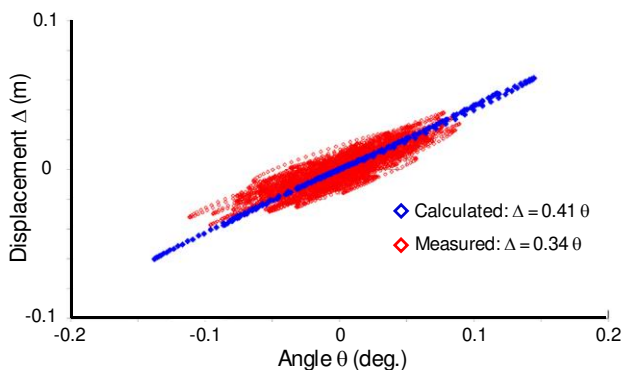


Figure 99 Comparison between measured and calculated riser motions for a small environmental event with low-estimate soil properties (modified from Kannala et al., 2016).

Figure 100 shows a similar comparison for a VIV fatigue-critical environmental event. The predicted

stiffness ratio, using a best estimate soil profile, is now matching the measured value of 0.41m/deg.

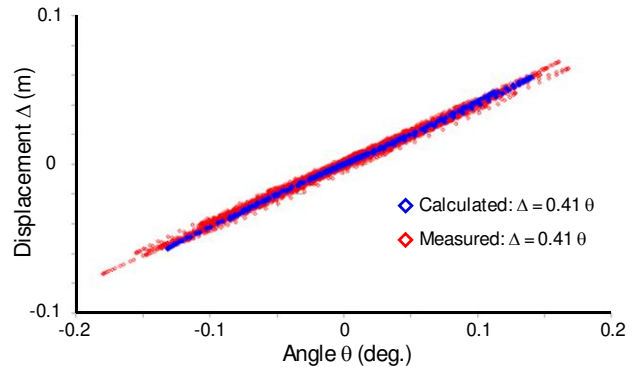


Figure 100 Comparison between measured and calculated riser VIV motions with best-estimate soil properties (modified from Kannala et al., 2016).

Another riser system monitoring case record from Mercan et al. (2015) provides similar conclusions. The ISO 19901-4:2025 framework provides a much improved match with the measured data, if used with best-estimate soil properties, while the current ISO 19901-4:2016 recommendations underestimate the system stiffness and overestimate its displacements.

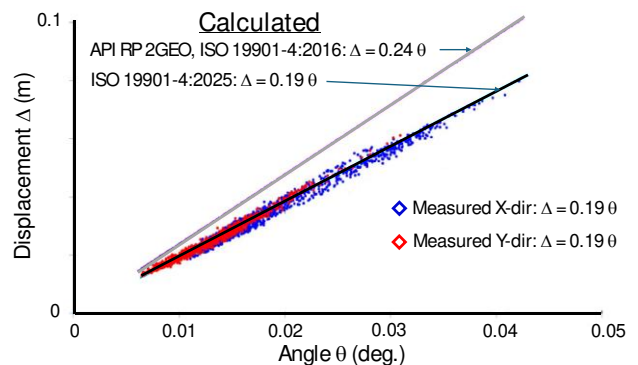


Figure 101 Comparison between measured and calculated riser motions with two soil spring models (modified from Mercan et al., 2017).

8.3 Learning

When used with best-estimate soil properties, the framework of Zakeri et al. (2015) to model soil-conductor interaction for fatigue analyses, as implemented in ISO 19901-4:2025, has not been proved to be wrong by the reported field instrumentations.

The soil model can have a large impact on the calculated fatigue life. In the case investigated by Mercan et al. (2017), the fatigue life estimated when using the ISO 19901-4:2016 framework was overestimated by a factor of 20 for the parts of the conductor and casing above the seafloor and was underestimated by a factor of 4,000 for the parts below

the seafloor. Therefore, one model is not more “conservative” than the other and the current ISO 19901-4:2016 model can be both “conservative” and “unconservative” at the same time, depending on which component of the system is of interest.

9 PERFORMANCE OF MAGNUS JACKET PILE AT SERVICEABILITY LIMIT STATE

9.1 Introduction

The Magnus jacket structure sits in Block 211/12 of the Northern North Sea in 186m of waters. It is supported by four groups of nine 2.134m (86in) diameter piles with an average penetration of 85m BSF and a constant wall thickness of 63.5mm above the driving shoe (Sharp, 1993).

When the platform was installed in 1982, design methods used for offshore foundations were extrapolated from onshore experience although the pile size was very much larger. It was decided to monitor the performance of the foundation system of one leg of the platform, leg A4, to verify the design methods (Figure 102).

The objectives included the measurements of the environmental load acting on the pile group during storms, the proportion of the load taken by the mudmats and by the piles, and the distribution of axial and lateral loads along the piles. The cost of the project was GBP 2.8m in 1982 (Sharp, 1993) or roughly GBP 10m (US\$12.6m) in 2025 money.

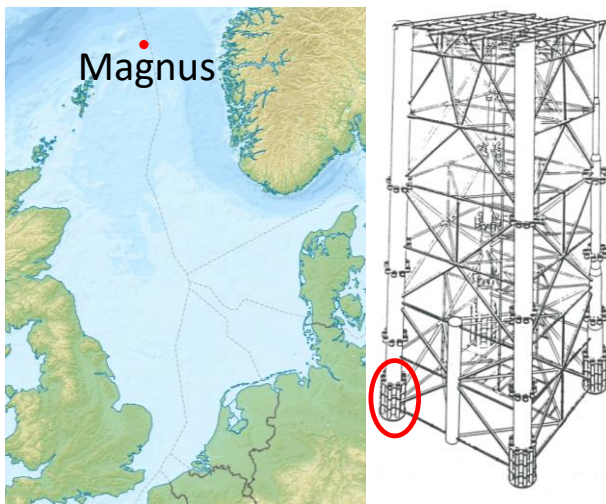


Figure 102 Magnus jacket and Leg A4 instrumentation

Instrumentation which included accelerometers, strain gauges, and mudmat pressure cells was installed on the jacket leg/mudmat/piles system and monitoring

took place continuously between August 1982 and April 1985 and over the 1985/86 winter.

Accelerometers data were used to obtain displacements and rotations at the seafloor. The two most severe storms occurred on 22 January 1984 and 10 January 1986 when significant wave heights of 10.7m and 12.6m were experienced respectively (Kenley and Sharp, 1993). For the 1984 storm the maximum peak to trough wave height was 17m (Horsnell et al., 1993).

9.2 Site Conditions

The site conditions consist mostly of very stiff silty clays. The upper stratum is believed to be a till 18kyears to 20kyears old deposited during the late Weichselian ice maximum. Overconsolidation of the till is probably due to desiccation rather than pre-loading. The thin units of fine to coarse sand with fine gravel at about 12m and 20m are probably erosion channel deposits formed about 25kyears ago. Below the sands to about 50m penetration is a pre-loaded glacio-marine silty clay about 25kyears to 75kyears in age, which corresponds to the Weichselian interstadial complexes (Semple and Rigden, 1983).

9.3 Hindcast of measurements

Horsnell et al. (1993) performed a series of laterally loaded pile analyses to match the measured data (i.e. bending moment distribution along the pile and seafloor lateral displacements) and showed that the best match was obtained by:

- Modifying the soil strength to account for consolidation due to the weight of the structure
- Including the presence of the mudmat by incorporating additional Winkler springs
- Incorporating pile-mudmat interaction by using a “y-shift” approach
- Modelling a single pile with the lateral soil resistance p-y curves of Reese et al. (1975) with $\varepsilon_{50} = 0.5\%$
- Adjusting the pile head/leg fixity.

The shear strength profile used by Horsnell et al. (1993) was obtained from UU triaxial tests on 72mm thin wall pushed and hammered samples acquired between 1975 and 1981. It included the profiles prior to the installation of the platform and after the soil had consolidated under the weight of the structure, which was modelled as a pressure of 50kPa acting on the mudmats (Figure 103).

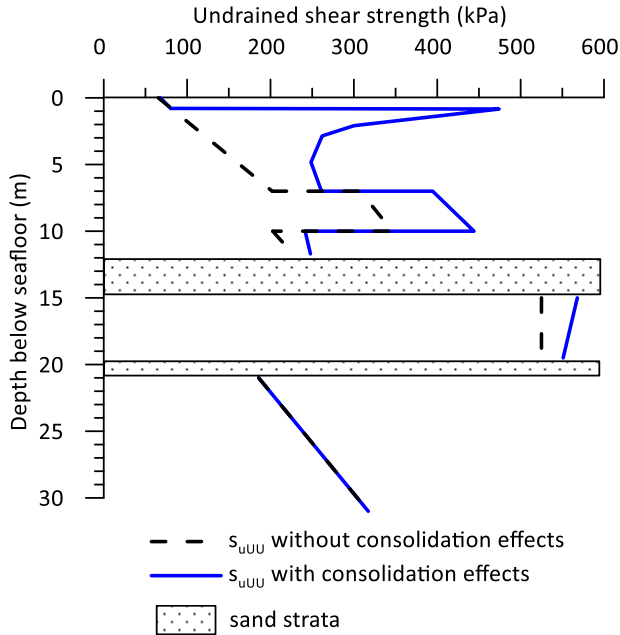


Figure 103 Shear strength profiles for Magnus jacket (Horsnell et al. 1993)

As per Figure 104, the best overall comparison resulted in a rotation at mudline of 0.34 milli-radians ($19.5 \cdot 10^{-3}$ degrees) and a mudline deflection of 4.1mm, which represents a low normalised displacement y/D of $4.1/2134 = 0.19\%$. These are surprisingly low numbers given the large wave (17m height) experienced by the platform.

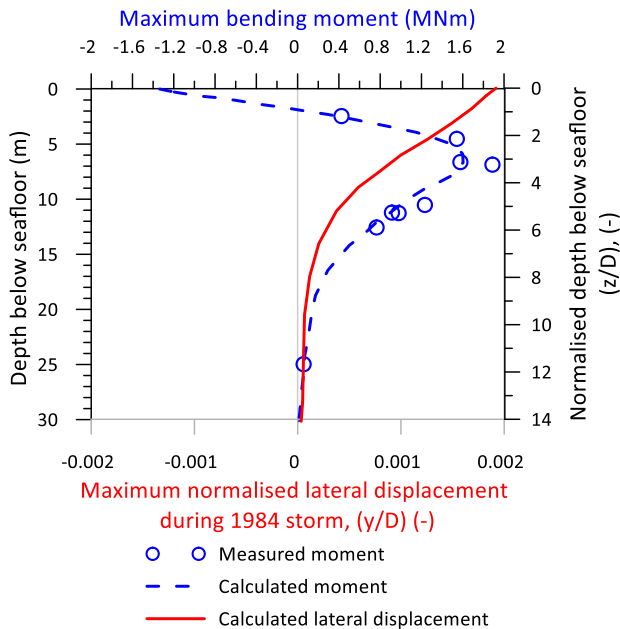


Figure 104 Pile monitoring results and hindcast (modified from Horsnell et al., 1993).

9.4 Comparison with ISO 19901-4:2025 methodology

This paper does not intend to hindcast the measured bending moment diagram as this would require a complex structural model but rather to compare the cyclic p-y curves generated with the new ISO 19901-4:2025 framework with those of the Reese et al. (1975) framework, which were determined to be a key input that gave the best match with the measured data.

The UU triaxial shear strength profile of Figure 103 must first be converted to values measured by the DSS tests, as required by ISO 19901-4:2025. Direct correlations between these two values are not widely published. From the North Sea database of Lunne et al. (1994), it can be deduced that s_{uUU} is about 0.5 to 0.8 times s_{uTC} . In addition, the worldwide database of offshore clays of DeGroot et al. (2019) suggests that s_{uDSS} is about 0.8 times s_{uTC} , which is consistent with the results of Liedtke et al. (2019) on Gulf of Mexico clays. The conversion factor from UU to DSS therefore ranges between 1.0 and 1.6 (0.8/0.5) and is strongly affected by disturbance of the sample when performing UU tests.

At the Magnus field, 21 No. isotropically consolidated triaxial compression tests were performed and reported by McClelland Engineers (1977). The ratio of s_{uTC} / s_{uUU} was 1.19 with a COV of 0.22. Using a ratio of 0.8 for s_{uDSS} / s_{uTC} , s_{uDSS} is essentially equal to s_{uUU} . This conversion factor of 1.0 falls at the low end of the range of published data. Therefore, the post-consolidation UU strength profile of Horsnell et al. (1993) (Figure 103) was taken as the DSS profile to calculate the cyclic ISO p-y curves, which were derived at arbitrary depths of 7m (3.3D), 9m (4.2D), 19m (8.9D), and 21m (9.8D) BSF using the Reese et al. (1975) method with $\varepsilon_{50} = 0.5\%$ and the ISO 19901-4:2025 method with the following input parameters:

- $I_p < 30\%$
- $OCR = 10$, except for the depth of 21m where $OCR = 4$
- API axial friction factor $\alpha = 0.47$, as the average factor calculated in the top 20D.
- Cyclic modification factors as per “North Sea stiff clays” conditions.
- Although ISO 19901-4:2025 suggests that gapping conditions should be used given the high values of the shear strength, non-gapping conditions were used because of the very small displacements mobilized during the storm. As explained by ISO, the development of a gap on the back side of the pile requires level of displacement

that are not believed to have been experienced during the storm.

The curves and the maximum mobilised displacement at the corresponding depths during the storm are shown on Figure 105. The normalised pressure vs normalised displacement curve of the Reese et al. (1975) method is unique because the p-y curves are all controlled by the deep failure mechanism and they all have the same moduli. They can therefore be normalised by $s_u D$.

The ISO normalised curves are not unique as they depend on OCR and tend to increase with depth as the cyclic effects diminish.

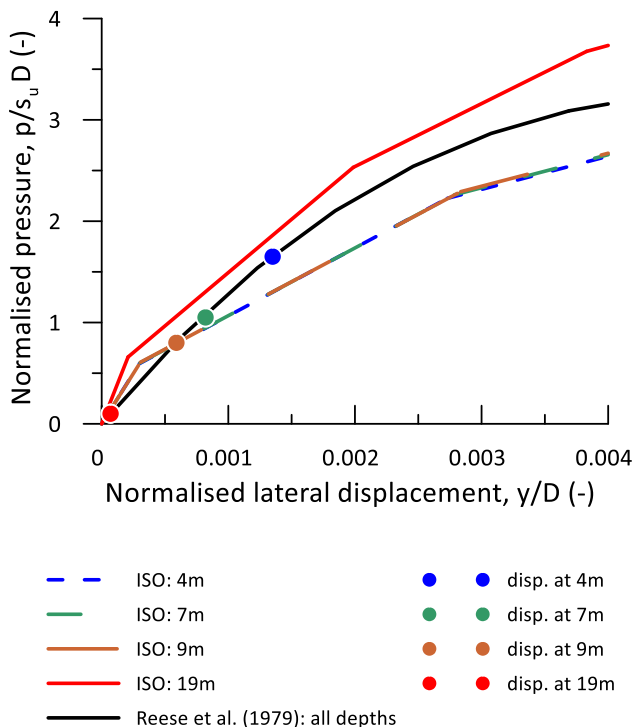


Figure 105 ISO and Reese et al. (1975) p-y curves with mobilized displacement at depths of 4m, 7m, 9m, and 19m

9.5 Learning

Figure 105 suggests that, for the very low displacements mobilised by the Magnus piles during the 1984 storm (i.e. $y/D < 0.2\%$), the cyclic p-y curves of ISO 19901-4:2025 are consistent with those of Reese et al. (1975), which were used by Horsnell et al. (1993) to obtain the most satisfactory hindcast of the measured field data.

Therefore, the new ISO method has not been proven to be wrong by the results of the Magnus pile instrumentation.

10 CONCLUSIONS AND LEARNINGS

The field performance of the seafloor and of structures has been analysed and key learnings have been documented.

First anthropogenic activities have been shown to potentially affect the seafloor and shallow seabed by depositing heterogeneous sediment mixtures of drill cuttings and cement which can pose a hazard to the installation and performance of shallow foundations. Such activities can also destabilize the seafloor, either by dragging objects or by overloading the seabed. These anthropogenic geohazards are underrepresented in the literature and should not be underestimated.

The Valhall pile buckling incident has highlighted the influence of the pile tip details and documented that external chamfers can significantly increase the chance of pile refusal and buckling in dense and very dense sands.

The performance of MODU anchors during GoM hurricanes has been shown to be consistent with back-analyses using advanced modelling techniques. It has highlighted the fact that the structural capacity of the anchor, and not its geotechnical capacity, can control its overall capacity and is often the limiting factor when the anchors are loaded out-of-plane.

Last, the lateral soil-structure framework of ISO 19901-4:2025 for clays was used to hindcast the field performance of structures at all the limit states of interest in design. The framework was used for the FLS for a GoM tripod structure and for drilling risers, for the SLS for the Magnus platform driven piles, for the ULS for GoM jackets, and for the ALS for a GoM free-standing caisson. All these hindcast were performed using best-estimate soils properties measured by DSS testing.

Using the scientific method context of Feynman (1964), this framework has not been proved wrong by any of the above performances, given it the highest form of technical justification for its inclusion in industry codes and standards.

11 SYMBOLS AND ABBREVIATIONS

ALS:	Abnormal limit state
AUV:	Autonomous Underwater Vehicle
BOP:	Blow out preventer
BSF:	below seafloor
CPT:	Cone penetration test
CU:	Consolidated Undrained
D:	pile diameter
DEA:	Drag embedment anchor
DSS:	Direct Simple Shear
FE:	Finite Element
FEA:	Finite Element Analyses

FLS: Fatigue limit state
 GoM: Gulf of Mexico
 I_p : index of plasticity
 LMRP: Lower marine riser package
 M: mobilised moment load
 M_{ult} : Peak torsional moment capacity of anchor
 MBES: Multibeam echosounder
 MODU: Mobile Offshore Drilling Unit
 MV: Mini Vane
 OCR: overconsolidation ratio
 q_c : cone tip resistance
 R: reduction factor of soil-pile adhesion
 ROV: Remotely operated vehicle
 SBP: Sub-Bottom Profile
 SLS: Serviceability limit state
 SRD: Soil resistance to driving
 s_{uUU} : undrained shear strength measured in UU triaxial compression tests
 s_{uDSS} : undrained shear strength measured in DSS tests
 s_{uTC} : undrained shear strength measured in CU triaxial compression tests
 SSS: side-scan sonar
 UC: Unconfined Compression
 ULS: Ultimate limit state
 UU: Unconsolidated Undrained
 VIV: vortex induced vibrations
 VLA: Vertically loaded anchor

ε_{50} : strain at a stress of 50% of the strength in UU triaxial compression tests

AUTHOR CONTRIBUTION STATEMENT

First Author: Conceptualization, Investigation, Methodology, Data curation, Formal Analysis, Writing- Original draft. **Other Authors:** for selected sections: Investigation, Methodology, Writing- Reviewing and Editing,

ACKNOWLEDGEMENTS

The authors are grateful to their employer and to Aker BP for permission to publish.

Thanks are expressed to John Stiff (retired, ABS), Senol Ozmütlu (Vryhof), Charles Aubeny (Texas A&M University), and Liv Hamre (DNV) for their personal communications.

Present and former bp colleagues whose work is part of this paper include Ayaz Ahmad, Jiun-Yih Chen, Eric Liedtke, and Dan Spikula.

The first author is very grateful to his wife, Thu Hang, for her support throughout the last 30 years and

for giving him the space to grow his career and write many technical papers and keynote lectures.

Thanks are also expressed to the many industry colleagues and the service companies who have fostered the career of the first author. In particular, a number of friends who supported him throughout his career include Knut H. Andersen, Jean-Louis Briaud, Ed Clukey, Robert Gilbert, Suzanne Lacasse, Don Murff, Niall Slowey, and Alan Young.

REFERENCES

- ABS (2012). Post mortem failure assessment of semi-submersible MODUs during Hurricanes Katrina & Rita with additional information from Hurricanes Gustav and Ike. Report ABSC/1514096/LB-08 rev 1. Prepared for MODU mooring strength and reliability JIP.
- Aldridge, T.R., Carrington, T.M., and Kee, N.R. (2005). Propagation of pile tip damage during installation. *Proc., First International Symposium on Frontiers in Offshore Geotechnics*, Gourvenec and Cassidy (eds) Perth, Australia, September, ISBN 0 415 39063 X. DOI:[10.1201/NOE0415390637.ch94](https://doi.org/10.1201/NOE0415390637.ch94)
- Alm, T., and Hamre, L. (1998). Soil model for driveability predictions. *Proc. Offshore Tech. Conf.*, Houston, Paper no. 8835. DOI:[10.4043/8835-MS](https://doi.org/10.4043/8835-MS)
- Alm, T. and Hamre, L. (2001). Soil model for pile driveability predictions based on CPT interpretations. *Proc., 15th International Conf. on Soil Mechanics and Foundation Engineering*, Istanbul, Vol. 2, pp. 1297–1302. https://www.issmge.org/uploads/publications/1/30/2001_02_0104.pdf
- Alm, Torstein, Snell, Richard O., Hampson, Kevin M., and Olaussen, Arne (2004). Design and Installation of the Valhall Piggyback Structures. *Proc. Offshore Tech. Conf.*, Houston, Paper no. 16294. DOI:[10.4043/16294-MS](https://doi.org/10.4043/16294-MS)
- Andersen, B.G. and Borns Jr., H.W. (1994). *The Ice Age World*, ISBN 82-00-21810-4, Scandinavian University Press, Oslo; Distributed world-wide by Oxford University Press. ISBN 10: 8200218104 ISBN 13: 9788200218104
- API RP 2A (1993). Recommended practice for planning, designing and constructing fixed offshore platforms – Working stress design, 20th Edition,
- API RP 2SK (2024). Design and Analysis of Stationkeeping Systems for Floating Offshore Structures, Fourth Edition, February

- API Technical Report 2PY (2020). Effect of best-estimate geotechnical p-y curves on performance of offshore structures.
- Aubeny, C.P. (2024). Personal communication.
- Aubeny, C.P., Han, S.W., and Murff, J.D. (2003). Inclined load capacity of suction caisson anchors, *Intl. J. for Numerical and Analytical Methods in Geomechanics*, Vol. 27, pp. 1235-1254, <https://doi.org/10.1002/nag.319>
- Barbour, R.J., and Erbrich, C. (1995). Analysis of soil skirt interaction during installation of bucket foundation using ABAQUS, *Proc. ABAQUS Users Conf.*, Paris, June.
- Brown, R.J. (2006). Past, Present, and Future towing of pipelines and risers, *Proc., Offshore Technology Conference*, Paper 18047, <https://doi.org/10.4043/18047-MS>
- Chen, J.-Y. (2011). [Analysis of performance and reliability of offshore pile foundation systems based on hurricane loading \(utexas.edu\)](https://utexas.edu) Ph.D. dissertation, The University of Texas at Austin.
- Cheon, J.Y., Spikula, D., Young, A.G., Gilbert, R., and Jeanjean, P. (2015). A perspective on selecting design strength: Gulf of Mexico deepwater clay. *Proceedings, Frontiers in Offshore Geotechnics III. Meyer (Ed.)*, DOI: [10.1201/b18442-206](https://doi.org/10.1201/b18442-206)
- Energio (2010). Assessment of damage and failure mechanisms for offshore structures and pipelines in Hurricanes Gustav and Ike. Report MMS TAR 642 to the Minerals Management Service.
- Energio (2019). Effect of best-estimate geotechnical p-y curves on performance of offshore structures. Report E18140 to the American Petroleum Institute.
- Dan, G. Sultan, N., and Savoye, B. (2007). The 1979 Nice harbour catastrophe revisited: Trigger mechanism inferred from geotechnical measurements and numerical modelling. *Marine Geology* 245 (2007) 40–64. <https://doi.org/10.1016/j.margeo.2007.06.011>
- DeGroot, D.J., Lunne, T., Ghanekar, R., Knudsen, S., Jones, C.D., and Yetginer-Tjelta, T.I. (2019). Engineering properties of low to medium overconsolidation ratio offshore clays. *AIMS Geosciences*, 5(3): 535-567. <https://doi.org/10.3934/geosci.2019.3.535>
- Delmar (2005a). Noble Jim Thompson Kepler MC 383 in Hurricane Ivan. Report 3280-R1-1 to bp.
- Delmar (2005b). Marianas Hurricane Rita postmortem analysis for Puma (GC821). Report 3474-R-0 to bp.
- Delmar (2024). Personal communication
- Feynman, R. (1964). Messenger lectures: The character of physical law, Cornell University.
- Accessed on Youtube at www.youtube.com/watch?v=EYPapE-3FRw
- Gilbert, R. B., Choi, Y. J., Dangyach, S. and Najjar, S. S. (2005). Reliability-Based Design Considerations for Deepwater Mooring System Foundations, *Proc., First International Symposium on Frontiers in Offshore Geotechnics*, Perth, Western Australia, 317-324. DOI: [10.1201/NOE0415390637.ch29](https://doi.org/10.1201/NOE0415390637.ch29)
- Gilbert, R.B., Chen, J.Y., Materek, B., Puskar, F., Verret, S., Carpenter, J., Young, A., and Murff, J.D. (2010). Comparison of observed and predicted performance for jacket pile foundation in Hurricanes. *Proc. Offshore Tech. Conf., Houston, TX*, May, Paper no. 20861. DOI: [10.2523/20861-MS](https://doi.org/10.2523/20861-MS)
- Hamre, L. (2024). Personal communication.
- Horsnell MR, Norris VA, and Ims B (1993). Mudmat interaction and foundation analysis. In *Large-scale pile tests in clay*, Edited by J. Clarke, Thomas Telford, ISBN 0-7277-19181. *Proceedings of the conference Recent large-scale fully instrumented pile tests in clay* held at the Institution of Civil Engineers, London, on 23-24 June 1992. ISBN: 0-7277-1918-1.
- ISO 19901-4:2016. Petroleum and natural gas industries – Specific requirements for offshore structures. Part 4: Geotechnical and foundation design considerations.
- ISO 19901-4:2025. Petroleum and natural gas industries – Specific requirements for offshore structures. Part 4: Geotechnical and foundation design considerations. Third edition.
- Jeanjean, P. (2006). Setup characteristics of suction anchors for soft Gulf of Mexico clays: Experience from field installation and retrieval. *Proc. Offshore Tech. Conf.*, Houston, USA, Paper 18005. DOI: [10.4043/18005-MS](https://doi.org/10.4043/18005-MS)
- Jeanjean, P. (2012). State of Practice: Offshore Geotechnics throughout the Life of an Oil and Gas Field. In *Geotechnical Engineering State of the Art and Practice: Keynote Lectures from GeoCongress 2012* <https://doi.org/10.1061/9780784412138.0024>
- Kannala, J., Zakeri, A., and Ge, M.L. (2016). Performance evaluation of recently developed soil models in well conductor fatigue analysis using field measurements, *Proc. Offshore Tech. Conf* Houston, USA, Paper no. 27186. DOI: [10.4043/27186-MS](https://doi.org/10.4043/27186-MS)
- Kenley RM and Sharp DE (1993). Magnus foundation monitoring project instrumentation data processing and measured results. In *Large-scale pile tests in clay*, Edited by J. Clarke, Thomas Telford, ISBN 0-7277-19181. *Proceedings of the conference Recent large-scale fully instrumented pile tests in clay* held

- at the Institution of Civil Engineers, London, on 23-24 June 1992. ISBN: 0-7277-1918-1.
- Kulikov, E.A., Rabinovich, A.B., Thomson, R.E., and Bornhold, B.D. (1996). The landslide tsunami of November 3, 1994, Skagway Harbor, Alaska. *Journal of Geophysical Research*, Vol. 101, NO. C3, pages 6609-6615. <https://doi.org/10.1029/95JC03562>
- Liedtke, E., Andersen, K.H., Zhang, Y., and Jeanjan, P. (2019). Monotonic and cyclic soil properties of Gulf of Mexico clays, *Proc. Offshore Tech. Conf* Houston, USA, Paper no. 29622. <https://doi.org/10.4043/29622-MS>
- Lunne, T., By, T., and Lacasse, S. (1994). Laboratory testing for offshore structures. *Proc. XIII ICSMFE*, New Delhi, India. https://www.issmge.org/uploads/publications/1/32/1994_04_0073.pdf
- Masing, G. (1926) Eigenspannungen und Verfestigung beim Messing. *Proceedings of Second International Congress of Applied Mechanics*, Zurich, 332-335.
- McClelland Engineers (1977). Soil and Foundation Investigation. Magnus Field, Block 211/12. U.K. Sector, North Sea. Report No. UK77-006-1 to BP Trading Ltd.
- Mercan, B., Chandra, Y., Campbell, M., and Ge, M. (2019). Soil model assessment for subsea wellhead fatigue using monitoring data. *Proc. Offshore Tech. Conf.*, Houston, USA, Paper no. 27662 <https://doi.org/10.4043/27662-MS>
- MMS (2008). MMS Completes Assessment of Destroyed and Damaged Facilities from Hurricanes Gustav and Ike, News Release #R-08-3932, November 26 2008 <https://www.bsee.gov/sites/bsee.gov/files/news/hurricanes/081126a.pdf>
- Newlin, J. (2003). Suction anchor piles for the Na Kika FDS mooring system. Part 1: site characterization and design. *Proc. Int. Symp. On Deepwater Mooring Systems*, Houston, Oct. <https://doi.org/10.1061/9780784407011>
- OTRC (2009). Analysis of potential conservatism in Foundation Design for Offshore Platform Assessment. Offshore Technology Research Center, Final Project Report prepared for the Minerals Management Services under MMS award/contract M08PC20002, MMS Project Number 612, 264pp.
- Petruska, D. (2005). Presentation “Mississippi Canyon 383 Rig mooring Failure” made at *Hurricane Readiness & Recovery Conference*, see Ward et al. 2005, Hurricane Readiness & Recovery Conference Report, Final Conference Summary
- Report prepared for the MMS by OTRC, MMS Project 559
- Randolph, M.F. (2018). Potential damage to steel pipe piles during installation. Special contribution. *IPA NewsLetter*, Volume 3, Issue 1, March. <https://www.press-in.org/upload/files/Newsletter/topics/special%20contribution/special%20contribution%20by%20Prof.%20mark.pdf>
- Reese L, Cox W, and Koop F. (1975). Field testing and analysis of laterally loaded piles in stiff clays., *Proc. Offshore Tech. Conf.*, Houston, USA, Paper 2312. <https://doi.org/10.4043/2312-MS>
- Sejrup, H.P., Larsen, E., Landvik, J., King, E.L., Haflidason, H., Nesje, A. (2000). Quaternary glaciations in southern Fennoscandia: evidence from southwestern Norway and the northern North Sea region. *Quaternary Science Reviews* 19 (2000) 667-685. [https://doi.org/10.1016/S0277-3791\(99\)00016-5](https://doi.org/10.1016/S0277-3791(99)00016-5)
- Semple, R.M., and Rigden, W.J. (1983). Site Investigation for Magnus. *Proc. Offshore Tech. Conf* Houston, USA, paper no. 4466. <https://doi.org/10.4043/4466-MS>
- Sharp, D., E. (1993). Magnus foundation monitoring - an overview. In *Large-scale pile tests in clay*, Edited by J. Clarke, Thomas Telford, ISBN 0-7277-19181. *Proceedings of the conference Recent large-scale fully instrumented pile tests in clay* held at the Institution of Civil Engineers, London, on 23-24 June 1992. ISBN: 0-7277-1918-1.
- Sharples, M. (2006). Post Mortem failure assessment of MODUs during Hurricane Ivan. Report 0105PO39221 to the Minerals Management Services, Sept.
- Shelton, J. T. (2007). OMNI-Max Anchor Development and Technology. *Proceedings of the 2007 Oceans Conference*, Vancouver, B.C., Canada. DOI:[10.1109/OCEANS.2007.4449415](https://doi.org/10.1109/OCEANS.2007.4449415)
- Vryhof (2024). Personal communication.
- Ward, E.G, Mercier, R.S., Zhang, J., Kim, H., Aubeny, C., and Gilbert, R.B. (2008). No MODUS adrift. Report prepared for the Minerals Management Service, MMS Project 574.
- Wu, F., Chen, C-H, and Litton R.W. (2020). Effect of best-estimate clay p-y curves on performance of offshore structures, *Proc. Offshore Tech. Conf*, Houston, USA, Paper OTC 30889 <https://doi.org/10.4043/30889-MS>
- Young, A., Quiros, G.W., and Ehlers, C. (1983). Effects of Offshore Sampling and Testing on Undrained Soil Shear Strength, *Proc. Offshore Tech. Conf*, Houston, USA, Paper OTC 4465. <https://doi.org/10.4043/4465-MS>
- Young, A. (2019). Personal communication

- Zakeri, A., Clukey, E., Keadze, B., Jeanjean, P., Walker, D., Piercey, G., Templeton, J., Connely, L., and Aubeny, C. (2015). Recent advances in soil response modeling for well conductor fatigue analysis and development of new approaches. *Proc. Offshore Tech. Conf* Houston, USA, Paper no. 25795 <https://doi.org/10.4043/25795-MS>
- Zimmerman, E.H., Smith, M.W., and Shelton, J.T. (2009). Efficient Gravity Installed anchor for deepwater mooring. *Proc. Offshore Tech. Conf* Houston, USA, Paper no. 20117. <https://doi.org/10.4043/20117-MS>

INTERNATIONAL SOCIETY FOR SOIL MECHANICS AND GEOTECHNICAL ENGINEERING



This paper was downloaded from the Online Library of the International Society for Soil Mechanics and Geotechnical Engineering (ISSMGE). The library is available here:

<https://www.issmge.org/publications/online-library>

This is an open-access database that archives thousands of papers published under the Auspices of the ISSMGE and maintained by the Innovation and Development Committee of ISSMGE.

The paper was published in the proceedings of the 5th International Symposium on Frontiers in Offshore Geotechnics (ISFOG2025) and was edited by Christelle Abadie, Zheng Li, Matthieu Blanc and Luc Thorel. The conference was held from June 9th to June 13th 2025 in Nantes, France.